12-2007

Mechanics of Burrowing in Muddy Sediments

Kelly M. Dorgan

MECHANICS OF BURROWING IN MUDDY SEDIMENTS

By

Kelly M. Dorgan

B.S. University of California, Santa Cruz, 2001

A THESIS

Submitted in Partial Fulfillment of the

Requirements for the Degree of

Doctor of Philosophy

(in Oceanography)

The Graduate School

University of Maine

December, 2007

Advisory Committee:

    Peter A. Jumars, Professor of Oceanography, Advisor

    Bernard P. Boudreau, Professor of Oceanography

    Eric N. Landis, Associate Professor of Civil Engineering

    Lawrence M. Mayer, Professor of Oceanography

    Les E. Watling, Professor of Oceanography

MECHANICS OF BURROWING IN MUDDY SEDIMENTS

By

Kelly M. Dorgan

B.S. University of California, Santa Cruz, 2001

A THESIS

Submitted in Partial Fulfillment of the

Requirements for the Degree of

Doctor of Philosophy

(in Oceanography)

The Graduate School

University of Maine

December, 2007

Advisory Committee:

Peter A. Jumars, Professor of Oceanography, Advisor

Bernard P. Boudreau, Professor of Oceanography

Eric N. Landis, Associate Professor of Civil Engineering

Lawrence M. Mayer, Professor of Oceanography

Les E. Watling, Professor of Oceanography

LIBRARY RIGHTS STATEMENT

In presenting this thesis in partial fulfillment of the requirements for an advanced degree at The University of Maine, I agree that the Library shall make it freely available for inspection. I further agree that permission for "fair use" copying of this thesis for scholarly purposes may be granted by the Librarian. It is understood that any copying or publication of this thesis for financial gain shall not be allowed without my written permission.

Signature:

Date:

MECHANICS OF BURROWING IN MUDDY SEDIMENTS

By Kelly M. Dorgan

Thesis Advisor: Dr. Peter A. Jumars

An Abstract of the Thesis Presented
in Partial Fulfillment of the Requirements for the
Degree of Doctor of Philosophy
(in Oceanography)
December, 2007

Marine muds are elastic solids through which animals move by propagating a crack-shaped burrow. Dilations previously considered anchors serve to exert dorso-ventral compressive stresses on the burrow walls that, through elastic behavior of the medium, focus strongly at the tip of the burrow. This focused stress breaks adhesive or cohesive bonds, propagating a crack for the animal to follow. The force exerted by the polychaete, *Nereis virens*, to propagate a crack has been measured in gelatin, an analogue of muddy sediment, through photoelastic stress analysis. Finite element analysis was used to convert measured forces to those exerted in natural sediments based on differences in stiffnesses between gelatin and mud. From linear elastic fracture mechanics theory, it is predicted that a crack propagates when the stress intensity factor, a measure of stress amplification at the crack tip, exceeds a critical value, the fracture toughness. Stress intensity factors, calculated from measured forces using finite element modeling, fall within the range of critical values measured in gelatin and exceed those in natural sediments. Stress intensity factors were also calculated from the shapes of worms burrowing in transparent gels with varied mechanical properties, and fell close to or

exceeded respective critical values. These results, using two independent measurements, strongly support that the mechanism underlying burrowing is crack propagation. Behavioral differences were observed by worms burrowing in gels with different mechanical properties, and can be explained by the differences in mechanics.

This mechanism of burrowing by fracture is consistent with descriptions of burrowing across phyla and helps explain long-puzzling anatomies and behaviors of burrowing animals. Understanding of this mechanism raises questions about the reputed high energetic cost of burrowing, feeding guild classifications—specifically surface deposit feeders, and identifies some potential artifacts in benthic studies of chemistry and bioturbation. Both behaviors of burrowers and responses of sediments to forces exerted by burrowers depend on the mechanical properties (stiffness and fracture toughness), and understanding of that relationship will lead to advances in automaton modeling of bioturbation. Any serious mechanical analysis of swimming involves relevant physical properties of the medium. Going forward, the same will now be true of burrowing.

ACKNOWLEDGMENTS

TABLE OF CONTENTS

LIST OF TABLES

LIST OF FIGURES

Chapter 1

INTRODUCTION

In many marine environments, bioturbation contributes to sediment mixing more significantly than do physical processes, altering sediment compaction and structure, oxygenation, and carbon burial. Propagation of acoustic waves depends on the degree of compaction, and higher porosity and the presence of burrows facilitates diffusion and advection of material into and out of the sediment. Oxygen flux into the sediment changes the biological community and chemical environment. Fates of contaminants are strongly influenced by bioturbation through burial, resuspension, and gut passage. This mixing creates 'noise' in the geological record, posing problems of resolution for both paleontologists and geologists. Burial of organic material is the primary long-term, global sink of carbon, the quantity of which is affected by digestion and bioturbation.

This dissertation seeks a deeper understanding of bioturbation by relating the mechanical properties of sediments to the forces that animals use to manipulate them, just as a deep understanding of swimming mechanics requires quantification of both the work done by the animal and the response of the medium. Recent work on methane bubble growth and movement in muddy sediment shows that bubbles move by propagating a crack and moving upward into the crack (Johnson et al. 2002). Growth was modeled through explicit theory from linear elastic fracture mechanics (LEFM), assuming that sediment is an elastic solid. This mechanism of movement by bubbles both suggests an analogous mechanism for burrowing animals and provides an explicit, testable model for studying sediment mechanics.

The hypothesis that animals burrow by crack propagation was tested in Chapter 2 using gelatin as an analog for muddy sediments (based on similar mechanical properties; e.g., Johnson et al. 2002). Gelatin is not only transparent, enabling visualization of animal behavior, but is also birefringent, enabling stress visualization and measurement by photoelastic stress analysis (e.g., Full et al. 1995). Edges of the burrow are clearly visible under polarized light and show a discoidal crack, shaped like a tongue-depressor, with the dorsal and ventral surfaces of the animal holding the crack open. The crack extends laterally beyond the setae and anteriorly to the tips of the antennae. When the worm everts its pharynx, stress applied to the crack walls, visualized using photoelastic stress analysis, is amplified at the crack tip. The crack extends and the worm moves forward into the burrow.

The mechanism of burrowing by crack propagation lends insight into some previously unexplained behaviors and anatomical features of burrowers and has implications regarding bioturbation, burrowing energetics, and some methods used to study burrowers. A literature review, presented in Chapter 3, discusses these implications and suggests that this mechanism is widespread in muddy sediments, but does not apply to burrowing in clean sands, which have very different mechanics.

The mechanism of burrowing by crack propagation raises questions about previous experiments that suggested that burrowing is more energetically expensive than other forms of locomotion (e.g., Trevor 1978, Hunter & Elder 1989). In Chapter 4, forces exerted during pharynx eversion by the polychaete *Nereis virens* were calculated through explicit consideration of sediment mechanics. These forces are lower than those previously measured (Trevor 1978) and depend on the stiffness of the sediment.

According to verified predictions from LEFM, the aspect ratios of bubbles growing by fracture depend on the ratio of fracture toughness to stiffness of the material. Similarity in the mechanism of bubble growth and burrow extension suggests that the shapes of burrows around worms should also depend on this ratio of material properties. Use of gelatin as an analog for muddy sediments is justified by similarity of these ratios between the two materials. Kinematics of burrowing worms observed in Chapter 4 suggested that worms shape their bodies as medium-appropriate wedges to extend the crack. Stable, wedge-driven fracture theory predicts a dependence of wedge shape on the same ratio of fracture toughness to stiffness. In Chapter 5, the dependence of burrowing behavior on this ratio of mechanical properties was predicted from theory and then tested against worm behaviors in gels with different properties.

Chapter 2

BURROW EXTENSION BY CRACK PROPAGATION

Until now, the analysis of burrowing mechanics has neglected the mechanical properties of impeding, muddy, cohesive sediments, which behave like elastic solids (Johnson et al. 2002). Here we show that burrowers can progress through such sediments by using a mechanically efficient, previously unsuspected mechanism — crack propagation (Johnson et al. 2002, Boudreau et al. 2005) — in which an alternating 'anchor' system of burrowing serves as a wedge to extend the crack-shaped burrow. The force required to propagate cracks through sediment in this way is relatively small: we find that the force exerted by the annelid worm *Nereis virens* in making and moving into such a burrow amounts to less than one-tenth of the force it needs to use against rigid aquarium walls (Hunter & Elder 1989).

Using gelatin as an analogue for sediment (on the basis of its similar mechanical properties; e.g., Menand & Tait 2001, Johnson et al. 2002, Boudreau et al. 2005) and polarized light to visualize the burrow around *N. virens*, we investigated whether these worms burrow by crack propagation. Gelatin is birefringent, which enables its stress to be analysed (Full et al. 1995) during burrowing.

We found that the edges of the burrow were visible and that they showed evidence of a discoidal crack, which was held open by the dorsal and ventral surfaces of the animal (Figure 2.1A, B). The arc of the crack extends laterally beyond the setae and anteriorly to the tips of the antennae. Visualization of stress fields by photoelastic stress analysis (for methods, see Appendix A) reveals a force exerted dorsoventrally by

4
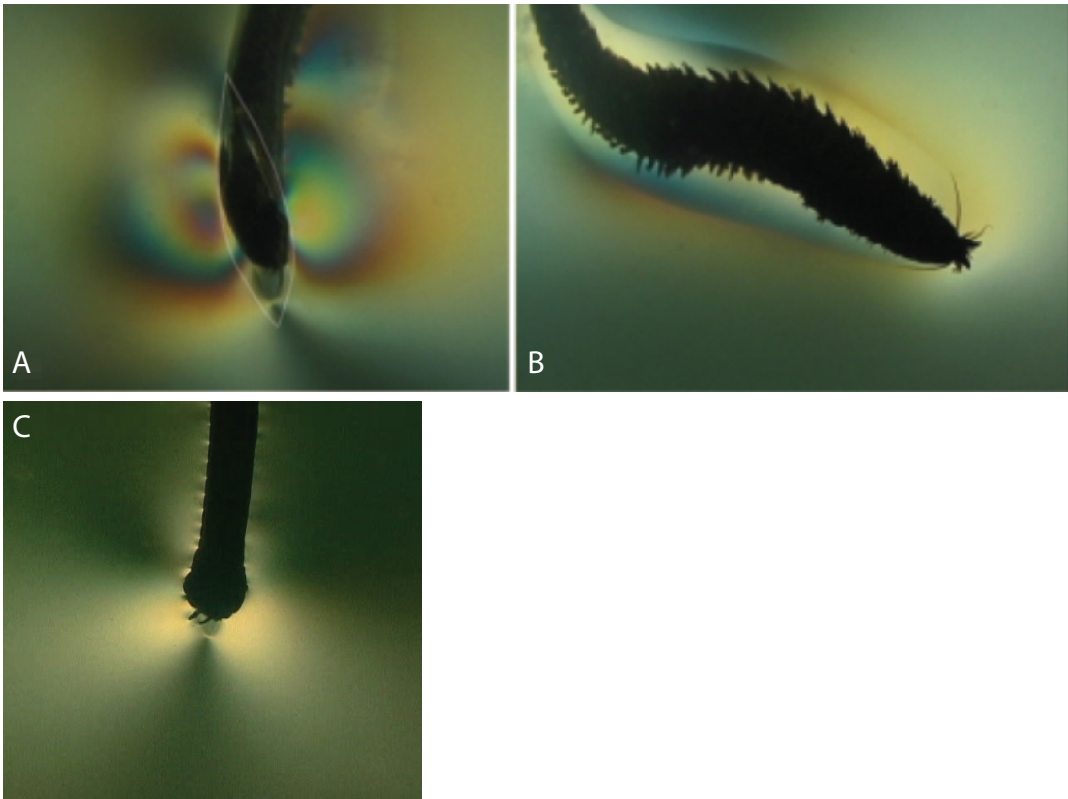
Figure 2.1. The crack-shaped burrow around *Nereis virens*. A) Anterior view in cross-polarized light, showing the longer axis, W, of the discoidal crack oriented parallel with the setae in the crack and the dorsal and ventral surfaces against the gelatin. The stress field shown here results from displacement of the gelatin by the worm's body and reflects the elastic properties of the medium. The worm is not actively propagating the crack in this frame. B) Dorsal view in cross-polarized light, showing the shape of the burrow around the animal and the low-force undulatory motion of the animal moving forward into the crack. C) Side view in circularly polarized light, showing the stress field dorsal and ventral to the worm along the shorter axis, T, of the discoidal crack and the crack extending anteriorly.

eversion of the animal's pharynx against the relatively flat wall of the crack (Figure 2.1C).

According to linear elastic fracture mechanics, the stress intensifies at the crack tip, propagating it when the critical stress intensity is reached (Broek 1978, Johnson et al. 2002). Here, the everted pharynx acts as a wedge, with the radial force intensified at the tip of the crack, which propagates, allowing the animal to move forward (Figure 2.2). The crack's aspect ratio (T/W in Figure 2.2) is a function of the material properties of the sediment (the critical stress intensity and Young's modulus). Expansion of a subterminal body portion has previously been considered as an anchor (Elder 1980); we infer instead that a terminal or subterminal lateral expansion acts as a wedge in elastic mud.

We measured the maximum force required to propagate a crack as 0.023 ± 0.002 N (mean $\pm$ s.e.m.; n = 5),which is less than 10% of the 'radial' force of 0.6 N that is exerted by a worm against an aquarium wall (Hunter & Elder 1989). Sediment behaves like an elastic solid that deforms under stress, as evidenced by acoustic (e.g., Hamilton 1980) and bubble-growth experiments (e.g., Johnson et al. 2002). The relatively small forces exerted by growing bubbles in sediment are well predicted by linear elastic fracture mechanics from the mechanical properties of the medium (Johnson et al. 2002). According to the theory of elasticity, a closer, rigid boundary necessitates greater force for a given displacement, resulting in substantial effects of nearby rigid walls on burrowers.

Crack propagation may also be a likely mechanism of movement for burrowers from several other marine phyla. For example, clams and echinoids, which are both found in muddy sediments, could exploit their wedge-like shape — and some echinoids have

6
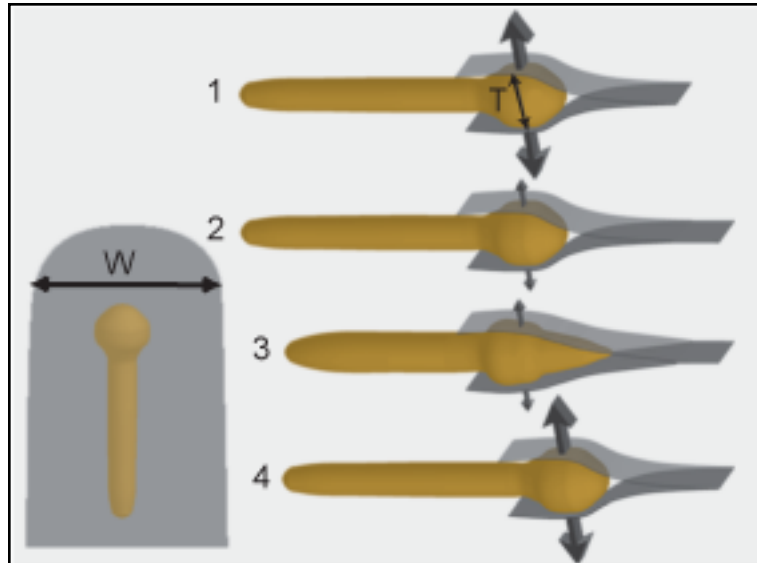
Figure 2.2. Diagrammatic lateral oblique view of crack propagation during burrowing. Filled arrows extending laterally from the crack and parallel to the minor axis, T, indicate measured stress magnitudes. The worm propagates the crack by everting the pharynx and exerting a force normal to the direction of movement (1). The stress is amplified at the crack tip, and when it reaches a critical value (K_{Ic}) the crack propagates and energy is released (2). The worm then retracts the pharynx and moves forward into the crack (3) before beginning the cycle again (4). Burrowing has previously been described as a dual-anchor system with alternating terminal anchor (1) and penetration anchor (3). Inset shows dorsal view diagram of crack showing disk shape. The aspect ratio (T/W) is a function of the material properties of the sediment (K_{Ic} and Young's modulus, E).

been reported to push directly into the frontal sediment, rather than excavating it, and to move through the sediment by means of a repeated rocking motion, unlike more globular, excavating echinoids living in sands (Kanazawa 1992). Gammarid amphipods could exploit their resemblance to oblate bubbles (Johnson et al. 2002) and subterminal expansions in earthworms indicate that they may burrow, and roots grow (e.g., Abdalla et al. 1969) by an analogous mechanism.

Burrowing by crack propagation also bears on bioturbation, the movement of sediment grains and fluids by living organisms. Bioturbation models have generally ignored the polymeric matrix that leads to elastic behaviour and that keeps sediment grains in the same relative position to each other, instead considering particles as separate, "randomly wandering" elements (Meysman et al. 2003). But cracks open new surfaces from which animals can feed, leading to unsteady release and uptake of solutes. Crack propagation focuses stresses at the propagating crack tip. These stresses are probably the highest experienced by sediments after their deposition and bear on issues such as the permanence of clay–grain associations and the mechanical protection of organic material from decay.

Chapter 3

MACROFAUNAL BURROWING: THE MEDIUM IS THE MESSAGE

3.1. Chapter Abstract

Burrowing by benthic infauna mixes both sediment grains and interstitial fluids, affecting sedimentary redox conditions and determining fates of organic matter and pollutants. Explicit, quantitative analyses of material properties of sediments, however, have been applied only recently to understand mechanisms of burrowing. Muds are elastic solids that fracture under small tensile forces exerted by burrowers, and are dominated by adhesive forces between sediment grains and the surrounding mucopolymeric gel and (or) by cohesion of this gel. By contrast, in clean sands behaving as granular materials, gravity is a much more significant force holding grains together than is adhesion or cohesion. Burrowers in muds have diverse structures that act as wedges to propagate cracks and elongate their burrows. In sands, increased rugosity on a small, and liquefaction on a larger scale, facilitate displacement of the grains that carry compressive forces along distinct force chains or arches. The classic dual-anchor system described for burrowers is reinterpreted as having several additional functions. The characteristic dilations or expansions function primarily as wedges that exert lateral tensile forces to propagate cracks forward, secondarily as double O-ring seals holding fluid pressure in the advancing burrow (maintaining tensile stresses needed to open a crack), and thirdly as anchors (to pull the shell along in bivalves in particular). Burrowing bivalves are wedges. In the case of burrowing gammarid amphipods, the dorsal exoskeleton mirrors the shape of half a sedimentary bubble and constitutes a

9

wedge. A great many anatomical features of burrowers can now be understood

analogously. The identification of the mechanisms of burrowing by crack propagation

suggests that a substantial revision of the previously described feeding guilds of

polychaetes is required.

3.2. Introduction

Roughly 70% of Earth's surface is covered by marine sediments, and the majority

are muds. This extensive biome is also one of the most poorly understood because

observations are difficult in muds especially in muds underlying deep water. The

relationships of animals living in this biome with their environments are particularly

intimate. Not only do they move through sediments, but the vast majority subsist by

eating them, *i.e.,* by deposit feeding. This kind of intimacy leads to rich intra- and

interspecific interactions (e.g., Edmonds et al. 2003).

Burrowing deposit feeders have both global and local importance. They literally

gate the burial of organic matter, controlling how much organic carbon is moved out of

contact with the global ocean and atmosphere. A substantial fraction of the nutrients

used in coastal ocean primary production arises from nutrient cycling within the deposit-

feeder-modulated seabed, and evidence grows that this feedback from deposited organic

particles is a strongly positive one that may 'run away', causing coastal eutrophication

and 'dead zones' (Grall & Chauvaud 2002). Among the subtle but important effects are

those on bioavailability of nitrogen, whose remineralization pathways (N_2 vs. NO_3^-) are

critically determined by local redox conditions controlled by respiratory irrigation (Aller

1988).

One consequence of moving and feeding is bioturbation, the mixing of sediments and their pore waters. Bioturbation is the process that in most locations limits resolution of the microfossil-based stratigraphic record. Outside areas of unusually high sedimentation rate and (or) permanent bottom-water anoxia, it is difficult or impossible to resolve $\leq 10^3$ yr stratigraphically (Schiffelbein 1984). Biogenic structures produced by deposit feeders also largely control the bottom roughness of marine muds and thereby influence bottom boundary-layer structure, bed shear stresses and the drag experienced by near-bed currents; these structures typically result in roughly doubled drag over a smooth-bed configuration (Nowell et al. 1981). By affecting erodibility in response to given shear stresses, deposit feeders further influence net deposition and sediment stability (e.g., Rhoads et al. 1978, Roast et al. 2004).

Across ocean depths, deposit feeding is the overwhelmingly dominant strategy used by macroscopic marine faunas to locate and consume food, and animals that feed on sediments in turn fuel many bottom-dwelling fishes and crustaceans of commercial importance. Unfortunately, the surfactants used by deposit feeders to strip hydrophobic food from ingested particles are also effective at removing hydrophobic pollutants (e.g., Voparil et al. 2003), and the high organic concentrations reached in deposit-feeder digestive processes make them also effective at solubilising heavy metals (e.g., Chen & Mayer 1999). Thus deposit feeders are major entry points of pollutants into marine food webs and frequently are casualties of this entry. In some cases their effects on sediment transport and deposition combine through bioturbation to exacerbate pollution problems. Witness the gradual resurfacing of massive, previously buried DDT deposits on the Palos Verdes shelf off Orange County, California (Sherwood et al. 2002). Exactly what deposit

feeders do—and where on and under the sediment surface they do it—becomes extremely important to the fate and effects of the residual DDT and its breakdown products.

A fundamental issue of deposit-feeder ecology is the identification of the mechanism and frequency of infaunal movement through sediments. Movement through sediments is generically referred to here as burrowing, and this movement is the subject of the present review. A review is timely for two reasons. One is simply that it has been over two decades since the topic has been systematically analysed (e.g., Trueman 1975, Trueman & Jones 1977, Elder 1980). The second and more important reason is that understanding of mechanical properties of heterogeneous materials such as sediments has increased enormously over those same two decades (e.g., Duran 2000, Torquato 2001). The goal of connecting sediment nano- and microstructure with its bulk behaviour seems nearly within reach. Moreover, parameterisation and measurement of bulk sediment properties at scales relevant to burrowing has just seen dramatic advance (Johnson et al. 2002), with immediate application to burrowing mechanics (Dorgan et al. 2005). One could hardly imagine analysing how a copepod or fish swims without incorporating fluid density and dynamic viscosity, yet no prior review of burrowing has explicitly identified and quantified the mechanical properties of sediments that interact with burrowing forces. It is time to move from qualitative to quantitative description of the burrowing process.

Previous burrowing studies have implicitly assumed that sediment deforms plastically around burrowing animals or that movement requires liquefaction of sediment. This assumption now is clearly refuted for those marine muds in which material behaviour has been quantified. These muds are solids that deform elastically and fail by fracture (Johnson et al. 2002), in stark contrast to both the granular behaviour of beach

12

sands that was previously implicitly assumed to apply across broad sediment types and to plastic deformation.

This review focuses on the physical constraints imposed by the material behaviour of sand and mud, distinguishing elastic behaviour of muds from granular mechanics of sands. Neither decapod burrowing, which has been reviewed by Atkinson & Taylor (1988), nor burying, recently reviewed by Bellwood (2002) is discussed. Similarly, the extensive literature on speed of burrowing (or burrowing rate index) versus grain size is not reviewed in any detail. Although the scaling of burrowing rate index with body size is a clever one (Stanley 1970) that likely will find continuing applicability, grain size alone—except at the extremes—has proven to be a poor predictor of bulk sediment properties relevant to burrowing forces. Also excluded to a large extent is the extensive literature that invokes dilatancy or thixotropy (defined below) as burrowing mechanisms but does not provide further explication or quantification.

Many anatomical features and behaviours of burrowing animals can be explained as mechanisms to overcome specific physical constraints of sediments. For example, anterior dilations serve to propagate a crack and elongate the burrow rather than simply to anchor animals in mud (Dorgan et al. 2005). Physical differences between sands and muds can explain morphological and behavioural differences among their inhabitants, while functional similarities exist across phyla with vastly different forms. Finally, implications of mechanical constraints on burrowing to distribution and biomechanics of animals in the sediment, nutrient acquisition and effects on biogeochemical cycling, bioturbation, and methods of studying benthic communities are discussed. This review

13

focuses on marine sediments, but similarities with soils necessitate some discussion of terrestrial burrowing, and many of the questions arising are relevant to both systems.

Because the aim is to advance the field beyond classification toward equation-level analysis and description, the terminology used is perhaps less precise than some might prefer. Namely, any method that both makes an opening and results in translation of an animal through sediments fits the generic definition of *burrowing* used here. In particular, *excavation*, in which sediment is physically removed from the direction of translation, is one method. *Liquefaction* is a means, particularly in media displaying granular physics, of reducing the forces needed to move forward into the liquefied region (i.e. by relieving the weight of overlying sediment and friction between grains). In either case, the resultant tunnel may be shored up by either a mucus lining or a more elaborate tube incorporating selected sediments. Movement of an animal in a pre-existing tube or burrow is not included as burrowing. The term *burrowing* as used here specifically includes the acts of making the opening in the substratum and moving into it. *Reworking* is used to mean any biogenic movement of sediment, whereas the term *bioturbation* refers to the detectable disturbance of the complex sedimentary medium. Bioturbation thus depends on context (e.g., whether solute or particle is treated and whether disturbance is measured by chemical assay, inspection of microfossils or grain-size analysis).

Departure from common usage of the term 'cohesive' as applied to sediments is intentional because it is both chemically and mechanically misleading. Cohesive forces act between like molecules, whereas adhesive forces act between unlike molecules. Cohesive forces between sediment grains can be appreciable (relative to grain weight)

only for grains in the clay size range. Most natural marine sediments adhere through

mucopolymers whose production and consumption are largely controlled by the billion

bacteria that typically inhabit each millilitre of pore water (Schmidt et al. 1998).

Sediment grains thus are surrounded by polymeric organic matter (e.g., Watling 1988).

Organic material associates with mineral grains differently depending on the size (and

weight) of the grains. Larger sand grains are encrusted with organic material, whereas

smaller silt and clay grains are almost always found in larger aggregates—effectively

embedded in polymer (Johnson 1974). Johnson (1974) clearly distinguished among

organic-mineral aggregates, encrusted minerals, and free mineral particles in his

microscopic study of particulate matter at the sediment-water interface, and he suggested

that differences in sedimentological properties likely result from these distinct particle

forms. Watling (1988) showed a more continuous sedimentary matrix below the

sediment surface, suggesting that at least some of the "aggregates" described by Johnson

(1974) were likely artifacts of putting sediment on glass slides. Sediment structure is

governed by polymeric material both on a larger scale through the sedimentary matrix

and on a smaller scale through the fracture of aggregates rather than individual particles

from the matrix. Thus if cohesion is important to the physical properties of sediments it

is the cohesion of the mucopolymer matrix and not of the sedimentary particles above

clay size.

3.3. Background solid mechanics

3.3.1. Elasticity of mud

Before considering the mechanical constraints of sediments, it is necessary to briefly summarise the relevant mechanics, starting with solid mechanics, that is relevant to muds and sandy muds. Clean, granular sands exhibit unique behaviour, resisting strain like a solid, flowing like a liquid, falling fully into neither category. Only clean, coarse-grained beach sands behave like classic granular materials, whereas adhesion among grains leads to a transition between granular behaviour and elasticity. In order to clarify the relevant variables, it is suggested that a nondimensional 'stickiness' marks the transition in behaviour, namely the ratio between the adhesive or cohesive forces that hold two grains together relative to grain weight. This scaling makes it clear that granular behaviour is very strongly dependent on grain size but also depends on adhesion between grains at contacts or cohesion of the polymer matrix in which grains are embedded.

Solids deform under stress, and when the stress reaches a critical value, the material fails, either by fracture or plastic deformation (also called yield). Stress (σ) is defined as force per unit area, and forces can be either body forces (such as gravity), which act in the same way throughout a material, or surface forces (such as those exerted by animals) that operate either on the actual surface of the solid or on a surface defining a control volume of the solid. The stress exerted perpendicular to a surface is called normal stress, and can be either compressive or tensile, depending on its direction. Convention defines compressive stresses as negative and tensile stresses as positive. Stress exerted parallel to the surface is called shear (Figure 3.1). Many solids behave

16
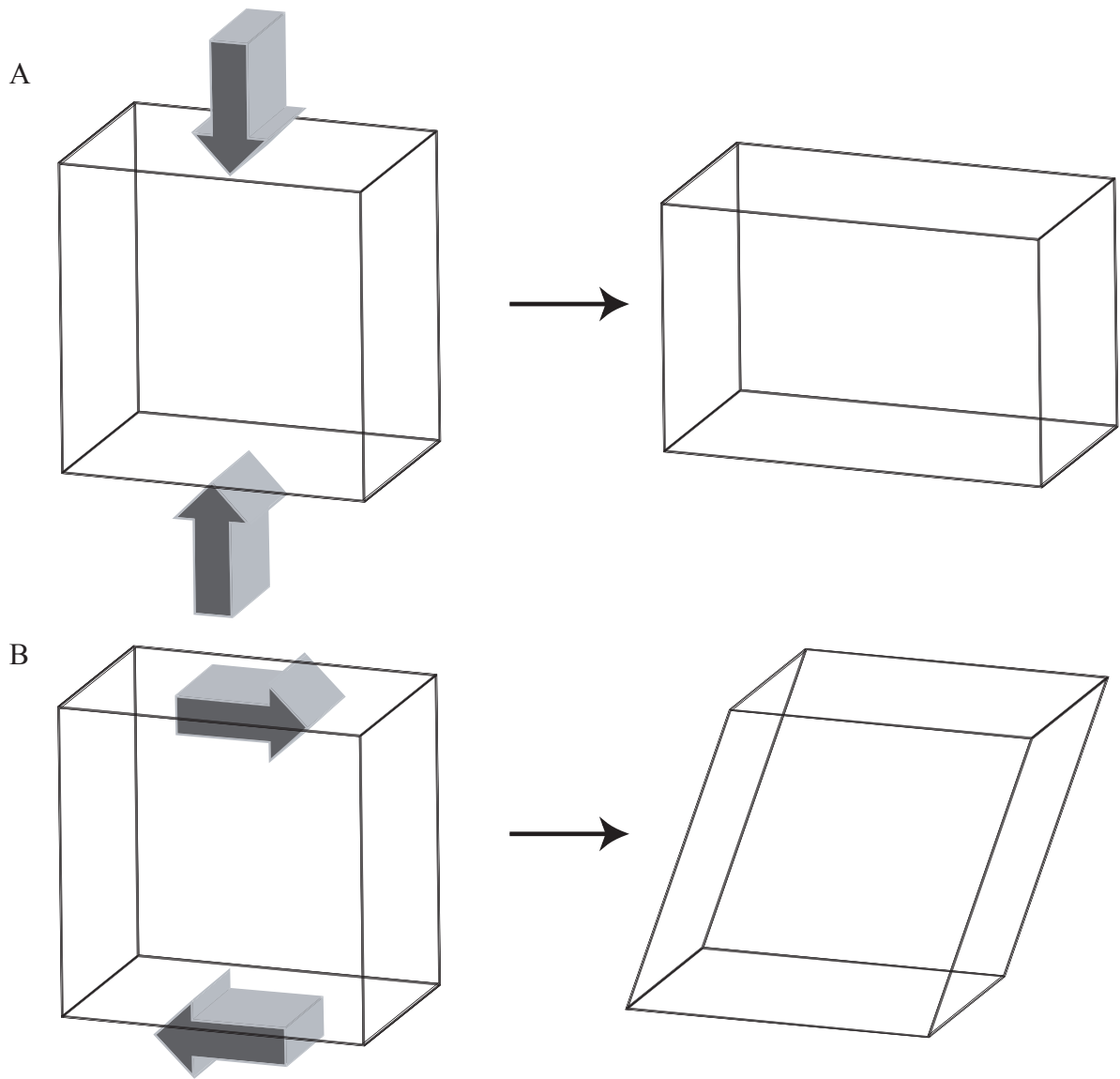
Figure 3.1. Normal and shear stress. A) Normal stress is stress exerted perpendicular to a surface; B) Shear stress is stress exerted parallel to a surface.

elastically under small stresses, so that a deformation is reversible: when the force is removed, the solid returns to its original shape. The force resisting a deformation is called the elastic restoring force. Yield stress (σ_Y) defines the threshold beyond which plastic deformation occurs; as long as the stress in the material does not exceed the yield stress, the material behaves elastically. The deformation resulting from stress per unit length of the material is called strain (ε), which is dimensionless. In an element of sediment, strain can be defined relative to an initial length scale or grain-to-grain distance before deformation. Within the linear elastic range, tensile stress in a material is a linear function of strain: $\sigma = E\,\varepsilon$, where E is the elastic modulus (dimensions of stress, $M\,T^{-2}\,L^{-1}$), also called Young's modulus. The elastic modulus is experimentally determined as the slope of the stress-strain curve (Figure 3.2). A material with a larger elastic modulus requires more stress to reach a given displacement and has greater stiffness.

3.3.2. Cracks and crack propagation

Tensile stresses are emphasized here because in order to make the opening, the sediment must be pushed or pulled apart, creating tension at the crack tip. Elastic solids under stress fail by fracture, which begins with some flaw or heterogeneity in the material. This material failure is success for an animal making or extending a burrow opening. An easily generalised model in fracture mechanics that proves remarkably relevant to burrowing geometries describes the behaviour of an elliptical flaw. Stress increases around the flaw, with a stress amplification factor over the far-field stress of ($1 + \sqrt{(a/r)}$), where a is half the length of the flaw (the longer radius of the ellipse) and r is the radius of curvature at the tip (Anderson 1995) (Figure 3.3). The longer and more

18
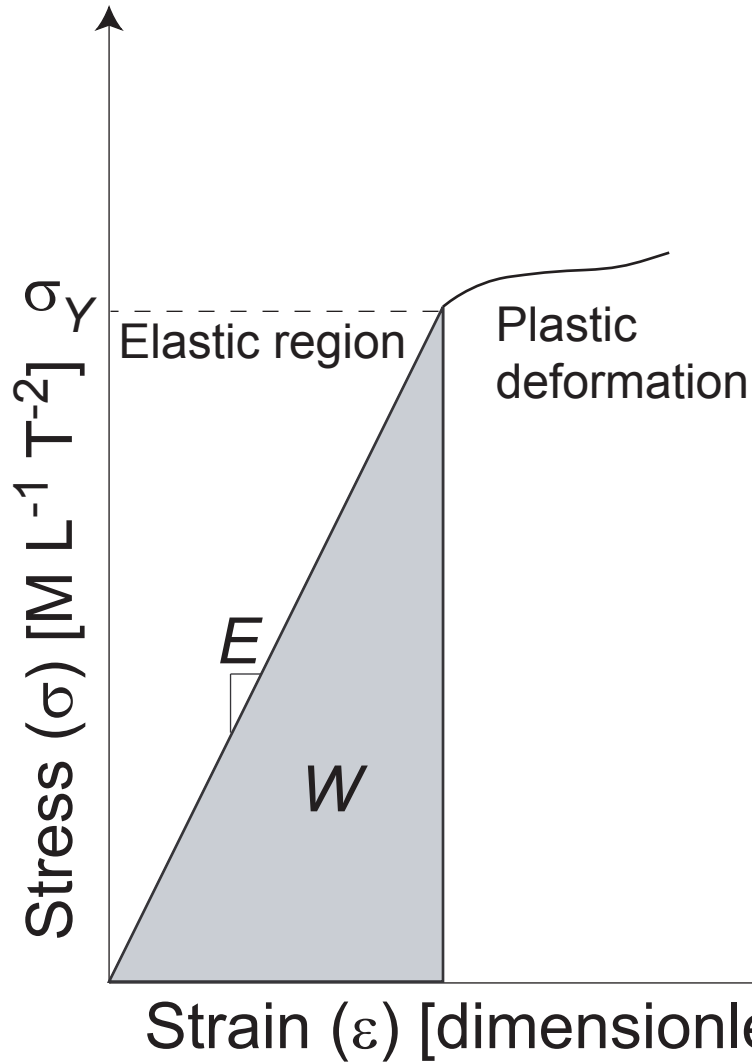
Figure 3.2. Stress-strain curve indicating elastic modulus, yield stress, and work of deformation. The elastic (or Young's) modulus is the slope of the linear portion of the stress-strain curve. When the stress exceeds the yield stress (σ_Y), the material deforms plastically, and the deformation is no longer reversible. The work done to deform an elastic material is the area under the curve. Some of the energy is stored as elastic potential energy, which is regained when the stress is removed
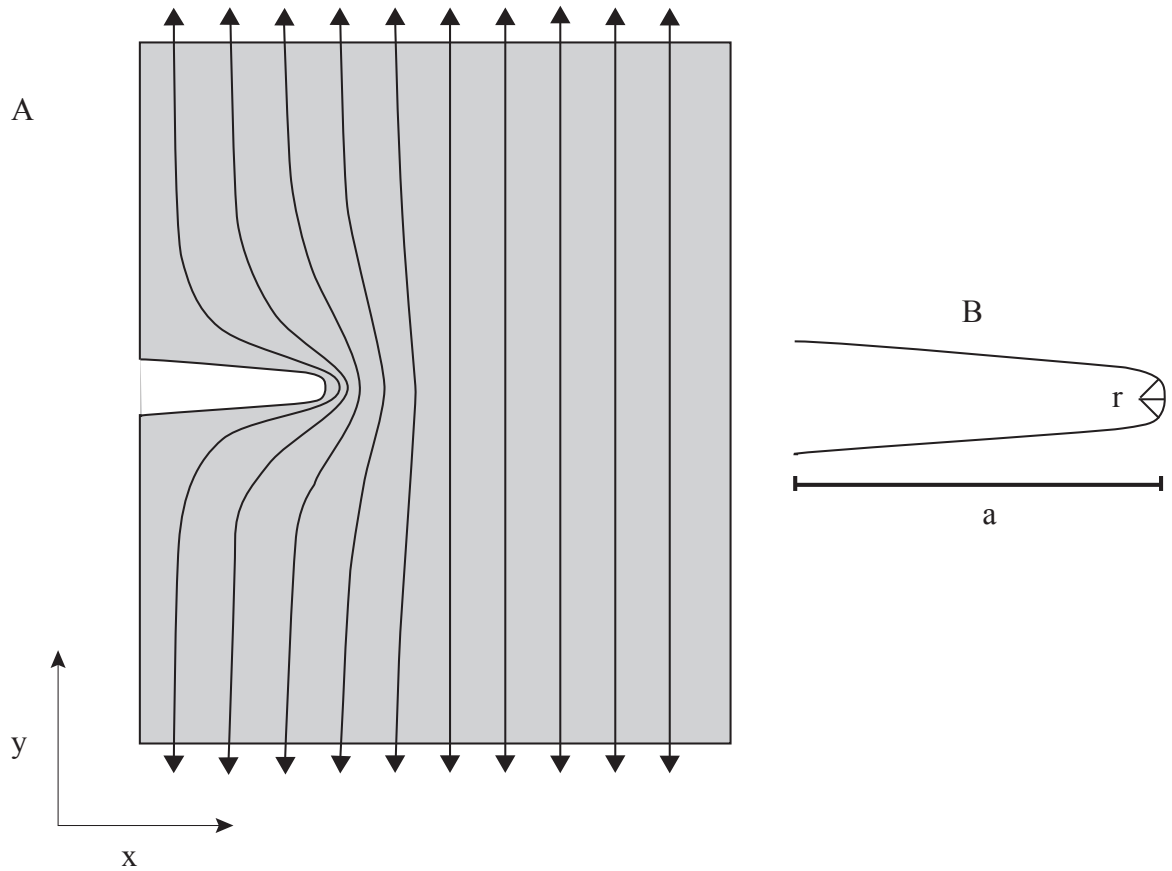
Figure 3.3. Stress amplification by elliptical flaw or crack. A) If a uniaxial tensile stress in the y direction is uniformly distributed in the x direction in an elastic solid (at large distance from a crack), the stress will be concentrated in front of the crack tip because stress cannot be transmitted through the flaw. Stress is amplified at the tip of an elliptical flaw or crack. B) The stress amplification factor over the far-field stress is $(1 + \sqrt{(a/r)})$, where a is the half-length of the crack and r is the radius of curvature at the crack tip.

pointed the flaw (i.e., the more crack-shaped), the greater is the stress at the tip. At the

most pointed extreme, r approaches zero and the amplification approaches infinity. Real

molecular dimensions preclude this mathematical singularity in real materials, although

amplification can result in stress at the crack tip greater than the yield stress of the

material. This result produces a region of plastic deformation around the crack tip

(Anderson 1995).

Because the amplification factor includes the radius of the elliptical flaw, causing

mathematical problems in describing cracks, a stress intensity factor for cracks (K_I) is

defined to describe the stress field around the crack tip in linear elastic materials. The

subscript *I* refers to mode I fracture, in which the material is pulled apart under tension

rather than sheared. Mode I is the relevant geometry for bubbles and burrowers (cf.

Anderson 1995, Johnson et al. 2002). K_I is similar to the amplification around an

elliptical flaw, but takes into account the small region of plastic deformation at a pointed

crack tip. K_I is proportional to ($\sigma\sqrt{(\pi a)}$), where σ is the stress far away from the crack tip,

and depends on the geometry of the material. When K_I reaches a critical value,

appropriately termed the critical stress intensity factor (K_{Ic}), the crack propagates.

Plastic deformation at the crack tip requires energy, which means that when a

force is exerted, some of the work that would otherwise result in strain is used instead for

plastic deformation, and the stress-strain relationship is no longer linear. But if the area

in which plastic deformation occurs is very small, the material behaves linearly, and

linear elastic fracture mechanics (LEFM) apply.

The critical stress intensity factor is a material property describing ease of fracture

and is experimentally determined for diverse materials. A material with a higher K_{Ic}

requires either more stress or a longer crack for fracture to occur than one with a lower K_{Ic}. The stress intensity factor enables comparison between cracks of different sizes under different stresses. (A smaller crack under larger stress should behave similarly to a larger crack under smaller stress.) Materials with similar K_{Ic} have similar fracture behaviour.

Another way of defining how easily a linearly elastic material fractures is the crack resistance (R), which is the rate of energy release required to propagate a crack [J m^{-2}]. Crack propagation is a way of releasing energy: when a ball hits a window, kinetic energy of the moving ball is transferred to elastic potential energy stored in the glass. Crack propagation occurs when the energy available exceeds the amount of energy required for the crack to grow (R). Energy release rate (G) is a measure of the amount of energy available for crack growth, with "rate" referring to a change in energy with increasing crack area rather than with time. Analogous to the stress intensity factor, a parameter is measured (G or K_I), and when that parameter exceeds a critical value that has been experimentally determined for a given material (i.e., when $G > R$ or $K_I > K_{Ic}$), fracture occurs (Anderson 1995).

Cracks propagate in the direction of least resistance. In a homogeneous, isotropic material (e.g., gelatin), a crack will propagate perpendicular to the direction in which the force is exerted. An animal burrowing by crack propagation in an elastic solid such as gelatin theoretically can make the crack turn by applying force at an angle. Heterogeneous materials (e.g., mud) exhibit small-scale variation in material properties, such as K_{Ic} and R, which can result in stochastic changes in the direction of crack

propagation (Figure 3.4). Excess energy can be released by crack branching, which in a heterogeneous material could be a mechanism of particle release.

When a crack approaches an interface, if the adhesion at the interface is much less than the cohesion of the material, as is generally the case, the crack will follow the interface (Cook & Gordon 1964). The stress field in front of a crack pointed toward a perpendicular interface has tension pulling the material away from the interface toward the crack. This tension can result in separation at the interface before the crack reaches it, so that when the crack tip hits the interface, a crack oriented along the interface has already been formed and crack resistance is low (Figure 3.5). The crack preferentially follows the interface, and additional energy is required for the crack to branch away.

Materials that resist crack propagation have high toughness compared with easily fractured brittle materials (Gordon 1976). Toughening mechanisms include plastic deformation, interfaces, crack bridging, and crack-tip blunting. Crack bridging is common in polymeric materials (like the mucopolymer matrix in muds) and involves fibers extending across the crack that take energy to break before the crack can propagate. Styrofoam provides a classic example of crack tip blunting: a crack in a porous foam reaches a pore and the crack tip radius is significantly increased, reducing the stress amplification factor. When the plastic zone at the crack tip is large, energy is used for plastic deformation in addition to the energy to propagate the crack.

Marine muds, similar to polymer gels (because they appear to comprise grains embedded in polymer gels cf. Watling 1988), are viscoelastic, and viscous flow or creep may be an important toughening mechanism on particular spatial and temporal scales. The behaviour of viscoelastic materials is time-dependent: under high strain rates, the
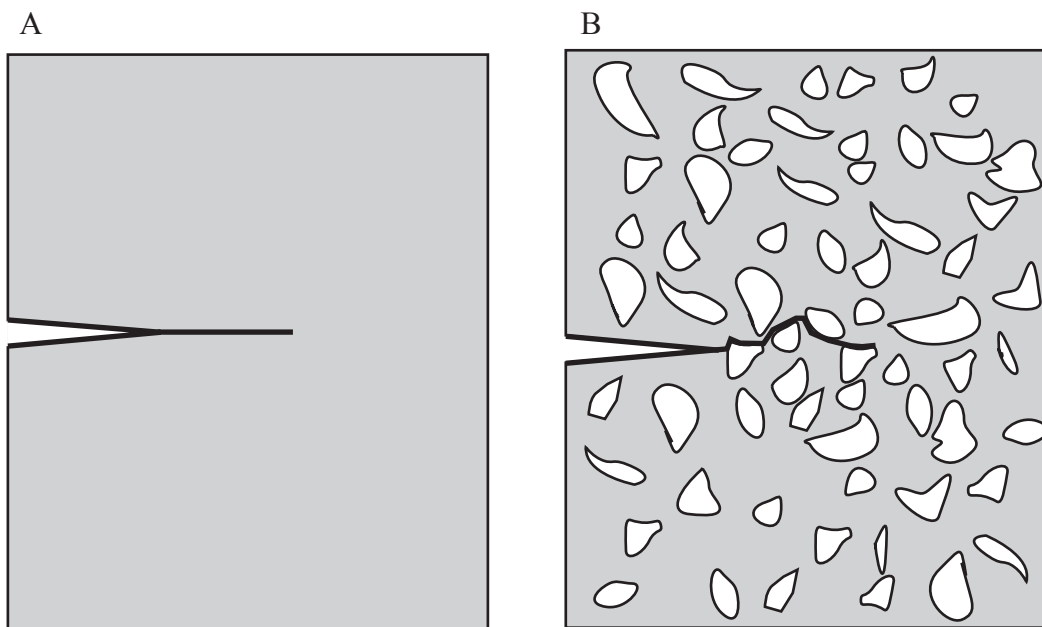
Figure 3.4. Crack propagation in (A) a homogeneous material and (B) a heterogeneous material. The crack propagates in the direction of least resistance, which means in a heterogeneous material, the path moves stochastically around much stronger grains. The crack depicted follows grain contours, implying adhesive failure of the polymer matrix attaching to the grain. Cohesive failure may instead occur within the polymer matrix, in which case the crack would move farther from grain surfaces.
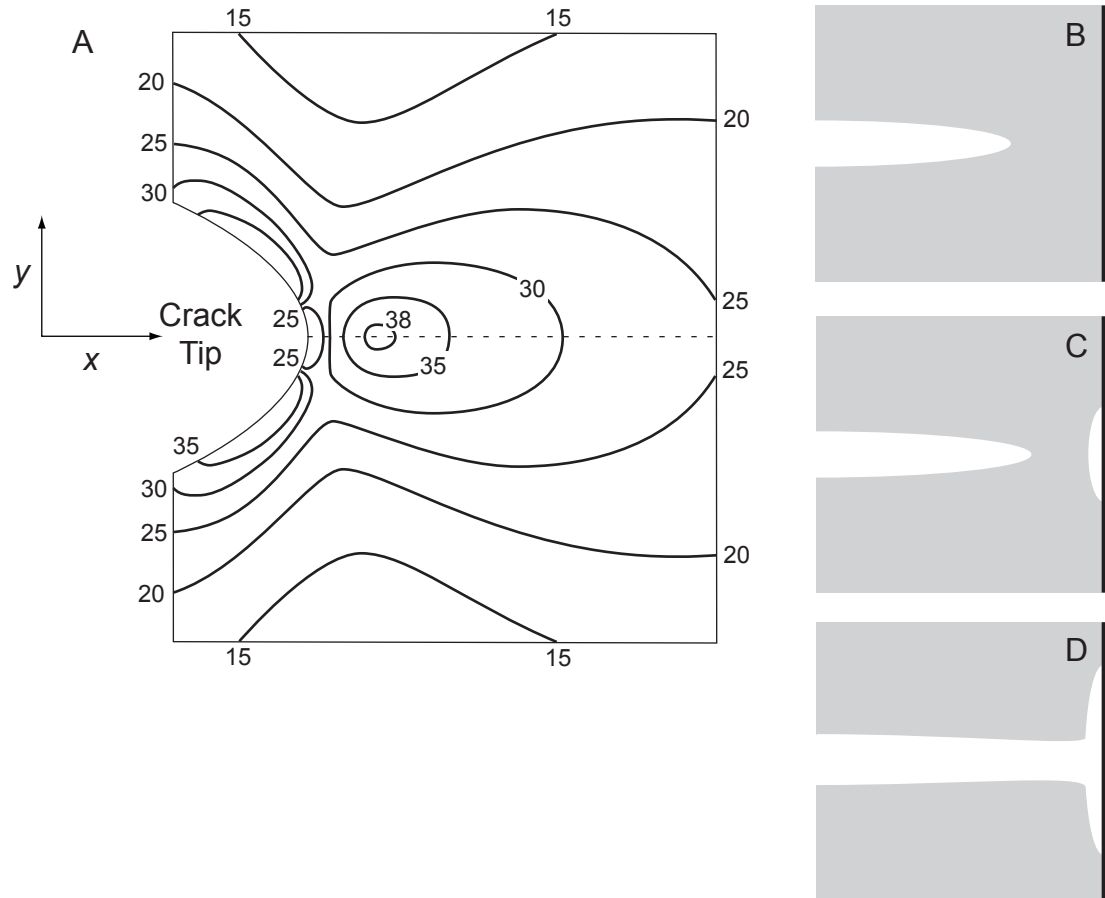
Figure 3.5. The effect of material interfaces on crack propagation. A) The stress field (σ_X) around a crack tip. The stress in the x direction (parallel to the direction of crack propagation) relative to the far-field stress [dimensionless] is shown. Maximal stress a short distance in front of the crack is tensile, so that when the crack approaches a weak interface (B), separation occurs at the interface before the crack reaches it (C). When the crack tip reaches the interface, the crack follows the interface (D). A weak interface is one for which cohesion of the material is much greater than adhesion between the two materials at the interface (Cook & Gordon 1964). In the illustration the dark black lines represent a rigid surface, such as an aquarium wall. Reproduced with permission from the Royal Society.

material behaves elastically, whereas under low strain rates, viscous flow occurs. The

dimensionless "Deborah number (*De*)" is defined as the ratio of the time a process takes

to the time required for significant plastic deformation to occur (Reiner 1964). Solids

have very small values of *De*, fluids very large. Viscoelastic materials have Deborah

numbers much closer to unity, falling between solids and fluids. Silly putty[®] (Binney &

Smith, Easton, PA, USA) provides a classic example of a viscoelastic material. It

bounces elastically in response to the short but high strain rate of hitting the floor. When

left on a table, however, the long but low strain rate of gravity results in flow. Fracture of

viscoelastic materials can often be approximated using linear elastic fracture mechanics,

but the approximation applies only over the limited range of strain rates and time scales

under which elastic behaviour dominates viscous (Anderson 1995).

3.3.3. Granular materials

Clean, coarse sands such as those found on wave-swept beaches behave

differently from more continuous solids. Mechanical behaviour of granular materials

depends on particle size, surface characteristics, heterogeneity, and packing structure, as

well as the viscosity of the interstitial fluid and the length scale being studied (Duran

2000, Goldenberg & Goldhirsch 2005). Extensive research on granular materials has

focused on materials composed of large (e.g., 1-mm), non-cohesive grains in air, for

which environmental influence (e.g., viscosity of the surrounding fluid) is minimal

(Duran 2000). Granular materials, when agitated at high frequency, behave like

molecules in a fluid. When particles are not agitated, they can still flow under shear, but

only in distinct layers lacking the smooth velocity gradient of a fluid (e.g., a snow

avalanche). The stochastic behaviours of granular materials result in part from randomness in contacts between particles. In a triangular packing scheme, an individual particle contacts six other particles, but it only needs two contacts below the center of gravity to be stable.

Stress in a granular material follows random chains of particles, such that some particles bear a disproportionate fraction of the load applied to the material, while others bear little or none (Figure 3.6) (e.g., Geng et al. 2001). Stress chains form arches that can block flow of granular materials through narrow discharge orifices, causing problems for distribution of grain and gravel, for example. A vertical stress is redirected laterally to varying extents depending on packing structure, which in turn depends on size and shape distributions of grains. Granular materials exhibit a nonlinear stress-strain relationship because as stress increases, particle packing changes, resulting in more contacts and increased rigidity (Duran 2000).

Under shear, tightly packed particles exhibit dilatancy. When walking on a beach, footprints appear dry, a phenomenon first identified by Reynolds. When particles are tightly packed, they fill a minimal volume. In order to deform and begin to flow under shear, particles must move to a less tightly packed configuration, increasing the volume of the material. The footprint on a beach appears dry because shear exerted by the foot causes the sand grains to separate, the volume to expand, and the water to drain downward into the expanded interstices. A minimal packing density exists for dilatancy to occur; less tightly packed particles move under shear without volume expansion (Jaeger & Nagel 1992).
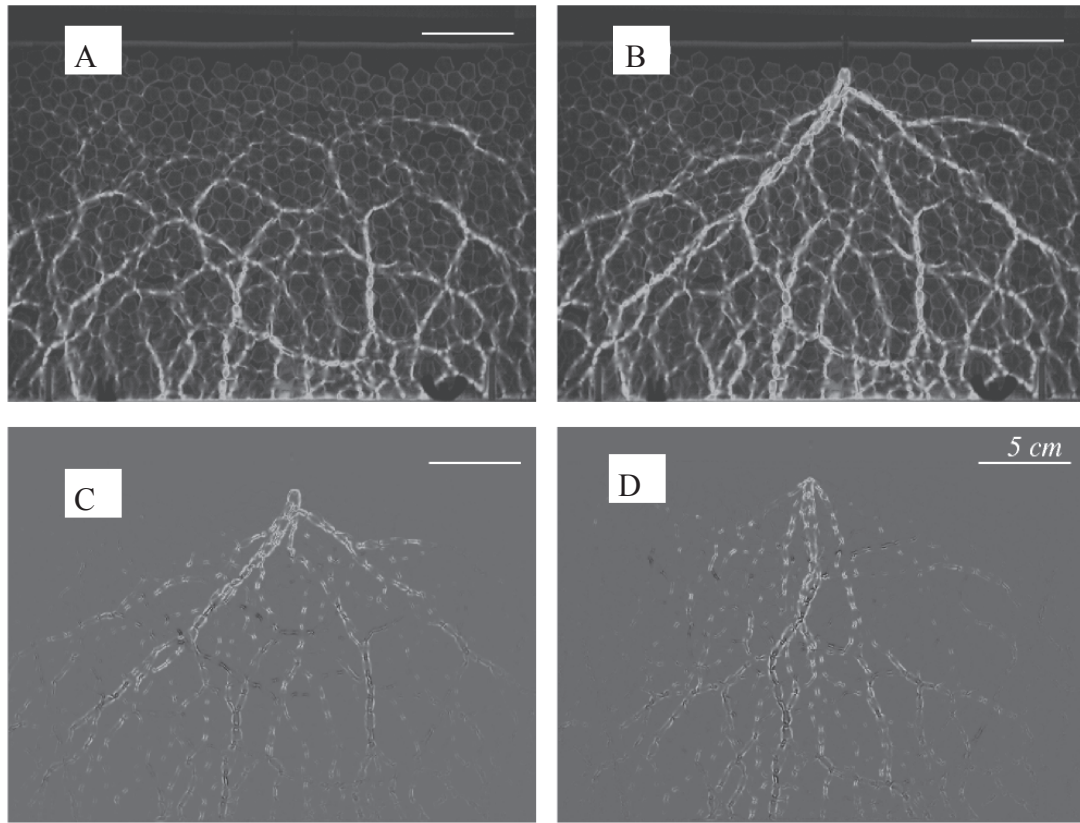
Figure 3.6. Light-colored stress chains in a 2-D granular medium (of birefringent disks) visualized using photoelastic stress analysis. A) stress resulting from gravity; B) stress resulting from a point force on the surface; C, D) stress resulting from a point force with stress from gravity subtracted using two different methods (Geng et al. 2001). Reproduced with permission from the American Physical Society.

Fracture patterns have been observed in granular materials, generally following force arches. In a falling stack of grains, fracture patterns are visible below force arches, holding the overlying grains. Fractures generally begin at a wall, suggesting that friction against the wall holds the force arch in place while the underlying grains fall away. Additionally, fracture occurs around a larger grain moving upward in a bed of smaller grains by vibration (Duran 2000).

Behaviours of granular materials become more complex as grain sizes decrease, viscous forces begin to become important, and adhesive and cohesive forces become relatively stronger relative to grain weight. Behaviours depend on the scale of the material as well. Bulk granular material containing a large enough number of particles can be considered a continuum, a simplification that fails on a more local level. Increased friction of grains causes granular materials to behave more elastically, but only on a large enough spatial scale; on a smaller scale, characteristic stress chains dominate the mechanics (Goldenberg & Goldhirsch 2005).

3.4. Bulk mechanical properties of sediments at burrowing-relevant scales

Grain-scale structures of sediments have been discussed to foster some intuition about why bulk sediments behave mechanically as they do and because it is likely that bulk properties of sediments will soon be predictable from them (Torquato 2001). For the remainder of the review, however, the focus is on bulk properties. The justification again is a simple scaling argument, i.e., that the burrowers are many times the length scale of the grains.

The polymeric organic material in mud, when separated from the grains, shows elastic behaviour. Frankel & Mead (1973) separated the organic material from the grains and observed meiofauna moving through the material on a depression slide. After animals moved through the material, the clumps returned elastically to their original shapes and positions. The clump of material through which the animal was moving would commonly be moved in the direction of the animal's motion, but more slowly than the animal. They suggest that the response of the mucilaginous material indicates both "viscous, and elastic" elements, but the "viscous" response is likely an artifact of detaching the material from the sediment grains and putting it in a depression slide.

This elastic behaviour was recently confirmed through work on methane bubble growth and movement (Johnson et al. 2002). Bubbles injected in sediment are crack-shaped rather than spherical, with aspect ratios predicted by linear elastic fracture mechanics (LEFM) (Johnson et al. 2002, Boudreau et al. 2005). The small forces exerted by the surface tension and buoyancy of bubbles can propagate cracks in mud (Figure 3.7) (Johnson et al. 2002, Boudreau et al. 2005). The internal pressure required for crack propagation (P_c) by a bubble of volume V depends on the critical stress intensity factor (K_{Ic}) and elastic (Young's) modulus (E) as

$$P_c = \frac{K_{Ic}^{\frac{6}{5}} p^{\frac{4}{5}} (\frac{1}{12})^{\frac{1}{6}}}{E^{\frac{1}{5}} V^{\frac{1}{5}}}$$ (equation 3.1)

(Johnson et al. 2002). While K_{Ic}, the material property governing fracture, is much more important than E in determining critical pressure, the aspect ratio of the bubble (b_c/a_c) depends much more strongly on E, as
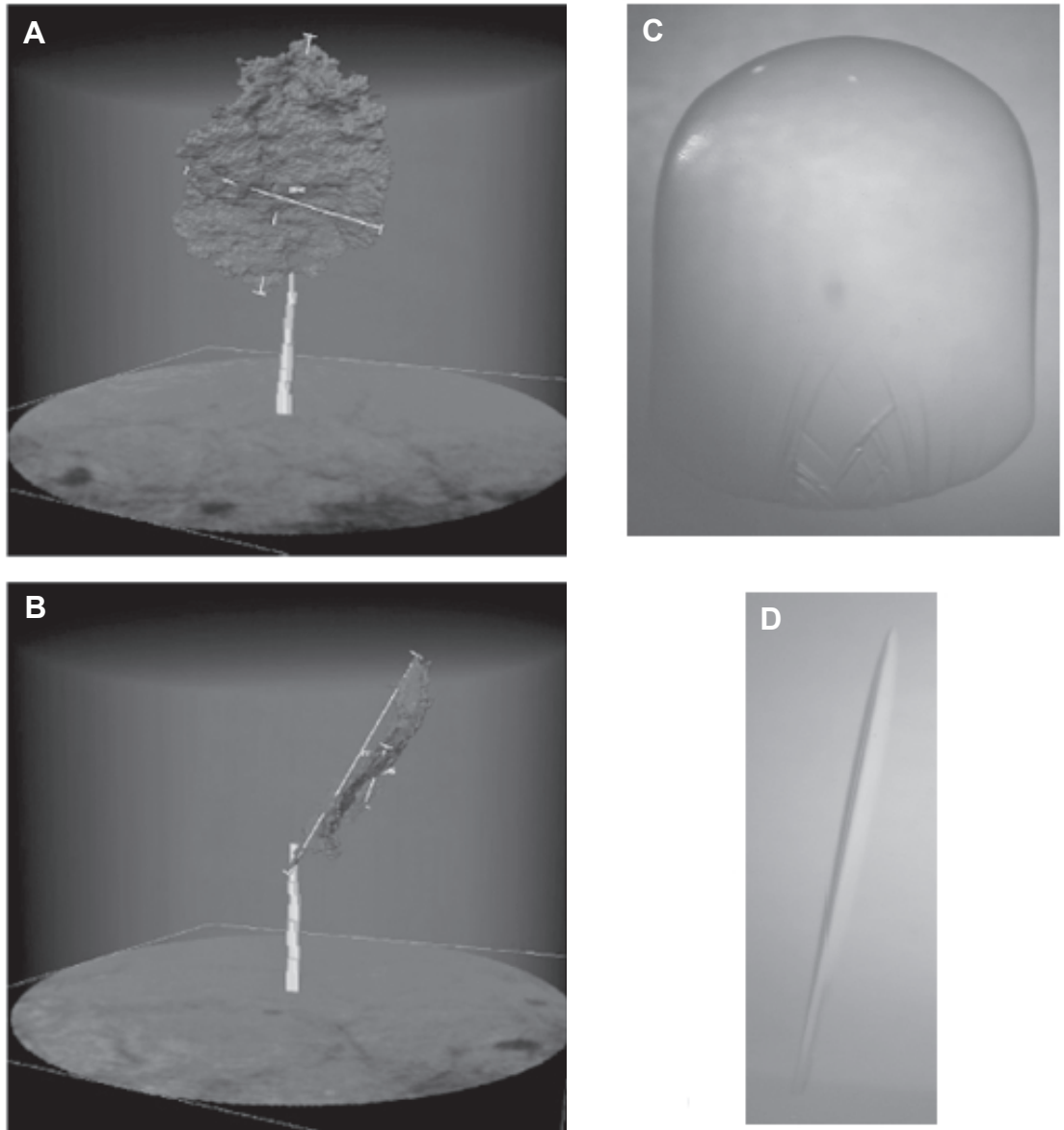
Figure 3.7. Bubble shape in mud and gelatin. A, B) A high-resolution CAT-scan of a bubble injected into sediment from Cole Harbor, Nova Scotia. The bright object is the injection capillary, and the sediment has been made transparent. The bubble is about 20 mm across and 0.7 mm thick, with a resulting volume of 300 mm^3. The sample is from the 25-35 cm depth interval of this core. C, D) Plan and cross-sectional views of a bubble rising in double-strength gelatin. The bubble is 38 mm wide and 1 mm thick. All panels are from Boudreau et al. (2005). Reproduced with permission from The Geological Society of America.

$$\frac{b_c}{a_c} = \frac{K_{Ic}\sqrt{p}}{E\sqrt{a_c}} \, .$$ (equation 3.2)

Although mud is elastic on the temporal and spatial scales of bubbles, it will flow when small forces are exerted over long periods (e.g., by gravity), demonstrating viscoelastic behaviour. For forces exerted over short intervals the material behaves elastically but over longer periods, viscous properties and creep may need to be considered, particularly for high-porosity muds. If a material creeps when under constant displacement, the elastic restoring force decreases over time, resulting in loss of elastic potential energy and permanent deformation. Beyond the limit of elastic behaviour, plastic deformation occurs. Although plastic deformation is not important for bubbles, it is likely to be more important on the larger scales of animals. LEFM accurately predicts the aspect ratio of bubbles in sediment and gelatin (a clear analogue with similar E and K_{Ic}) (Johnson et al. 2002, Boudreau et al. 2005), but some animals exert a much larger displacement than observed with bubbles. If the aspect ratio is larger than predicted by LEFM, the material is behaving nonlinearly, and significant plastic deformation or creep may occur.

Marine sediments exhibit both thixotropic and dilatant properties (Chapman 1949). The term thixotropy, originally used to describe the isothermal, reversible gel-sol transition of colloids, has been generalised to include changes in load-deformation behaviour with time, specifically a decrease in viscosity with increased rate of shear or with time under a constant shear (Chapman 1949, Santamarina et al. 2001). Thixotropic behaviour results from the breakdown of the polymeric matrix among particles, but the exact mechanism is unknown.

Dilatancy has been described as an increase in resistance with increased shear (Chapman 1949), but more accurately refers to an increase in volume due to expansion of pore space when particles begin to move (Duran 2000). Whereas shear decreases particle contacts, a direct pressure increases the number of grain contacts and consequently resistance to penetration. Thus dilatancy is a mechanism that could be used to *reduce* the force required for burrowing, and exertion of shear rather than normal stress should be a more efficient burrowing mechanism in sands. Granular materials such as sands exhibit dilatant behaviour, whereas thixotropy is characteristic of viscoelastic materials, or muds. In muds, the polymeric matrix surrounding grains dominates mechanical behaviour. Sands on wave-swept beaches fall on the other end of the continuum, behaving like dry, granular materials. The field of granular mechanics reveals why a transition from granular mechanics to solid mechanics might be expected as grain size decreases (Figure 3.8). The weight of an individual large sand grain is sufficient to bring it into contact with its neighbours below, and the transmitted forces are large compared with the adhesive forces of the organic polymers connecting grains. It is not yet clear where in terms of grain size or other characteristics the transition from granular mechanics to viscoelastic mechanics occurs. What is apparent, from the limited measurements made to date (Boudreau, unpublished data), is that even fairly coarse silts with considerable sand content behave more or less elastically. That is, elastic or viscoelastic behaviour dominates below the sand-silt grain size transition (< 62 μm diam), and may extend into heterogeneous fine sands as well, or even beyond.

This transition zone is mechanically complex but relevant to biology, as it likely includes a range of sand-silt habitats in productive coastal areas. Granular materials
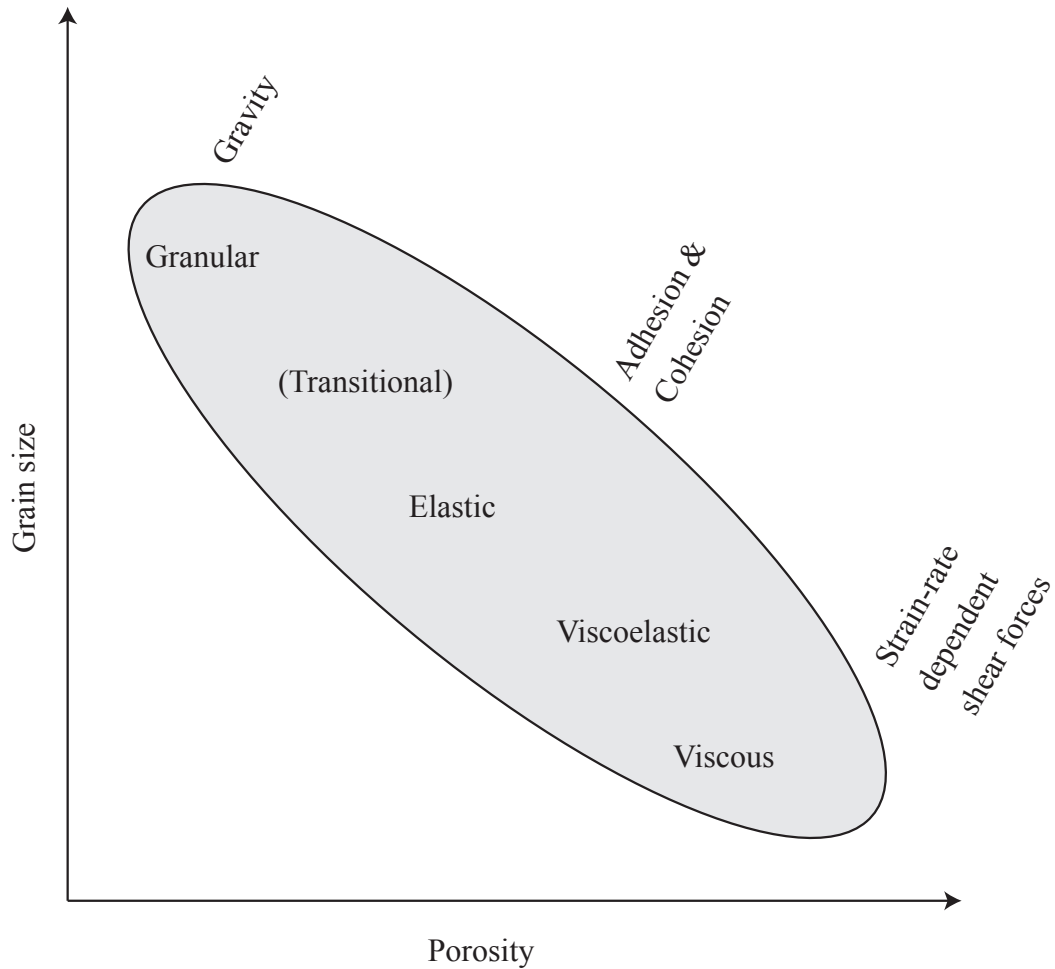
Figure 3.8. Conceptual diagram outlining dependence of mechanical behaviour on grain size and porosity of marine sediments. The ellipse encompasses the range of grain sizes and porosities found in natural sediments. Sands behave like granular materials, muds like elastic solids, and resuspended fluid mud layers viscously. A transition zone exists between sands and muds in which gravitational forces at grain contacts are comparable with adhesive forces between the polymeric matrix and grains. Sand grains within a matrix of fine grains and polymers likely fall within this transition zone. At the other end, muds that are highly porous but not resuspended behave viscoelastically.

show more elastic behaviour when friction becomes more important for non-adhesive

particles (Goldenberg & Goldhirsch 2005), and adhesive forces would increase friction

and consequently result in more elastic behaviour. In addition, elastic behaviour is

important on large spatial scales, while stress chains are important on smaller scales

(Goldenberg & Goldhirsch 2005). As grains are randomly distributed, mechanical

behaviour in this transition zone is likely highly heterogeneous, with small volumes of

elastic behaviour around arches of sand grains.

Effects of the static load of overburden are common to both muds and clean sands

but differ in the manner by which the pressure is transmitted. In both cases mean total

pressure at depth z equals the hydrostatic pressure at the sediment-water interface ($z = 0$)

plus z times bulk density of the sediment above z multiplied by the acceleration of

gravity. In the case of impermeable muds, this load should be effectively isotropic and

add to the elastic restoring force. In the case of clean, permeable sands, force arches

(Figure 3.6) lend some anisotropy and a great deal of grain-scale variation in local forces.

In both materials, however, this load must be overcome to open a burrow and to keep it

open. Temporary alleviation is possible through time-dependent processes such as

liquefaction and grain rearrangement in general. Through feedbacks with burrowing,

bulk density increases with depth in sediments as porosity decreases (Mulsow et al.

1998). Consequently, as sediment depth increases, this overburden force must add

nonlinearly to the forces required for burrowing.

3.5. Burrowing in mud

3.5.1. Description of the mechanism

Early studies of burrowing in marine sediments took a largely biological perspective, focusing on detailing muscle and appendage movements, giving little consideration to sedimentary variables. Clark (1964) described a general burrowing strategy of alternating anchors; a penetration anchor holds the body in place while the anterior end of the animal moves forward into the sediment. The anterior end then dilates to form a terminal anchor while the posterior end is pulled forward. The dual-anchor burrowing mechanism has been described across phyla and has been reviewed by several authors (Clark 1964, Trueman 1975, Trueman & Jones 1977, Elder 1980, Trueman 1983, Trueman & Brown 1992). Implicitly assumed in this mechanism is that sediment either flows or deforms plastically, is compacted around the animal, excavated, or ingested, and that the movement of particles is discrete and irreversible.

The polychaete *Nereis* has been shown to burrow by crack propagation (Dorgan et al. 2005), and preliminary observations suggest that other polychaetes, as well as *Yoldia,* a bivalve, use a similar mechanism (Figure 3.9). Anchoring is only a secondary or tertiary function of anterior dilations; the primary function is to exert a force perpendicular to the direction of motion. The resulting stress in the sediment is amplified at the tip of the burrow, which elongates as a propagating crack when the critical stress intensity factor (K_{Ic}) is reached (Anderson 1995, Johnson et al. 2002, Dorgan et al. 2005). The 'terminal anchor' is not necessarily stationary and thus is a misnomer or at least an incomplete description. *Nereis*, for example, drives the everted pharynx forward as a wedge to extend the crack-shaped burrow.
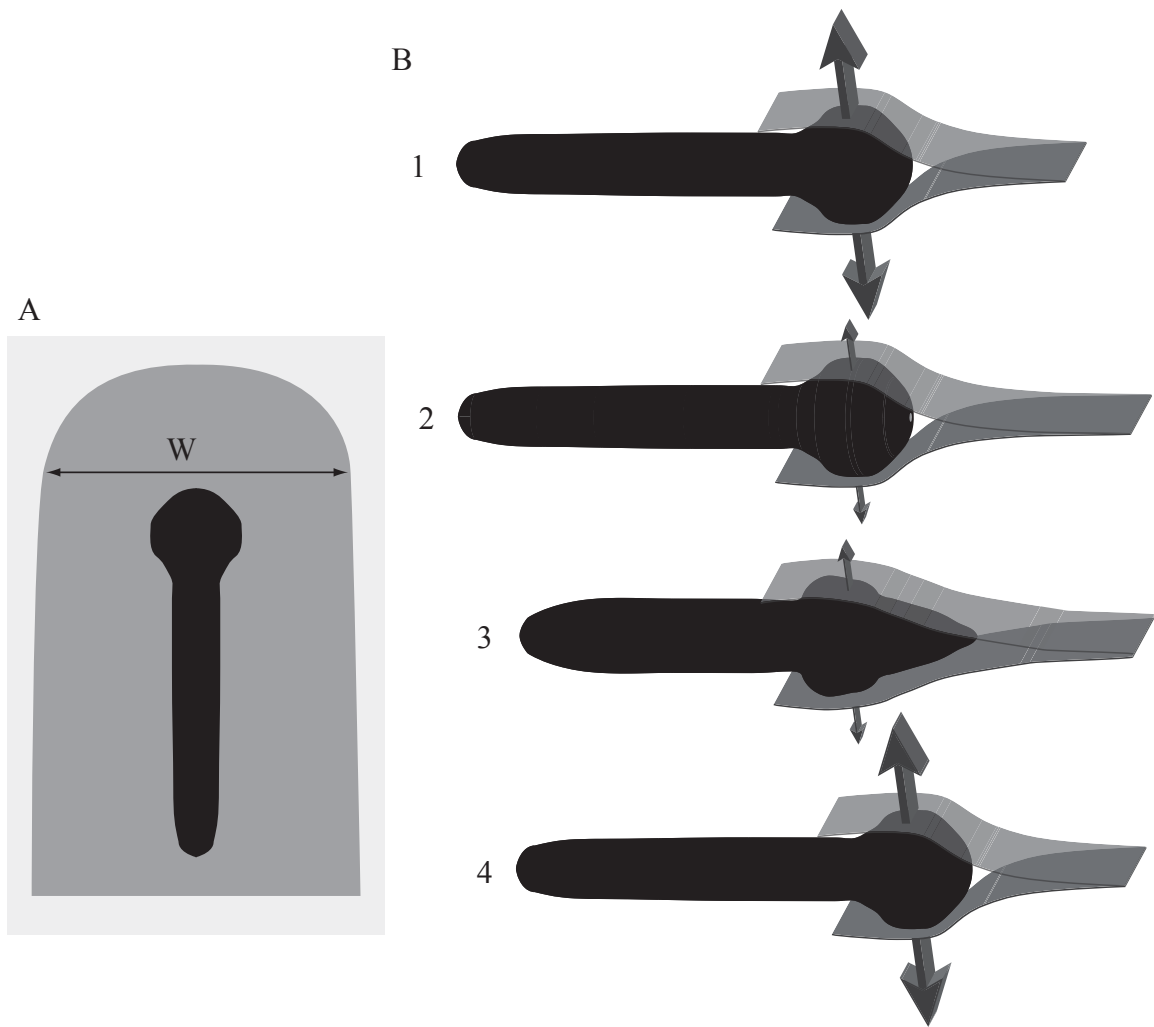
Figure 3.9. Scheme showing dorsal view of crack shape and lateral oblique views of crack propagation during burrowing. A) Dorsal view of crack shape and B) Lateral oblique views of crack propagation during burrowing (Dorgan et al. 2005). Arrows extending vertically from the crack indicate forces. The worm everts its pharynx and exerts a force normal to the direction of movement (1), which causes the crack to propagate, releasing energy (2). The worm then retracts the pharynx and moves forward into the crack (3) before repeating the cycle (4). W is the longer diameter or width of the discoidal crack. Its shorter diameter matches that of the pharynx. Reproduced with permission from the Nature Publishing Group.

For 'burrowing' by bubbles, how to calculate net tensile force is evident, and the oblate spheroidal shape is a simple one from which to calculate that force from internal pressure (cf. Johnson et al. 2002). A natural question to ask is what shape should be assumed for an animal's wedge and how to calculate the net force on the sediments. It is difficult to lever a crack in mud, and soft-bodied animals in general may use liquid pressure generated in front of their advance to produce an oblate spheroidal geometry and tensile stresses analogous to those in a gas bubble. Subterminal expansions thus may serve O-ring functions as well. Observers are encouraged to consider the possibility that dual expansions may comprise mechanisms that act first to wedge open a crack, second to seal and maintain fluid pressure in front of the wedge and third as an anchor to pull the remainder of the body along.

Setae are used by annelids to prevent backward slip during peristalsis and for parapodial locomotion within the crack. As longitudinal muscles contract to dilate a segment, protrusion of the setae occurs; then the setae are retracted as the segment elongates and moves forward (Seymour 1969). Setae exert small, very localised forces that may displace individual grains or aggregates, potentially releasing particles from the sedimentary matrix. The friction resulting from setae explains observations that polychaetes can burrow in gelatin whereas many bivalves are unable to gain purchase and move in the low-friction medium (P. A. Jumars and K. M. Dorgan, personal observation).

3.5.2. Ubiquity of crack propagation

The dual-anchor system of burrowing has been described for burrowers across many phyla (Clark 1964), and those descriptions are briefly reproduced here. Naticid

gastropods have a wedge-shaped foot, with the propodium acting as the terminal anchor

and the shell and metapodium the penetration anchor (Trueman & Brown 1992). A

bivalves opens its shell to form a penetration anchor, then partially closes the valves,

moving fluid into the extended foot, which dilates to form the terminal anchor (Trueman

1983). Scaphopods use a similar mechanism, with the epipodial lobes around the foot

increasing the radial expansion to compensate for reduced pedal dilation compared with

bivalves, which close their shells to drive more fluid into the foot (Trueman 1983).

Burrowing anemones dilate the physa to form a terminal anchor, then use the dilated

column as the penetration anchor (Ansell & Trueman 1968, Ansell & Peck 2000).

Priapulus, the nemertean *Cerebratulus*, and sipunculids all have long, eversible

probosces that serve as terminal anchors, while the head or anterior part of the body

serves as the penetration anchor (Clark 1964, Hunter et al. 1983). The long proboscis

allows these animals to move forward in large steps, progressing rapidly (Hunter et al.

1983). In *Priapulus*, both the longitudinal and circular muscles contract synergistically,

generating high internal pressures to evert the long proboscis (Clark 1964). It is

suggested that in all these cases the primary function of the subterminal expansion is a

wedge to drive a crack.

The polychaete *Nephtys* and other worms with smaller pharynges were described

as using the pharynx to "excavate a hole into which the animal then crawls" (Clark 1964).

Nephtys is distinguished from worms with a larger proboscis in that it likely does not use

the proboscis retractor muscles to pull the animal forward as the proboscis is retracted

(Clark 1964). Similarly, *Polyphysia* is described to use only a penetration anchor, and to

progress slowly in small steps (Hunter et al. 1983). The echiuran *Urechis* and

holothuroid *Caudina* use their proboscis and oral tentacles, respectively, to 'scrape' and excavate a cavity into which to move (Clark 1964). Burrowing by *Nereis diversicolor* has been similarly described (Trevor 1977), and we now know that the pharynx is not excavating, but exerting an outward force to propagate a crack (Dorgan et al. 2005), suggesting that these animals use crack propagation to extend their burrows, and that the 'scraping' releases particles, enabling surface deposit feeding from the crack wall.

Clams not only use the extended foot to exert a force and propagate a crack in muddy sediment, but also are shaped like a wedge and may use the shell shape to passively exert force on the sediment for fracture and also resist the elastic restoring force. The stages of burrowing by bivalves are: (1) valves open to form a 'penetration anchor' while the foot probes forward, (2) valves close, moving fluid away from the body and resulting in dilation of the foot ('terminal anchor'), and (3) retractor muscles contract, pulling the shell down toward the expanded foot (Trueman 1983). The stress exerted by the open valves in the first stage is amplified at the tip of the crack, which likely elongates under, or even before, light probing by the foot. Dilation of the foot results in a smaller deformation than the open valves, but acts like a wedge driven much closer to the crack tip. The valves are then closed as they are pulled into the crack, allowing them to fit into the narrowing crack and reducing friction as they move. Many clams exhibit a forward-backward rocking motion when burrowing, which is more common for less elongate species (disk- rather than blade-shaped; Stanley 1970). This rocking behaviour is a likely alternative for elongating a crack and moving forward, and may be more effective in muds that are more resistant to penetration.

Echinoids living in muddy sediments are wedge-shaped, "push directly into the frontal sediment rather than excavating it and move through the sediment by means of a repeated rocking motion", unlike the shapes and behaviours of more globular, excavating echinoids living in sands (Kanazawa 1992). This rocking motion, combined with transport of sediment by spines, resulted in a volume of sediment reworked by burrowing 60-150 times greater than that ingested by the heart urchin, *Brissopsis lyrifera* (Hollertz & Duchene 2001). Hollertz & Duchene (2001) observed cracks on the surface above burrowing urchins, which initially burrow into the sediment by excavating with their spines until the body angles slightly downward, and then move forward in a rocking motion. This rocking could, in addition to moving the urchin forward, exert a normal force against a burrow wall to propagate a crack. Unlike clams and worms that can expand against both walls at once, the hard test of urchins may require them to exert force against the two walls alternately. Urchins burrow relatively slowly (2-5 mm h^{-1} (Schinner 1993)) compared with other burrowers, possibly due to a less efficient technique of burrowing or a more efficient technique to access particles in the surrounding medium for ingestion, i.e., through manipulation with spines.

Many burrowers are shaped like wedges, but even *Nereis,* which does not appear to have a wedge shape, uses its everted pharynx as a wedge to drive into the crack. The ultimate goal of propagating a crack allows comparisons between seemingly different anatomical features (Figure 3.10). For example, the ornate wedge of some trichobranchid polychaetes, large ovoid proboscis of *Artacama valparaisiensis* (Polychaeta: Terebellidae), and muscular anterior region of cirratulids and cossurids are all feasible crack-propagating mechanisms for worms (cf. Hartman 1955, Hartman 1958, Rozbaczylo

41

Figure 3.10. Polychaetes with morphologies suitable for propagating cracks. A) Many cirratulids have muscular expansions at both anterior and posterior ends that could be used to exert a force to propagate a crack (drawing from Hartman 1958, p. 201). B) the terebellid, *Artacama valparaisiensis*, has a large, ovoid proboscis (drawing from Rozbaczylo and Mendez 1996, their Fig. 1a); Reproduced with permission from the Biological Society of Washington. C) The trichobranchid *Artacamella hancocki* has an ornate, wedge-shaped anterior (drawings from Hartman 1955, p. 59). D) *Magelona* sp. (Magelonidae) has a broad, flattened prostomium that could be pushed forward into a crack, with an eversible proboscis to exert a lateral, wedging force (drawings from Jones 1968). Reproduced with permission from the Biological Bulletin.

A

feeding
palp

oblique
view

branchiae

B

C

branchiae

feeding
tentacles

side view

top view

D

sagittal section
(side view)

ventral view
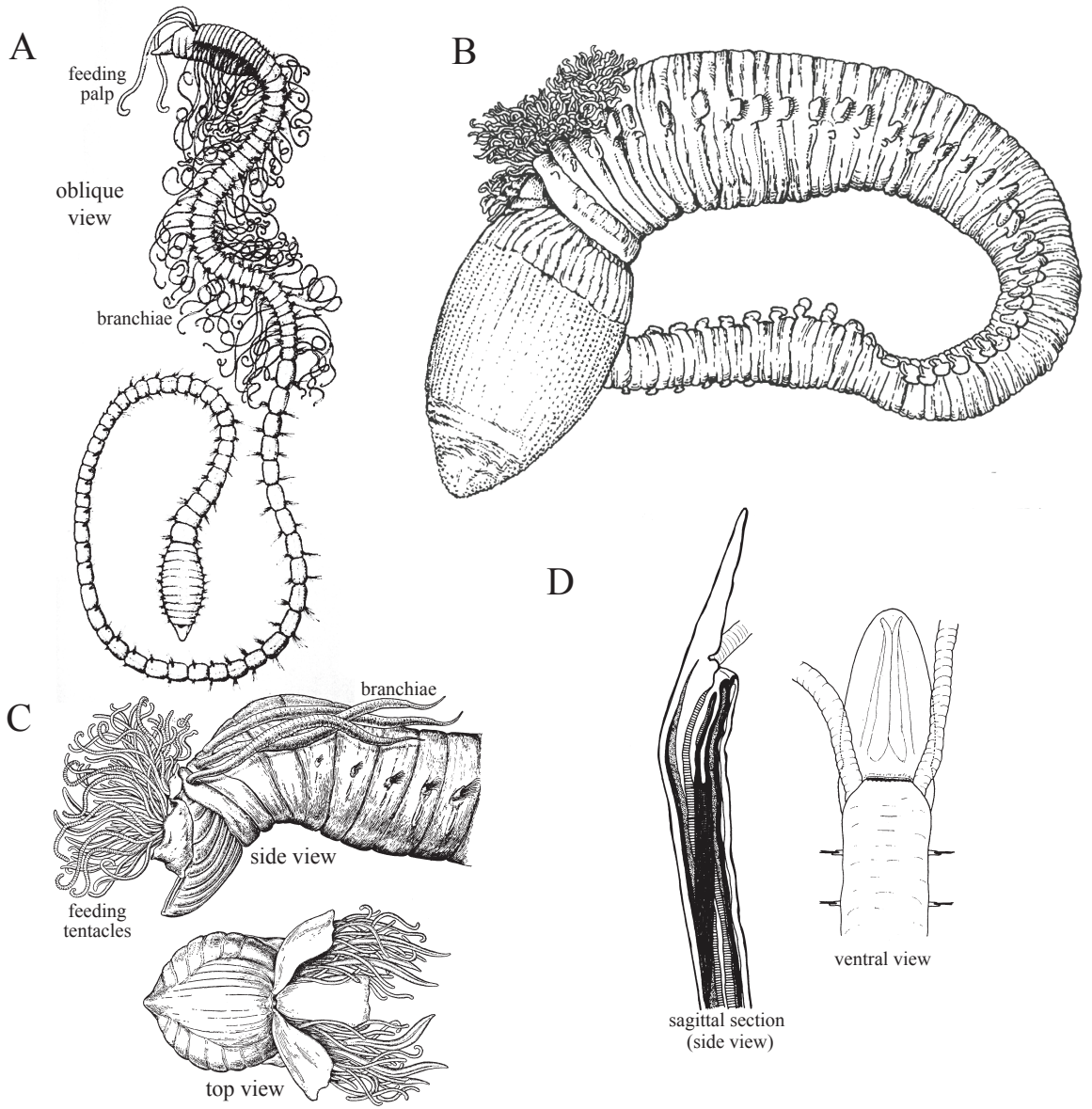
& Mendez 1996). Magelonidae have a broad, flattened, wedge-shaped prostomium and an eversible proboscis (Jones 1968), suggesting that they, too, utilise crack propagation.

Amphipod burrowing appears largely analogous with movement of bubbles. Indeed, the basic shape of a burrowing amphipod is an oblate hemispheroid, a half-bubble with legs for propulsion. The dorsal exoskeleton is the wedge, driven by the legs. If the deformation of the sediment caused by the amphipod's body is within the elastic limit of the sediment (i.e. the sediment is linear elastic), the aspect ratio of a burrowing amphipod (Figure 3.11) (body width relative to its diameter) may be predictable from the Young's modulus and the critical stress intensity factor (cf. Johnson et al. 2002). It is strongly suspected that this interaction with the sedimentary medium is the underlying reason for the body plan of some gammarids and may be one reason for their cuticular hydrophobicity.

3.5.3. Dependence on properties of mud

As discussed above, the aspect ratio of bubbles in sediment has been accurately predicted using linear elastic fracture mechanics (LEFM) and is directly proportional to K_{Ic} and inversely proportional to E (Johnson et al. 2002). Whereas a bubble has a constant volume, and the material properties of the sediment determine the shape, burrowers tend toward constant displacement. That displacement results in a stress determined by Young's modulus, E, which likely varies with depth in sediment, porosity, grain size, and organic content. K_I is directly proportional to the stress, and the ease of fracture and resultant length of the crack therefore depends on both E and K_{Ic}. If E increases and K_{Ic} remains the same, a burrower will exert more stress for a given
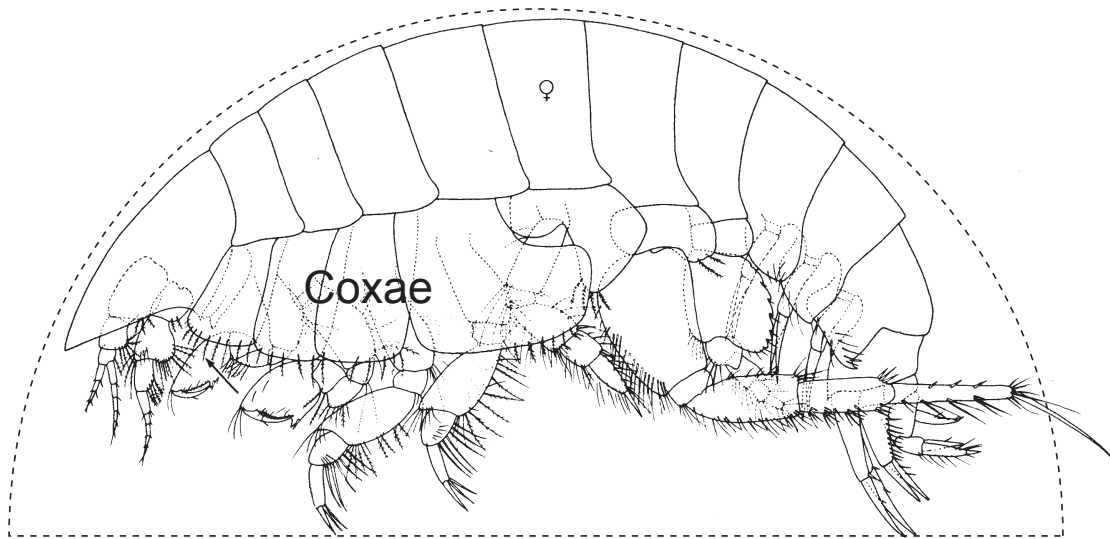
Figure 3.11. Lateral view of a gammaridean amphipod. *Harpinia propinqua* is shown with the outline of an oblate hemispheroid (drawing from Bousfield 1973).

displacement, and the crack will propagate farther, resulting in a more flattened discoidal

burrow shape. If K_{Ic} increases, more stress is needed to propagate the crack, and the

crack will extend a shorter distance and have a larger aspect ratio.

3.5.4. Burrowing with a hydrostatic skeleton

Many burrowers move using a hydrostatic skeleton, the physics of which has been

summarised for earthworms (Quillin 1998). A hydrostatic skeleton comprises an

extensible body wall containing fluid or tissue under compression and against which

muscles can work. The interior fluid is incompressible, allowing operation of

antagonistic muscles, the transfer of muscle forces to the environment and maintenance

of body shape (Quillin 1998). Cylindrical hydrostats of length L and radius r have a

constant volume of

$$V = \pi r^2 L .$$ (equation 3.3)

Rearranging and differentiating this equation gives

$$\frac{dr}{dL} = \frac{-r}{2L} .$$ (equation 3.4)

For a 1% shortening of the circular muscles, which elongate the segment when

contracted, there is a 2% elongation of the longitudinal muscles, which dilate the segment

when contracted (Alexander 2003). For worms, the whole body comprises one or more

hydrostatic skeletons used for locomotion, whereas mollusks use their hydrostatic feet in

coordination with the hard shell, and amphipods and echinoids have only hard

exoskeletons. Some annelids have septa that partition the fluid in segments, dividing the

worm into a series of separate hydrostats. In aseptate annelids and other worm-shaped

animals, the body comprises one large hydrostat.

Stresses in the body wall of a thin-walled cylinder under internal pressure are

$$\sigma_c = \frac{Pr}{t} \text{ and } \sigma_l = \frac{Pr}{2t},$$
(equation 3.5)

where σ_c is circumferential tensile stress, σ_l is longitudinal tensile stress, P is internal pressure, r is radius, and t is body-wall thickness. These stresses are calculated by balancing the force from the internal pressure with the force exerted by the muscle, assuming that the cylinder has no other forces acting upon it (Figure 3.12A) (Quillin 1998).

Worms that burrow in muddy sediments by crack propagation experience a force exerted by the burrow walls compressing the body dorsoventrally (Dorgan et al. 2005). Superposition of a dorsoventral force and a constant internal pressure results in an asymmetrical internal stress field, with higher stress being exerted laterally and lower stress dorsally and ventrally (Figure 3.12B). This internal stress asymmetry results in reduced circumferential stress on the sides of the worm extending dorsoventrally and increased circumferential stress on the dorsal and ventral sides extending laterally. Similarly, the dorsoventral compression results in an elliptical rather than circular cross-section of the worm's body. The radius of curvature of the shorter axis (the sides of the worm) is smaller than that of the longer axis, resulting in reduced lateral circumferential and longitudinal stresses from eq. 5.

Scalibregma inflatum (Scalibregmatidae) is named for its balloon-like shape when removed from sediments, and sternaspids (Sternaspidae) are nearly spherical when removed from the mud. When observed burrowing in gelatin, however, they are both dorsoventrally compressed, adopting the fundamental disk shape of the crack itself (K. M. Dorgan & P. A. Jumars, unpublished observations).

47
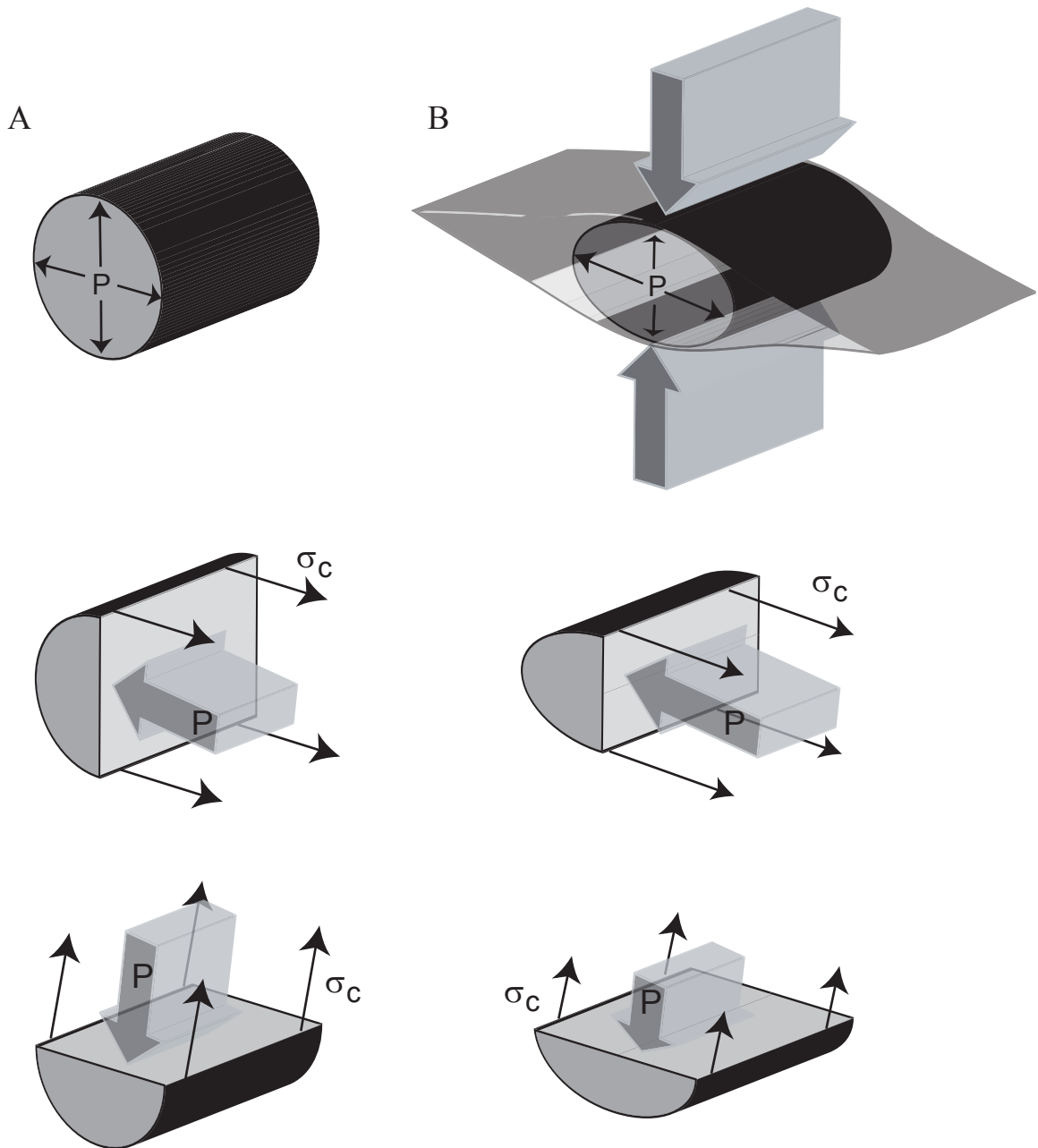
Figure 3.12.   Hydrostatic skeleton of a worm. A) Sections through the hydrostatic skeleton of a worm, showing circular muscles (which exert stress, σ_c) and internal pressure (P) (adapted from Quillin 1998); B) the same hydrostatic skeleton but dorso-ventrally compressed by the walls of the disk-shaped burrow through the elastic restoring force.

The polychaete *Cossura* sp. has longitudinal muscles, but its circular muscles are "very poorly developed" (Tzetlin 1994). Cossuridae burrow in muddy sediment (Rouse and Pleijel 2001) and may use the elastic restoring force of sediment to aid their circular muscles in elongating segments during peristalsis. Circular muscles are also completely absent in the burrowers Opheliidae, Sigalionidae, Nephtyidae, and representatives from numerous other polychaete families, including meio- and macrofauna (Tzetlin & Filippova 2005, Tzetlin et al. 2002). Tzetlin et al. (2002) point out that circular muscles are commonly less developed in parapodia-bearing taxa, and even absence of circular muscles is not uncommon in polychaetes. In fact, Tzetlin & Filippova (2005) hypothesize that the absence of circular muscles may be the plesiomorphic state in Annelida. Tzetlin et al. (2002) suggest that circular muscles may not be necessary for polychaetes that move using parapodia, as the dorso-ventral, transverse, parapodial, or other longitudinal muscles can act as antagonists for longitudinal muscles, but that circular muscles are necessary for burrowers. It is suggested here that circular muscles may not be necessary for burrowing if the elastic restoring force acts as an antagonist for the longitudinal muscles, but crawling by peristalsis does require circular muscles. It would be interesting to compare burrowing and non-burrowing species that are closely related.

3.5.5. 'Soupy' muds

'Soupy' appears to be a misnomer for deposited muds. Except for those that have very recently been resuspended, highly porous muds behave viscoelastically instead; a high strain rate results in more elastic behaviour of the sediment, whereas a low strain

rate results in viscous flow. This behaviour is apparent in gelatin; gelatin 'jiggles' when

shaken, but leave a half-eaten bowl of gelatin to respond to gravity and it flows passively.

The same behaviour can be seen in some muds left in a bucket. If the strain rate at which

a transition from elastic to viscous behavior is similar to that exerted by animals, that

threshold may affect animal behavior. In this case, animals may either move quickly,

heightening strain rates and invoking elastic behaviour to fracture the mud or move

slowly, lowering strain rates and swimming in slow motion through a highly viscous

fluid. It should be noted, however, that swimming at consequently low Reynolds

numbers cannot be accomplished by reciprocating mechanisms (Purcell 1977).

Viscoelastic materials experience creep, which may be important in highly porous muds.

Burrowing behaviour in soft muds by *Polyphysia* has been described (Elder

1973), but the mechanical behaviour of the sediments is unknown. *Polyphysia* burrows

by direct peristalsis, with both circular and longitudinal muscles contracting

simultaneously, resulting in an anterior wave of short, thin segments. In septate worms,

circular and longitudinal muscles work antagonistically; in *Polyphysia*, elastic fibres

restore body shape after contraction of both sets of muscles (Elder 1973). This direct

peristaltic wave displaces most of the coelomic fluid anteriorly (Elder 1973). It may be a

way to build up pressures over a large enough area and to high enough levels to fracture.

The anterior five segments of *Polyphysia* are segmented, and the head progresses

continually while the rest of the body progresses in episodic waves (Elder 1973).

Polyphysia moves its head from side to side while burrowing (Elder 1973, Hunter et al.

1983), a behaviour that has been observed in *Scalibregma* (in the same family,

Scalibregmatidae, as *Polyphysia*) and *Nereis,* both burrowing in gelatin (K.M. Dorgan,

personal observations). Hunter et al. (1983) suggest that *Polyphysia* is taking advantage of the thixotropic behaviour of mud and reducing the viscosity before moving forward. *Nereis,* however, which has been shown to burrow by crack propagation (Dorgan et al. 2005), exhibits the same behaviour, and preliminary observations of *Scalibregma* burrowing in gelatin reveal a crack-shaped burrow. Head movements of *Scalibregma* extend the crack tip laterally and slightly anteriorly, while the wider body holds the crack open (K.M. Dorgan, unpublished observations). In this way, the head is analogous to the probing foot of a clam, while the wider body holds the crack open, as does the clam's shell. In sediment, the head movement may additionally be used to free particles for feeding, in sensory behaviour, or as a way to mechanically 'sample' the resistance of sediment in different directions by driving the head into the crack.

Priapulus caudatus also burrows in soft sediments but uses a very different mechanism. *Priapulus* uses simultaneous contraction of circular and longitudinal muscles to build up high internal pressures to evert a large praesoma, which has been described as a terminal anchor (Hunter et al. 1983). The praesoma is dilated to a volume greater than the volume of fluid remaining in the trunk; then a direct peristaltic wave moves the body forward as the praesoma is retracted (Hunter et al. 1983). Burrowers in high-porosity sediments use mechanisms interpreted as ways to propagate a crack in a viscoelastic solid. Although the behaviour of burrowers suggests that elastic behaviour dominates over viscous flow even in highly porous sediments, an explicit understanding of the mechanical behaviour of these sediments is still lacking.

The two sediment behaviours may act largely in series (initially elastic, with creep becoming more important on longer time scales) and that this series may explain the

basic body plan of the burrowing polychaetes that dominate the muddy seafloor. The general body form is bilaterally symmetrical anteriorly but cylindrically symmetrical posteriorly, like that of *Scalibregma* or *Polyphysia*. It is suggested that the anterior is adapted to crack propagation and movement in the crack, whereas the hindmost cylindrical morphology is the form that will result from sediment creep reaching equilibrium with coelomic pressure. Following this reasoning, fast polychaete burrowers will lack a cylindrical region, whereas slow burrowers will lack a bilaterally symmetric region. However, to compare burrowing speeds properly, they should be normalised to the rate of sediment creep; burrowers in highly porous sediments that creep more easily may need to burrow more quickly to experience similar mechanics to a slower moving animal in stiffer sediment.

3.5.6. Peristalsis as a way to crack

Many worms and worm-shaped burrowers move by peristalsis, which involves waves of muscular contraction traveling either anteriorly or posteriorly along the body. In direct peristalsis, the wave of contractions moves in the same direction as the animal, while in retrograde peristalsis, the wave moves in the opposite direction (Elder 1980). In general, retrograde peristalsis is utilised by animals with septa separating coelomic fluid into segments of constant volume. Direct peristalsis occurs only in animals with an open body cavity, and segments do not maintain a constant volume as the wave passes.

In general, animals utilising retrograde peristalsis (e.g. earthworms) burrow in more compacted, less porous sediments. This compartmentalisation enables the animals to build up high internal pressures and exert strong forces within a small region of the

body while pressures remain low elsewhere. The animal has to do less work to exert the same force at that given body location than does an animal with an open body cavity. In addition to exerting force to propagate a crack, worms dilate segments against the elastic restoring force of the sediment. It takes work to maintain body shape in the crack, and the fatter the segments and longer the dilation is held, the more work is needed. In more compact muds with a higher elastic modulus and higher restoring force, it may be more efficient to increase the volume of the body that is contained in thin segments to reduce work done against the elastic restoring force of the sediment (in other words, to let more of the body be flattened). Septa, which are present in worms that move by retrograde peristalsis, help maintain the stiffness of the body wall so less internal pressure is required to maintain body shape. The earthworm *Lumbricus* has septa and a particularly stiff body wall and does not need to maintain internal pressure to keep the body's cylindrical shape against gravitational forces in air (Trueman 1975).

Direct peristalsis occurs primarily in animals burrowing in high-porosity sediments, such as *Polyphysia* sp., *Priapulus caudatus* (Hunter et al. 1983, Hunter & Elder 1989), and the holothuroid *Leptosynapta tenuis* (Elder 1980). The thin segments in which circular muscles contract are also short, increasing the area touching the sediment and resulting in fluid displacement among segments. In contrast, retrograde peristalsis involves segments of a constant volume, so thin segments become longer. Elder (1980) suggests that direct peristalsis may be advantageous to these animals as it reduces the area of the thin segments and increases the anchor area, which may be beneficial in 'soupy' sediments that deform easily. This suggestion can be reinterpreted to explain the benefits of increasing the area exerting the stress. These high-porosity sediments deform

under low stresses, prohibiting the animal from building up the higher internal pressures possible in more compacted sediments. A larger area of body wall in contact with the sediment allows the animal to exert more stress, possibly compensating for low internal pressures.

The direct peristaltic wave moves coelomic fluid anteriorly in *Polyphysia* (Elder 1973), resulting in expansion of the anterior region and increased internal pressure. *Arenicola marina* also uses direct peristalsis (Elder 1980), but in this case water flow is external, and the peristaltic wave pumps water through the burrow, likely aiding in liquefaction. Even in the sand that it inhabits, however, the pressure so produced may be used to propagate a crack upward as a head shaft (S.A. Woodin, personal communication).

In both types of peristalsis, the thinner segments are moving while the thicker segments are stationary, the latter withstanding the elastic restoring force of the burrow wall. By analogy with the common formulation of sliding friction, the frictional force (F_f) is directly proportional to the normal force (F_N), $F_f = \mu F_N$ where μ is the friction coefficient. In this case, the elastic restoring force dominates the normal force (although sediment overburden may be important as well), and most of the elastic restoring force is exerted by the sediment against the stationary, dilated segments. This conclusion suggests that frictional forces may be much less significant than inferred in previous studies in which friction has been considered important as a mechanism for particle mixing and a component of energetic calculations for burrowers (e.g., Trevor 1978).

3.6. Burrowing in sand

3.6.1. Differentiation from mud

Sand is a granular medium, in which forces distribute along stress chains; interfaces between some particles experience large stresses, while others bear little or no load (Duran 2000). To an animal burrowing in sand, some grains are easily moved, while others are part of a stress chain and are therefore much more difficult to displace. Depending on speed of locomotion and size of the animal, a macroscale or microscale approach to burrowing could be taken. Bulk movement of sand can be achieved by liquefaction or excavation, whereas individual grains can be moved by breaking stress chains. This section attempts to correlate observations in the literature with known behaviours of granular materials to generate hypotheses for future research.

Muddy sediments are adhesive and resist deformation, so forces exerted on an animal act from any direction in which the animal exerts a force. Sand differs in that grains rest on each other, with the result that the weight of the overlying sediment exerts an important but non-uniform force on an animal, whether stationary or mobile. Sea urchins that live in sands reflect this difference with their dome shape, which is able to sustain the downward weight of the sand (Kanazawa 1992). For animals that construct more permanent burrows, mucus may serve the dual purpose of reducing friction and providing adhesion for sand grains to stick together and maintain the structure of the burrow wall.

Penetrometer studies have shown that the force required to penetrate the surface of sand decreases dramatically with decreasing angle to the sand surface below 30˚. The gastropod *Bullia* has a disk-shaped foot, is a fast burrower, and moves by extension of the

propodium, forming a terminal anchor, then drawing forward the shell and metapodium, forming a penetration anchor. *B. digitalis* burrows at an angle of 10-15˚, whereas *Donax serra* burrows vertically. *D. serra* has the higher energetic cost of burrowing, with a ratio of 9:1 predicted by penetrometer data (Brown & Trueman 1991). These results are unsurprising, because the upward displacement of discrete particles should be much easier than horizontal, for which tight packing resists movement. The impermeability and cohesiveness of polymers in mud suggest that the angle of penetration should have a less significant effect on ease of penetration, although there appear to be no similar studies done in muds.

3.6.2. Description of the mechanism

Clean sands on wave-swept beaches have large, homogeneous grain sizes and are more closely mimicked by laboratory and theoretical studies on dry granular materials than are finer sands with higher organic contents. The mole crab, *Emerita*, burrows in sandy beaches by rapid excavation and resuspension of sand grains. Like other sandy beach burrowers (e.g., cirolanid isopods; Yannicelli et al. 2002), *Emerita* can burrow only in wet sand (Trueman 1970). It has been suggested that dry sand is too hard (Trueman 1970) or less thixotropic (Yannicelli et al. 2002), but more likely the animals are using the increased density of sea water over air to facilitate suspension of sand grains. The first three pairs of thoracic limbs move the body backwards into the burrow and sand forward, while the fourth pair of limbs and the uropods excavate the burrow (Trueman 1970). Burrowing occurs much more rapidly than in the fastest bivalves studied (Trueman 1970, Lastra et al. 2002). Amphipods burrow in sands by a completely

different mechanism. Setae that bend in only one direction help produce forward (and probably slightly upward) motion in sands (Nicolaisen & Kanneworf 1969). Perhaps they are driving a wedge.

Mole crabs are considered generalist burrowers, in that burrowing rate is not greatly affected by sediment grain size (Trueman 1970, Lastra et al. 2002). Burrowing rate index, defined as BRI = (mass(g))$^{1/3}$/burrowing time x 100, has been used to compare burrowing speeds among animals of varying sizes (Stanley 1970). (N.B. Alexander et al. (1993) use 10^4 instead of 100 in their calculations to give BRI values of 1.0 or greater). The burrowing rate index is generally constant throughout the size range of a species (Stanley 1970). Species for which BRI depends strongly on grain size are considered specialists, many of which burrow most quickly in fine to medium sands. *Donax serra* and *D. sordidus* show fastest burrowing times in 125-500 μm sands (Nel et al. 2001), cirolanid isopods in 'fine' rather than 'coarse' sediments (Yannicelli et al. 2002), the mysid, *Gastrosaccus psammodytes*, in 125-1000 μm sand (Nel et al. 1999), and many of the bivalves studied by Alexander et al. (1993) showed BRI maxima in fine to medium sands. Burrowing times increase in finer sands (Nel et al. 1999, 2001).

Displacement of a single particle in a granular material requires work to overcome friction and, depending on the packing structure, work to lift overlying particles. In a loosely packed structure, a displaced particle may be moved into pre-existing void space with minimal displacement of other particles. The smaller the particle size (assuming uniform particle size distribution), the less overlying load it carries, given that it is part of a stress chain, because there are more stress chains in a given area. Stress chains are more easily broken in finer-grained granular materials: The stress chain bears less

weight, and the weight is more easily redistributed along newly formed stress chains. Contacts per volume increase with decreasing grain size. Furthermore, the frictional force between two particles depends on the overlying weight and while (assuming constant void ratio) the total load is the same at a given sediment depth for smaller grains, the load is distributed over a greater area. For these reasons, smaller grains should be more easily displaced than larger grains. The fact that burrowing rates decrease in sands with grain sizes < 125 μm suggests that different mechanics are at work. Changes in permeability or adhesion would affect burrowing performance. Contacts per volume also increase with decreasing sorting, although this likely leads to increased resistance to stress more than facilitating redistribution of stress chains, as dense packing could inhibit redistribution of grains.

The features of sand burrowers that increase their rugosity may be adaptations to displace grains bearing larger loads. Examples of these features include papillae on the pharynges of worms, setae, bivalve shells with surface relief comparable in scale to grain size, and sea urchin spines.

3.6.4. Use of fluidisation

Fluidization entails the injection of fluid in such a manner as to eliminate a substantial proportion of grain contacts and cause the bulk material to flow as a fluid. Many clams eject water from the mantle cavity during rapid adduction of the valves; adduction also results in foot dilation (Trueman 1975, Trueman & Brown 1992). Among gastropods, Trueman & Brown (1992) compare *Bullia,* which burrows in sandy beaches, with natacids, which burrow deeper in muddy sediments. *Bullia* ejects water, helping to

liquefy the sand, while natacids do not eject water, a process that would be less beneficial in low-permeability muds except to maintain pressure in the small volume of crack preceding the animal.

Arenicolid polychaetes pump water down from the tail end of their J-shaped burrows toward the head. The water moves upward toward the sediment-water interface from the anterior end of the burrow within a localised area in the sediment (Timmerman et al. 2002). Although movement of fluid has been studied by several authors (Riisgård et al. 1996, Timmerman et al. 2002), explicit modeling of particle movement is lacking. *Arenicola marina* is assumed to use the pumped water to loosen or fluidise the sand in front of the head, feeding in this region (Trevor 1977). In order to move through sand by using pumped water to fluidise the sand, either the entire overlying bed of sand through which water passes must be fluidised, or a localised region around the head, in which case the weight of the overlying sediment must be distributed around the animal by stress chains. The upper layer of sand may be supported by stress chains arching around the small, fluid region into which the animal can move.

Fluidisation may be practical only within the upper region of sand with low resistance to flow. Flow through a packed bed increases with increasing permeability and depth of sand, following Darcy's law

$$u = -\frac{\kappa}{\mu}(\nabla p - \rho g) \qquad \text{(equation 3.6)}$$

where u is velocity, k is permeability, μ is the viscosity of the water, ∇p is the pressure gradient, ρ is water density, and g is gravity (Wilkes 1999). The 1-D discretised form is

$$u = -\frac{\kappa}{\mu}(\frac{p_1 - p_2}{L} - \rho g) \qquad \text{(equation 3.7)}$$

where L is the length of the bed, and p_1 and p_2 are the pressures at the bottom and top of the bed, respectively. Most of the variation results from permeability, which increases with increasing grain size, length of bed (depth in sediment), and the increase in pressure (which depends on the force with which water is forced by the animal) with depth. Fluidisation of a bed of particles occurs when the pressure drop between the bottom and top of the bed exceeds the stress caused by the weight of the particles, i.e., when

$$p_1 - p_2 = gL(1 - \varepsilon_0)\rho_s \qquad\qquad \text{(equation 3.8)}$$

where ε_0 is the void ratio (not to be confused with strain), and ρ_s is the density of the particles (Wilkes 1999). An animal burrowing at a greater depth must produce a greater increase in pressure to fluidise the bed, a depth dependence unsurprisingly similar to Darcy's Law because fluidisation occurs at a critical flow velocity.

Riisgård et al. (1996) found that *A. marina* attains a maximum pressure head of 20 cm water, a value comparable with that needed to fluidise the bed above itself, assuming that the animal is burrowing at a depth (*L*) of 10-15 cm with a void ratio of 0.5. However, their study involved animals in glass tubes, whereas in the natural environment, pumped water may find lateral escape routes into the surrounding sand, reducing the available pressure head to fluidise the overlying sand. In addition, stress is distributed laterally over relatively large distances in granular materials, whereas the region in which fluid moves upward from the worm's burrow is relatively small. The literature on fluidisation of beds of particles is extensive but generally considers fluidisation of the entire bed enclosed by an impermeable container with flow at a constant rate (Wilkes 1999). Burrowing animals pump water at an unsteady rate into an uncontained area, of which only a small portion is affected by the pumping.

60

Although fluidisation of the bed is unlikely at depth, the pumped water may reduce the load of the overlying sediment and reduce friction between grains, easing burrowing. Another hypothesis for the mechanism of burrowing by *Arenicola* is that the pumped water could be used to fracture the sand. Granular materials have been found to fracture below force arches (Duran 2000), and hydraulic fracture is an important mechanism in geological processes, including rocks and glaciers (Fountain et al. 2005). Fine sands may have enough adhesion to behave elastically, or at least to fall within the transition zone between elastic and granular behavior. Again, preliminary observations by S.A. Woodin (personal communication) support this hypothesis.

It is possible that the papillae of *Arenicola* are used to break stress chains and move grains that are not easily resuspended. However, the maldanid polychaete, *Proxillella affinis pacifica*, which lives in muddy sediments, has a papillated pharynx, while other sand-dwelling species of maldanids lack papillae (Kudenov 1977). In this case, the papillae may remove particles from the organic matrix and/or provide greater surface area to stick to particles and move them into the mouth.

3.7. Discussion and Implications

3.7.1. Terrestrial implications

Subterminal expansions suggest that earthworms may burrow, and roots grow, by analogous mechanisms. Roots grow axially until too much resistance is met, causing them to grow radially, creating a zone of stress relief into which axial growth extends (Figure 3.13) (Abdalla et al. 1969). The alternation between axial and radial growth by plant roots has been described as 'inverse-peristaltic' growth. By this means roots can
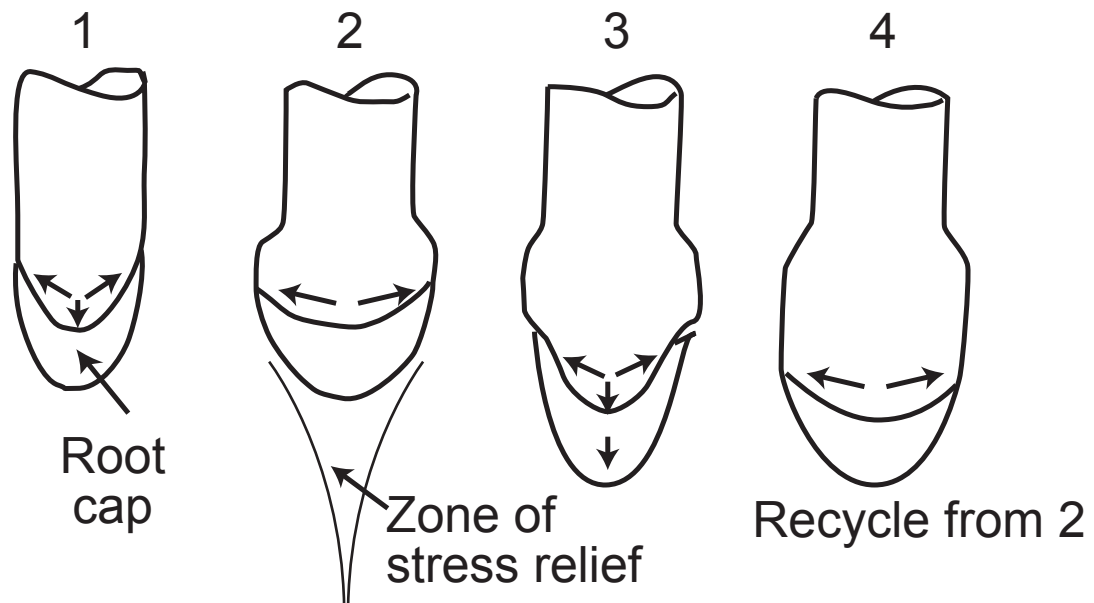
Figure 3.13. Scheme of root penetration in soil (Abdalla et al. 1969). When the root cap meets resistance (1), the root grows radially, creating a zone of stress relief (2). The root can then extend axially (3), until it again meets too much resistance (4). Reproduced with permission from Elsevier.

penetrate compact soils with five times the resistance that the root would be able to overcome by axial growth alone (Hettiaratchi & Ferguson 1973).

Earthworms also exert radial forces, which are higher than measured axial forces (Keudel & Schrader 1999, Quillin 2000). Highest internal pressures of burrowing earthworms occur when buried segments are dilated, described as a mechanism to anchor the worm and compact the surrounding sediment (Seymour 1969). Earthworms exert stronger forces near the anterior end; a retrograde peristaltic wave is strongest when beginning at the head end and it may die out before reaching the tail (Seymour 1969). Earthworms lose coelomic fluid through dorsal pores, which are only present on posterior segments of burrowing species (Stovold et al. 2003). Anterior sections maintain internal pressures, enabling worms to exert the same radial forces even when dehydrated (Stovold et al. 2003).

Although crack propagation seems a likely mechanism of burrowing in terrestrial soils, direct evidence is needed. Extensive literature on soil properties from the perspectives of civil engineers exists (e.g. Chandler 1984), but this literature has not been explicitly applied to the space and time scales of burrowing. Soils have been modelled using elastic-plastic fracture mechanics (Chandler 1984). It would be worthwhile to re-examine burrowing using a nonlinear fracture model. Previous studies of earthworm burrowing have measured forces of animals burrowing against rigid walls and, although they have yielded important ecological and ontogenetic comparisons among earthworms (Keudel & Schrader 1999, Quillin 2000), the values measured do not represent natural conditions. Internal pressures and measured forces depend on the material against which the animal is exerting the force.

3.7.2. Biomechanics of burrowing

While the use of a hydrostatic skeleton suggests similarities between the mechanisms of burrowing and crawling, environmental forces differ significantly. Animals burrowing in muds have two surfaces against which to push and are compressed by the elastic restoring force, resulting in different body wall stresses. Seymour (1969) measured internal pressures of earthworms burrowing and crawling and found different pressure records for the two behaviours. Crawling earthworms had maximal coelomic pressures of approximately 10 cm of water in segment 10 during circular muscle contraction (lengthening of segments), with a drop to approximately 5 cm water during segment dilation. For burrowers, coelomic pressure was higher (18-24 cm water) than for crawlers, and showed the reverse pattern, a reduction in coelomic pressure as segments were elongated (Seymour 1969). The two walls constrain radial expansion of the burrowing worm, requiring much higher pressures than unconstrained surface crawling. When burrowing, one direct peristaltic wave occurs at a time in *Polyphysia crassa*, whereas simultaneous passage of two waves occurs during crawling (Hunter et al. 1983). This difference allows higher internal pressures to build up during burrowing, even in soft muds with low resistance. Burrowing and crawling, although superficially, kinematically similar, are mechanically and dynamically different types of locomotion. Comparisons, both within and among species, should be made with caution.

A possible advantage to locomotion within an elastic solid is external storage of elastic strain energy. Elastic energy can be stored in tendons; the most common example is in kangaroos and wallabies (Alexander 2003). When a hopping kangaroo lands,

kinetic energy is stored in a spring-like tendon, then converted back to kinetic energy as the kangaroo ascends. Whereas energy storage is common in internal elastic structures, burrowers are unique in their access to an external elastic energy storage structure. The importance, or even occurrence, of elastic energy storage by burrowers in muds is yet unknown.

Terrestrial and aquatic environments differ in that terrestrial hydrostats must retain their body shapes against gravity, whereas most aquatic animals have densities close enough to the density of sea water that gravitational force is not a major concern for an animal at the sediment-water interface. Gravitational forces can, however, become significant with increasing sediment overburden. The cuticle and septa of *Lumbricus terrestris* help maintain body shape, allowing much lower resting internal pressures than in *Arenicola marina*, for which most of the body is aseptate (Seymour 1969). Negative pressures have been recorded in *Lumbricus terrestris* and have been attributed to elastic outward rebound of the body wall as circular muscles are relaxed (Seymour 1969).

Burrowing has in the past been calculated to be more energetically expensive than other forms of locomotion such as flying, swimming, and running (Trevor 1978, Hunter & Elder 1989). However, forces exerted by *Nereis virens* in gelatin are < 10% of those measured with solid force transducers in *Priapulus* and *Polyphysia* (Dorgan et al. 2005, Hunter & Elder 1989). It is quite likely that burrowing is less costly than previously suggested, but traditional methods of measuring energetic cost of transport are not feasible in marine sediments. Oxygen consumption rates are the standard means to calculate net cost of transport, but in marine sediments no way is known to estimate individual oxygen consumption rates because of the complex three-dimensional, time-

varying structure of oxygen concentration fields within and around a burrow whose geometry itself is time varying. Moreover, the uptake occurs together with that of abundantly and nonrandomly distributed smaller organisms, including bacteria at 10^9 cells ml^{-1} of pore water in natural sediments (Schmidt et al. 1998). Even the steady-state distribution of oxygen concentration under continuous pumping into a permanent burrow of fixed geometry is not trivial to model (Aller 1982).

3.7.3. Nonrandom distribution of animals

Most burrowers appear to exert constant displacements on the walls of their burrows determined by the sizes of their everted pharynges, dilated feet, or other 'terminal anchors'. The stress then exerted against the sediment depends on the elasticity of the sediment: $\sigma = E\varepsilon$. Because the elastic modulus (E) is a measure of the amount of stress required for a given strain, the elastic modulus is expected to increase with greater sediment compaction, reduced porosity and increased weight of sedimentary overburden (i.e. with depth in the sediment). A constant displacement exerted by an animal would result in increasing stress as E increases. Stress intensity factor (K_I) is proportional to stress, while the critical value at which fracture occurs (K_{Ic}) is a material property. K_{Ic} appears to increase with depth (B.D. Johnson and B.P. Boudreau, unpublished data), but similar profiles for E are lacking. Our analysis of the effects of overburden would argue for increasing E with depth, however, but not necessarily in proportion to K_{Ic}. Changes in the relationship between E and K_{Ic} with depth would change the ease and shape of fracture and could result in layers of high burrowing activity. For example, if E increases more quickly than K_{Ic}, the higher stress will propagate the crack more easily.

Because cracks propagate in the direction of least resistance, an already cracked path may become a highway for other burrowers. Similarly, methane bubbles can grow more easily in pre-existing, partially annealed cracks, as indicated by the pressure records of bubble-growth in Johnson et al. (2002). How quickly cracks anneal in sediments is unknown, but a comparison between the time of annealing and the time that elapses before another burrower encounters a crack (also unknown) could be used to predict the likelihood of highways forming in muds. Alternatively, cracks may be turned away from the compacted area around burrows, keeping burrowers away from recently formed burrows. Discoidal cracks can become cylindrical burrows with compacted sediment walls (e.g., Shull & Yasuda 2001). These two alternatives depend in part on whether most traces left by animals are crack-shaped and close after the animal passes or are cylindrical burrows, discussed in further detail below.

3.7.4. Bioturbation

The distribution of animals clearly has a direct effect on bioturbation. A nonrandom distribution of animals suggests a nonrandom probability of movement of particles by those animals. Perhaps more importantly, in bioturbation models, particles are considered discrete, an invalid assumption in elastic muds. Unless the polymer matrix holding grains together is broken, the movement of individual grains depends strongly on the movement of adjacent grains. The matrix is broken when a crack propagates, at which time grains may be released by crack branching or irregular crack growth resulting from sediment heterogeneity. However, release of grains from the matrix during ingestion by deposit feeders and their defaecation at another location is

likely the most important mechanism of particle mixing. Results of lattice automaton models of bioturbation highlight the importance of ingestion and egestion in particle mixing (Boudreau et al. 2001).

The question of how a crack becomes a permanent cylindrical burrow is important both in terms of bioturbation and interpreting the fossil record. Cylindrical burrows are clearly visible on the sediment surface and in x-radiographs and, once vacated, cave in or fill with sediment, resulting in particle movement. The presence of burrows necessitates some mechanism for transforming a crack to a cylinder, either passively resulting from sediment mechanics or by active behaviour of animals such as lining the burrow with mucus. Burrow presence does not, however, give an indication of how often this process occurs. Absence of evidence may not be evidence of absence: cylindrical burrows left in the sediment are obvious (e.g., cirratulid burrows; Shull & Yasuda 2001), but how could a crack, having closed up, be detected? It has been observed that larger macrofauna contribute disproportionately more to sediment mixing than smaller animals; for example, the volume of sediment reworked by burrowing by the heart urchin, *Brissopsis lyrifera*, is 60-150 times greater than that ingested (Hollertz & Duchene 2001), whereas ingestion contributes much more significantly to modelled mixing by small, capitellid-like deposit feeders (Boudreau et al. 2001).

Whether a crack closes after an animal passes depends on a number of factors. Viscoelastic creep results in reduced elastic restoring force over time, potentially compacting burrow walls, but the temporal and spatial scales over which creep is important are unknown. The elastic limit of the sediment is clearly important, and although no data on elastic limits of muds exist, intuition suggests that more porous, fine-

grained muds have lower elastic limits and flow more easily than more compacted

sediments. Coarser sediments may deform plastically, more similar to terrestrial soils.

Gelatin has been used to examine the mechanical effects of spicules in connective tissue

of sponges and cnidarians (Koehl 1982), with obvious implications for sediment grains in

a mucopolymeric matrix. Increased spicule volume fractions and surface area-to-volume

ratios result in increased stiffness, a result consistent with intuition about sediment: i.e.,

more highly porous muds have lower stiffness. Interestingly, the spicules have a stress-

softening effect on gelatin (and natural tissues) because repeated stresses are met with

decreased resistance (Koehl 1982). Consider a burrower moving through a crack with

repeated peristaltic contractions. The viscoelastic nature of mud suggests time

dependence; the slower an animal moves, the more time is allowed for the sediment to

creep. Perhaps most importantly, the size of the animal determines the deformation

because a larger animal is much more likely to exceed the elastic limit and leave a

permanent burrow.

Crack propagation as a mechanism of burrowing brings into question several

assumptions in bioturbation models. Meysman et al. (2003) distinguish between local

and non-local models of bioturbation, suggesting that local models are based on the often

invalid assumption that the step length of particles is much less than a length scale

associated with the tracer being used, and therefore that non-local models are preferable

in general. Local models additionally assume random particle movements (Meysman et

al. 2003), a questionable assumption given the elastic property of mud. Non-local

transition matrix models are based on the first-order Markovian assumption that

displacement of a particle is independent of previous movements of that particle

(Meysman et al. 2003). However, a particle moved by a burrower may be either sequestered from future movement by the compaction around the burrow or preferentially moved if another animal follows the path of least resistance. A particle's history is also important in granular mechanics, because the friction force depends on interactions with surrounding particles (Duran 2000). This history dependence may average out over many particles and be statistically unimportant. Alternatively, it could result in preferential movement of particles that have recently been moved while other particles remain in place, leading to overestimation of total mixing.

Development of the lattice-automaton bioturbation simulator (LABS) provides a mechanism-based way of studying bioturbation (Choi et al. 2002). In this computer simulation, sediment is modeled as a 2-D lattice of grains and water through which automatons, the modelled infauna, move. The automatons follow prescribed rules for movement and ingestion and egestion of particles that are designed to mimic natural behaviours of specific groups of animals, e.g., small, capitellid-like deposit feeders (Choi et al. 2002). LABS has successfully predicted values of the biodiffusion coefficient, D_B, similar to those measured in the field with similar animal densities (Boudreau et al. 2001). These results are particularly impressive, given the lack of data on basic features of the animals being modelled (e.g. velocities) and on the mechanical interactions between the animals and the sediment. Adding realistic mechanical constraints should improve next-generation models based on the elastic properties of sediment and fracture by animals and will contribute to mechanistic understanding of bioturbation. Models of fracture in heterogeneous materials such as wood and cement may be applicable to marine muds (e.g., Schlangen & Garboczi 1996).

3.7.5. Feeding in a crack

Because their scheme remains widely used, relevance of our new understanding of burrowing is reviewed with respect to the original feeding guild classification of Fauchald & Jumars (1979). First, it is recommended that potential users who do not resort to the primary literature update this guild classification by reference to the summaries in Rouse & Pleijel (2001). Our new understanding of burrowing by crack propagation, together with still-limited observation, suggests to us a number of changes. A clear recommendation is to be skeptical of observations made on one or a few specimens not known to be in good condition. Because animals are more easily observed at the surface, animals observed rarely there may not be performing representative behaviors when they are on the surface.

Sternaspids have been considered subsurface deposit feeders, and the authors have no disagreement with that classification. Several workers (e.g., Day 1967, cited in Rouse & Pleijel 2001) have suggested, however, that these worms sit at the sediment surface with the rear plate and gills at the sediment surface. However, this observation may have been based on moribund individuals, much like early depictions of *Yoldia* feeding at the sediment-water interface (e.g., Yonge & Thompson 1976). The authors have observed that *Sternaspis* is a vigorous subsurface burrower that rarely approaches the interface and suggest a new common name based on obvious analogy: the bubble worm. Specimens have been kept in mud in sea tables for months without any surface manifestations whatsoever (P. A. Jumars, personal observation).

Fauchald and Jumars (1979) classified scalibregmids as subsurface deposit feeders, yet *Scalibregma* appears to access surface materials quickly (Blair et al. 1996). In observations (P. A. Jumars and K. M. Dorgan unpublished) of *Scalibregma inflatum* (from Puget Sound, Washington) in laboratory microcosms, this species maintains a cylindrical surface opening, apparently for respiration. Such an opening may allow the animal to sense surface phytodetrital events and may serve to trap some depositing materials. A new question to which there is yet no answer is to what extent a crack-producing animal can steer its crack to the surface and take advantage of freshly deposited material there.

Cossurids often show distinct subsurface depth preference in sectioned cores (e.g., Jumars 1978). Tzetlin (1994), however, drew a conceptual diagram of surface deposit feeding in one live specimen. He offered caveats about the condition of this specimen, but subsequent citations have not carried along this warning. It is strongly suspected that this specimen was moribund and that cossurids typically feed below the primary sediment-water interface in cracks of their own manufacture. The fact that they can access surface sediments quickly (Blair et al. 1996), however, suggests that they can propagate cracks very near to or even to the sediment-water interface. Based on morphology and observation of a few individuals (P. A. Jumars, unpublished data), it may be that trichobranchids also feed similarly below the sediment-water interface. The morphology of magelonids is also strongly indicative of burrowing.

Most problematic for classifiers will be cirratulids and terebellids, which certainly across and perhaps within species, clearly span both the classical ideas of surface (sediment-water interface) deposit feeding and the newly identified guild of feeders on

surfaces created below the sediment-water interface by cracking. It is suggested that the majority of bipalpate cirratulids (and at least some other cirratulids) will be found to be crack makers and feeders, with some clear exceptions that make mudballs (Levin 1997)—and no doubt some more subtle exceptions.   Cirratulids also have been seen to access fresh phytodetritus quickly (Blair et al. 1996), again suggesting that the cracks they make may come close to the surface and perhaps cause subduction of surficial materials. A number of cirratulids and cossurids show a similar body plan in which segments are many and long. These species generally have muscular expansions near both the prostomium and the pygidium. The analogy is striking to a long train with an engine at either end; it is far easier to pull from either end than to push when the burrowing direction is reversed.

Burrowing by liquefaction in sands is known in terebellids (Nowell et al. 1989). Morphology will help (e.g., the *Artacama* illustration; Figure 3.10B), but in situ and laboratory observations will be needed where stronger evidence is required. The crack-utilising guild across polychaete families most commonly bears some variety of expandable wedge, gills to deal with this likely low-oxygen environment of high, unsteady oxidant demand and tentacles or spines to free particles from the matrix for ingestion. Because they had no concept of burrowing by crack propagation, Fauchald and Jumars (1979) were inclined to associate tentacles with surface deposit feeding in the absence of evidence to the contrary. No such association should be assumed.

Biogeochemical implications of fracture in marine muds include potential release of macromolecules trapped in the organic matrix and preferential access to some areas of sediment resulting from microscale differences in adhesion. Diffusion through a gel is

slowed little from that through the ungelled liquid for small molecules, but molecules larger than the pore size can be trapped in the matrix. Cracks may release trapped macromolecules for consumption or for diffusion or advection through or out of the sediment. Cracks propagate in the direction of least resistance, which suggests that animals preferentially follow a path recently cracked or containing less cohesive or adhesive material. Research on the dependence of K_{Ic} on organic content and lability of sediments could lead to predictions either of preferential ingestion of organic material or the possibility of pockets of sticky organic material sequestered from deposit feeders. The interface of a membrane-encased, compacted fecal pellet may cause cracks to go around the pellet, leaving it intact and the encased material unavailable to deposit feeders.

Biogenic, discoidal cracks do not appear to have been reported from the fossil record (Jumars et al. 2006). Perhaps they close and anneal quickly, but given their unexpected shapes (Johnson et al. 2002) no one may have thought to link such cracks with a biogenic mechanism. The existence of this mechanism of burrowing muddies the distinction between surface and subsurface deposit feeding, particularly if cracks are found to propagate close enough to the sediment-water interface that newly deposited materials can fall in. Moreover, the mechanical similarities between feeding on the sediment-water interface and feeding on a newly created surface in a propagated crack make it very likely that many species can do both.

3.7.6. Methodological considerations

Crack propagation is facilitated along an interface for which adhesion between the two materials is less than the cohesion in one material (Figure 3.5) (Cook & Gordon

1964). This phenomenon has direct relevance to marine sediments, both naturally in the presence of boulders and in observations and experimental designs involving walls in both lab and field studies. Benthic observational tools include transparent aquaria, time-lapse, sediment-profile imagery (Diaz & Cutter 2001, Solan & Kennedy 2002) and planar oxygen sensors (Koenig et al. 2001), all of which involve observing a 2-D vertical section of sediment through a rigid, glass barrier. These studies implicitly assume that the observed animals are representative of the community. However, the sediment-glass interface facilitates crack propagation along the interface, while the solid boundary allows worms to exert higher stresses with the displacement caused by pharyngeal eversion. Because of these two factors, it is likely that many burrowers in muds congregate at glass walls, resulting in overestimation of community abundance and activity in long-term studies. This increased activity may result in overestimation of bioturbation rates in laboratory studies, with wall effects increasing with decreasing container size. Both *Nereis virens* and *Yoldia* sp. burrowing in aquaria of gelatin tend to end up against a wall or the bottom and then follow the wall. Although gelatin makes these observations clearer, congregation near aquarium walls is frequently observed in natural sediment as well. The crack-shaped burrow extends further from *Nereis* burrowing against an aquarium wall than in the middle of the aquarium (8-10 cm from the wall) (Figure 3.14) (K.M. Dorgan, unpublished data).

Walls may have the opposite effect on animal distributions in granular materials. Because stress chains branch with distance from a point force, the area over which the force is distributed becomes much smaller closer to a wall with fewer stress chains to bear the load. In an elastic solid, the rigidity of a solid boundary allows the animal to
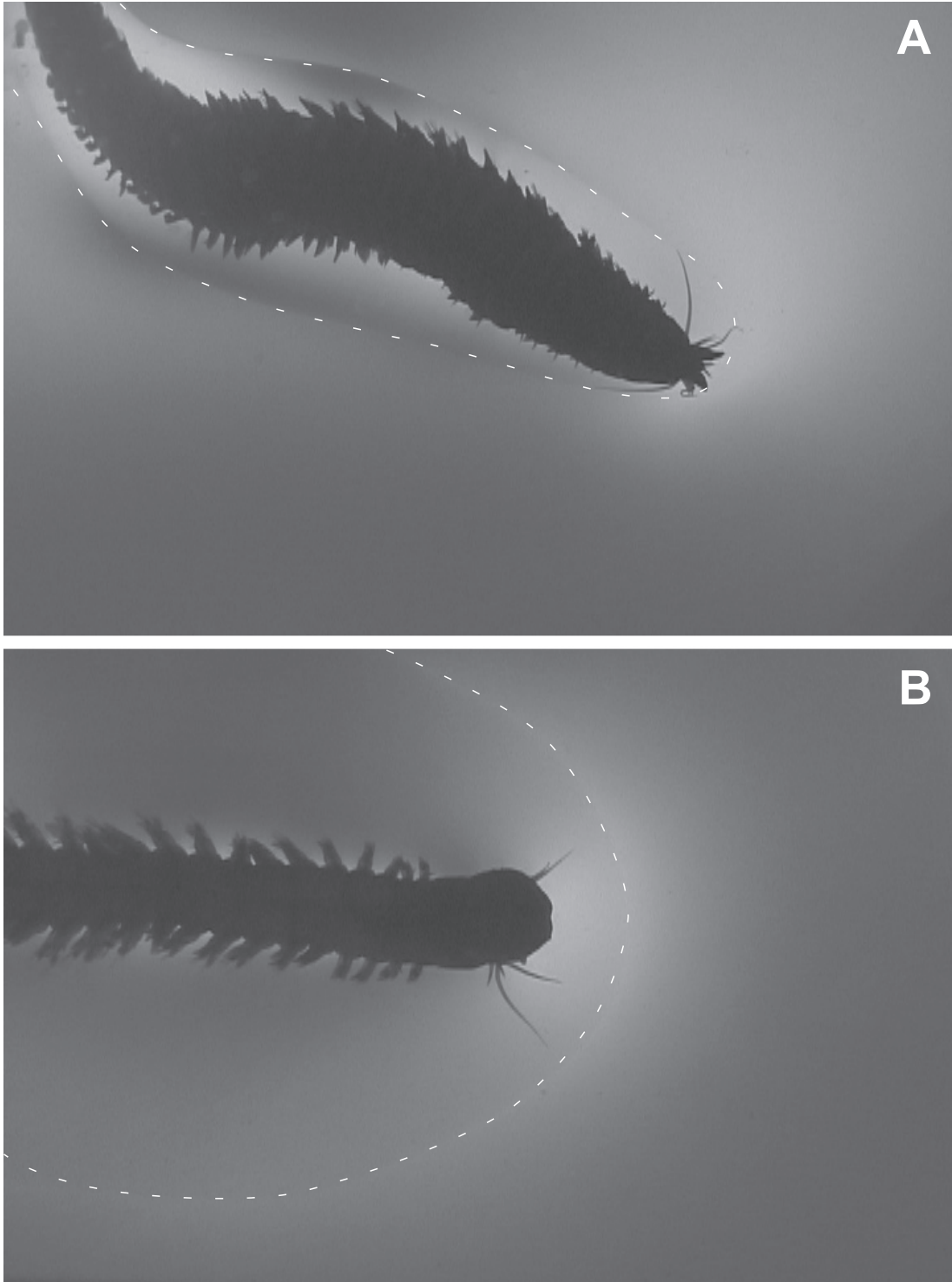
Figure 3.14. Burrow shape of *Nereis virens* in gelatin near a glass wall. A) Burrow shape of *Nereis virens* in gelatin 8-10 cm from glass wall compared with B) against glass wall of aquarium (K.M. Dorgan, unpublished data).

exert greater stress with a given displacement and more easily propagate a crack, but resistance to grain displacements in a granular material increases with increasing pressure, which is increased through the presence of a nearby wall (Figure 3.15; Dantu 1957). Animals are therefore likely to be passively directed away from rigid boundaries in sands.

Size, density, and food quality of particle tracers have been considered in terms of food selection by deposit feeders (Self & Jumars 1988), which affects mixing rates, but not in terms of mixing by burrowing. Granular materials separate by grain size, with larger grains moving upward during mixing (Duran 2000). In adhesive sediments, tracer particles added to the surface will behave more discretely than particles bound in the polymeric matrix, and may be preferentially moved, leading to overestimation of mixing rates in tracer studies. Surface characteristics such as roughness and hydrophobicity as well as size and density of particles affect mixing rates in sediments with both elastic and granular behaviours and thus need to be considered as potential sources of artifacts in tracer measurements.

3.8. Summary and Future Directions

Mechanical constraints of sediments on burrowers provide new insights into anatomy and behaviour of individuals; burrowers in mud are generally wedge-shaped or have muscular anterior regions to extend their burrows by crack propagation. This fracture may be facilitated hydraulically, with expansions serving as both wedges and O-rings to drive fluid into the crack tip. Burrowers are functionally similar across phyla with vastly different anatomies. At the same time, burrowers in mud and sand are often
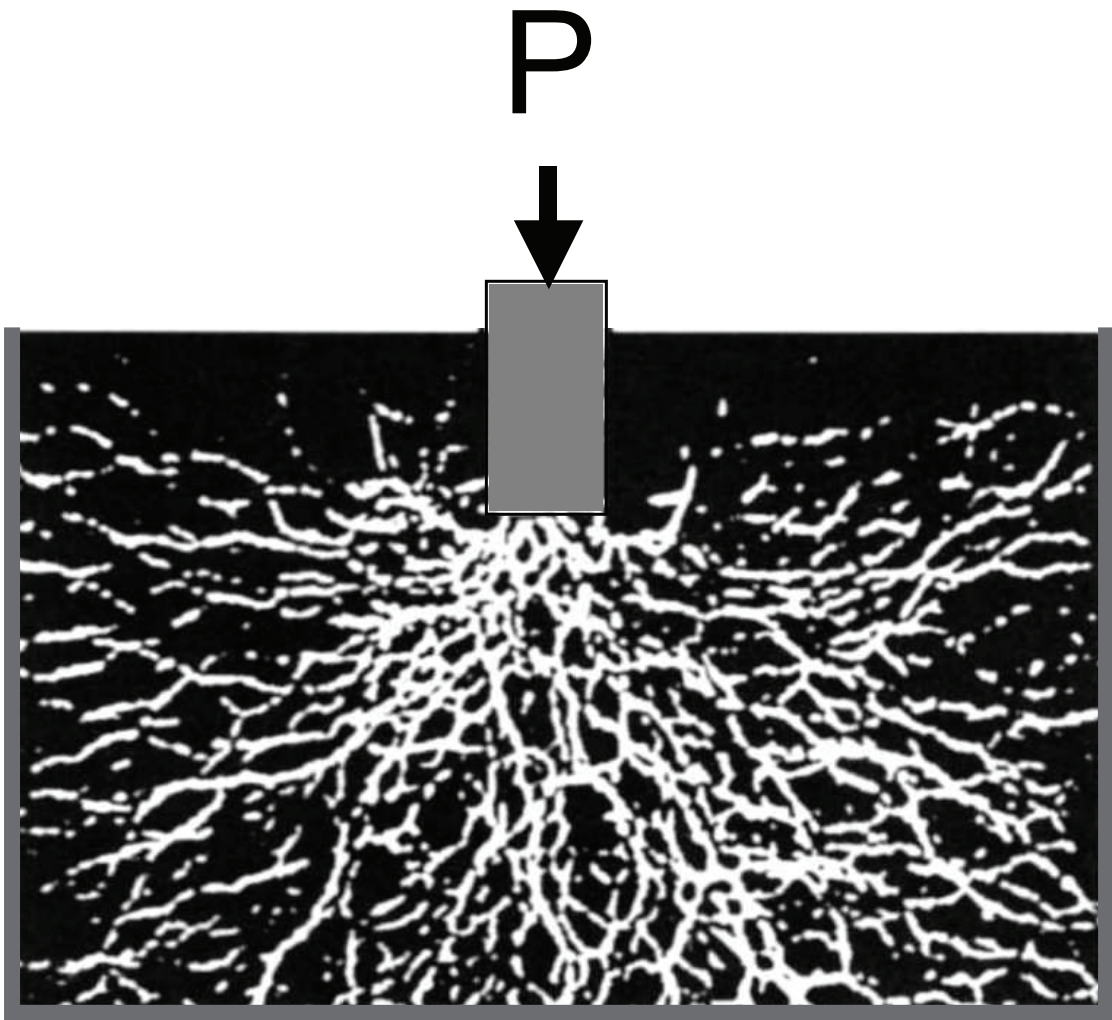
Figure 3.15. Light colored stress fields in a bounded granular medium, shown by photo-elastic stress analysis (Dantu 1957).

anatomically similar and have similar behaviours, but their physical mechanisms of burrowing differ between the two media.

In this review, behaviours and anatomies of burrowing animals are correlated with physical constraints of the sediment environment, but the observations are largely qualitative, and quantitative data are lacking. For example, amphipods are bubble-shaped, but do their aspect ratios match those predicted for bubbles in sediments? To what extent can interspecific differences in body shape be explained by differences in sediment properties? Obviously, the shapes need to be measured under the conditions in the burrow, not in a specimen bottle. Clearly there are trade-offs between energetics (cost increasing with deviation from the predicted aspect ratio, but how much?) and the need for gut (and other internal organ) capacity. Furthermore, the feedback mechanisms between behaviour of burrowers and sediment properties have not been quantified. For example, an animal may passively either follow or avoid the path of another animal depending on whether the trace left behind is a crack that has closed but not fully annealed (facilitating propagation of another crack-shaped burrow along the same path) or a cylindrical burrow with walls of compacted sediment (turning a crack away in another direction). An explicit mechanical model for burrowing provides a framework around which to generate and test such hypotheses.

Areas in which sediment mechanics should be included in benthic studies are also indicated. Most obviously, mixing of particles depends strongly on the material properties of the sediment. Particles behave discretely in granular sands, but the polymer matrix of muds holds nearby particles together, resulting in their non-independent mixing.

Key questions in furthering bioturbation research in muds are how, how often, and under what conditions a crack becomes a burrow. A crack that closes after an animal passes results in minimal particle mixing, whereas vertical cylindrical burrows cave in or fill with surface sediments. Bubbles have a flattened disk-shape and stay within the elastic limit of muds, but animals are much more three-dimensional. Animals may displace sediment beyond the elastic limit, resulting in permanent deformation and a cylindrical trace. Animals also actively line burrow walls with mucus, making them more permanent. The mechanical behaviour of heterogeneous, viscoelastic sediments depends on both temporal and spatial scales of deformations as well as stress history. Future research on the dependence of the stress-strain relationship on strain rate, time of deformation, and stress history will enable predictions about burrow formation.

Burrow formation is important in considering not only particle mixing, but also the biomechanics of burrowing. If sediment remains predominately elastic during the passage of an animal, the burrow will remain crack-shaped and the elastic restoring force will be important. This rebound would allow energy savings by storage of elastic strain energy and a reduced need for circular muscles in peristaltic burrowing.

Scaling is important not only in terms of the animal's size, but also the animal's size in relation to the grain size. Sediment heterogeneity is largely scale-dependent because infaunal sizes vary over orders of magnitude, and homogeneity may be largely a matter of perspective. Relative scaling of organisms and grain size becomes particularly important in the transition region between granular and elastic behaviour, and mechanical testing should be conducted on appropriate scales of both space and time. Granular materials can behave elastically on larger scales, whereas on smaller scales individual

grains are important and stress chains dominate behaviour (Goldenberg & Goldhirsch 2005). Moreover, much of the extensive literature on mechanical behaviours of viscoelastic solids and granular materials focuses on vastly different temporal or spatial scales and boundary conditions than experienced by burrowers. For example, equations governing fluidized beds are presented that are useful in gaining intuition, but their application to, for example, the small-scale unsteady pumping by *Arenicola* is questionable at best. They need modification for biological application.

In this review, we have speculated extensively about how mechanical properties of sediments may drive animal behaviour. Although it is known that burrowers in mud do propagate cracks and that cracks propagate in the direction of least resistance, it is not known whether animals necessarily move in that direction or can use sensory information and mechanical means to steer cracks. The application of a quantitative model to burrowing generates hypotheses based on predicted, energetically efficient behaviours. Energetic efficiency is only one component of animal fitness, and deviations from predicted behaviours suggest alternate fitness benefits.

An integrated approach to studying burrowing behaviour and resultant infaunal distribution, particle mixing, and geochemical profiles is essential to improving predictive capabilities. Burrowers both affect and are affected by material properties of sediments. Feedback mechanisms necessitate combining an explicit mechanical model of sediments with research on behaviour, including how closely animals follow predictions. Despite the length of this review, it has barely scraped the surface of the rich interactions that can be anticipated when realistic, quantitative descriptions of material properties of sediments are coupled with analyses of animal mechanics and behaviours.

Chapter 4

BURROWING IN MARINE MUDS BY CRACK PROPAGATION: KINEMATICS AND FORCES

4.1. Chapter Summary

The polychaete *Nereis virens* burrows through muddy sediments by exerting dorsoventral forces against the walls of its tongue-depressor-shaped burrow to extend an oblate hemispheroidal crack. Stress is concentrated at the crack tip, which extends when the stress intensity factor (K_I) exceeds the critical stress intensity factor, K_{Ic}. Relevant forces were measured in gelatin, an analog for elastic muds, by photoelastic stress analysis to be 0.015 ± 0.001 N (mean $\pm$ s.d.; n = 5). Measured elastic moduli (E) for gelatin and sediment were used in finite element models to convert forces in gelatin to those required in muds to maintain the same body shapes observed in gelatin. The force increases directly with increasing sediment stiffness, and is 0.16 N for measured sediment stiffness of $E = 2.7$ x 10^4 Pa. This measurement of forces exerted by burrowers is the first that explicitly considers the mechanical behavior of the sediment. Calculated stress intensity factors fall within the range of critical values for gelatin and exceed those for sediment, showing that crack propagation is a mechanically feasible mechanism of burrowing. The pharynx extends anteriorly as it everts, extending the crack tip only as far as the anterior of the worm, consistent with wedge-driven fracture and drawing obvious parallels between soft-bodied burrowers and more rigid, wedge-shaped burrowers (i.e., clams). Our results raise questions about the reputed high energetic cost of burrowing and emphasize the need for better understanding of sediment mechanics to quantify external energy expenditure during burrowing.

4.2. Introduction

Burrowing animals dominate marine sediments that constitute 70% of Earth's surface. Burrowers are considered ecosystem engineers, significantly altering their environments and microbial activities (cf. Meysman et al. 2006). In spite of their numerical and biomass dominance, however, they have been underrepresented in the literature on animal locomotion. Progress has been limited in two ways: observationally (marine sediments being literally "clear as mud") and conceptually by a lack of understanding of sediment mechanics on spatial and temporal scales relevant to burrowing macrofauna.

Newton's third law is commonly applied in biological fluid dynamics, for example to estimate drag forces on a body by measuring the opposite force (exerted by the animal on the fluid), i.e., the rate of momentum extraction from the fluid. The Navier-Stokes equations permit this estimate through explicit fluid parameters of density and dynamic viscosity. In this subfield of continuum mechanics it would be inconceivable to study animal locomotion without considering these material properties. That no study has estimated forces and work of burrowing by reference to explicit parameters of the solid elastic (or viscoelastic) continuum through which burrowers move and against which metabolically fueled forces operate signals a rudimentary state of understanding.

Forces exerted by both marine and terrestrial burrowers have been measured in various ways, although no methods, to our knowledge, have yet explicitly considered sediment mechanics. Coelomic (internal) pressure has been measured with a cannula

through the body wall (e.g., Ansell & Trueman 1968, Seymour 1969, Seymour 1971, Trueman & Foster-Smith 1976, Hunter & Elder 1989). In many of these studies, burrowers were close to rigid walls so that behaviors could be observed (e.g., Seymour 1971, Trueman & Foster-Smith 1976, Hunter & Elder 1989). Close proximity to a rigid interface increases stiffness of the sediment against which the animal exerts forces (Dorgan et al. 2006). Measured internal pressures from which forces are calculated are higher near walls than animals would exert in the natural environment to achieve the same burrow/crack opening (body thickness). In addition to cannulae, Hunter & Elder (1989) used an isometric force transducer attached by hook and thread to the tail of the worm to measure "tail-pulling" force as an empirical measure of the work needed to overcome friction. Trevor (1978) used a diaphragm to separate sediment from water connected to a pressure transducer to measure forces exerted against the diaphragm by the anteriors of burrowing worms. Force transducers have also been used to measure anterior and radial forces (Quillin 2000). Diaphragms and force transducers, however, offer resistances different from natural soils or sediments. Similarly, internal pressures of worms crawling on the surface or moving in water (e.g., Seymour 1969) are not representative of internal pressures of worms burrowing in natural sediments (Dorgan et al. 2006).

Bubbles in muddy sediments create disk-shaped cracks that grow and permit bubble rise by fracture. Their growth and aspect ratios have been modeled using linear elastic fracture mechanics (LEFM) theory, indicating that muddy sediments behave in a linear elastic manner on these small time and space scales (and under force magnitudes) typical of burrowing behavior (Johnson et al. 2002, Boudreau et al. 2005). LEFM theory

considers three material properties for two-dimensional problems in which the material is isotropic and the crack is loaded only in mode I (opening or uniaxial tension): elastic modulus (E), critical stress intensity factor or fracture toughness (K_{Ic}), and Poisson's ratio (ν). E is a measure of stiffness and the constant that relates stress, σ (force/area), and strain, ε (elongation/original length), as $\sigma = E\varepsilon$ in a linear elastic, isotropic material undergoing uniaxial deformation. Poisson's ratio (dimensionless) is the negative of the constant of proportionality between longitudinal and transverse strain under uniaxial stress. An incompressible material such as gelatin has a Poisson's ratio of 0.5, whereas lower values of Poisson's ratio indicate higher compressibility. Mode I stress intensity, K_I, is the coefficient of the dominant term in the series expansion of the stress field at a crack tip under mode I loading, and is used to compare stresses at cracks of varying configurations under varying loading conditions. The crack propagates when K_I exceeds the critical value, K_{Ic}, the fracture toughness. Another way of stating the fracture criterion is that when energy release rate (G) exceeds resistance of the material (R), the crack grows. If energy release rate increases as the crack grows, growth is unstable (e.g., shattered glass), whereas if energy release rate decreases as the crack grows, growth is stable and stops when energy release rate falls below material resistance. Relevant fracture mechanics have been recently reviewed (cf. Dorgan et al. 2006, Mach et al. 2007) and can be found in textbooks (e.g., Anderson 1995).

Adhesive and cohesive forces of the mucopolymer matrix holding grains together (resulting in elastic behavior) dominate mechanics of muds, whereas clean, monodisperse sands are granular materials for which the weights of individual grains are more

important in determining contacts (Dorgan et al. 2006). Burrowing mechanics differ between the two media, and only muds are considered here.

The burrow around the polychaete *Nereis virens* Sars is a planar crack (shaped like a tongue-depressor) and extends laterally away from the worm, with elastic rebound of the medium compressing the worm dorsoventrally (Dorgan et al. 2005). The most recently produced crack segment is an oblate hemispheroid that propagates when the worm everts its pharynx to exert dorsoventral forces against crack walls. These forces concentrate stress at the crack tip, producing fracture when stress intensity exceeds the critical value, K_{Ic} (cf. Anderson 1995).

Using photoelastic stress analysis (cf. Harris 1978, Full et al. 1995, Dorgan et al. 2005), a technique once widely employed by engineers to observe stress patterns (cf. Durelli & Riley 1965), we measure forces exerted by *Nereis virens* burrowing in gelatin as a clear analog for muddy sediments. We quantify differences in relevant material properties between gelatin and muddy sediment and use finite element modeling to calculate forces exerted by the polychaete *N. virens* in muddy sediments from forces measured in gelatin. Finite element analysis has largely replaced photoelastic stress analysis to evaluate stress distributions in engineering applications, yet, as shown here, the photoelastic method remains useful in an experimental context. This paper gives the first estimates of forces exerted during burrowing in natural sediments that explicitly consider the mechanical properties of sediments.

4.3. Materials and Methods

4.3.1. Animals

To enhance visibility of stress fields, large (> 5 g wet wt.) specimens of *Nereis virens* were selected. Animals were obtained from Harbor Bait (Edgecomb, ME) and kept in containers of mud under flowing seawater until use.

4.3.2. Gelatin as a mud mimic

Elastic behavior has been described for saturated, muddy sediments (e.g., Hamilton 1971, Dvorkin et al. 1999), the behavior of which is dominated by the muco-polymer matrix in which mineral grains are suspended. More recently, Johnson et al. (2002) found bubbles in muddy sediments and in double-strength (2X) gelatin in seawater (28.35 g L^{-1}) to have similar aspect ratios and to move by fracture. From LEFM, this aspect ratio is

$$\frac{\delta_c}{a_c} = \frac{\pi^{1/2} K_{Ic}}{2Ea_c^{1/2}}$$

(equation 4.1)

where δ_c is the half thickness and a_c is the half length of the bubble when it begins to grow, and their ratio is the aspect ratio. K_{Ic} is critical stress intensity factor, and E is elastic modulus (Johnson et al. 2002, from their eq. 19). The bubbles are oblate spheroids, with half width close to a_c. We suspect that the similarity in behavior arises from dominance of the bulk material properties of muds by gelatin-like mucopolymers that link sediment grains. Gelatin, a textbook example of a linear elastic solid (e.g., Sperling 2001), has also been used as an analog in studies of hydraulic fracture in the earth's crust (e.g., Menand & Tait 2002, Rivalta et al. 2005).

Johnson et al. (2002) measured critical stress intensity factor (K_{Ic}) and elastic modulus (E) for seawater-gelatin and mud. For mud from Cole Harbor, NS, K_{Ic} is 280 to 490 Pa m$^{1/2}$ and for gelatin, K_{Ic} is 50 to 220 Pa m$^{1/2}$. They measured E of sediment as approximately 1.4 x 10^5 Pa and of gelatin as 1.5 to 10 x 10^3 Pa (Johnson et al. 2002, Boudreau et al. 2005). Considerable variation exists, and sediment has higher E and K_{Ic} than gelatin, but the ratios K_{Ic}/E coincide approximately based on ranges of values for the parameters, and bubbles observed in both media have predictable and similar aspect ratios (Boudreau et al. 2005). The relevance of sediment mechanics to burrowers has been recently reviewed (Dorgan et al. 2006).

Because aspect ratios of bubbles depend on the K_{Ic}/E ratio of the medium, it seems reasonable to assume similar dependence for aspect ratios and extensions of animals' crack-shaped burrows. One difference between gelatin and muddy sediment is greater loss of stored elastic potential energy in sediment than in gelatin, resulting in a lower relative elastic restoring force and less dorsoventral compression of the body in mud (see results). However, the total forces exerted by animals in sediment are higher because stiffness is higher, so elastic restoring forces may be comparable in the two media. We have observed difficulty by *Sternaspis* burrowing in gelatin (appearing compressed and often failing to burrow; K. M. Dorgan and P. A. Jumars, unpublished), but *Nereis* seems to burrow without obvious difficulty. We are working to develop a better analog, but have not yet formulated a better, isosmotic, non-toxic material with the transparency necessary for photoelastic stress analysis.

4.3.3. Measurement of material properties

To reduce variability in measured E for gelatin (Boudreau et al. 2005) and therefore reduce uncertainty in the input parameters to our finite element model, we conducted additional tests of E for sediment and gelatin. Because we are interested in burrowing rather than bubble growth, we tested sediments in the top 0.10 m rather than from deeper cores (cf. Johnson et al. 2002). Cores of muddy sediment (0.15 m diameter) were collected from Lowes Cove, Walpole, ME, at low tide, wrapped in foam to restrict disturbance, and transported to Orono, ME. Lowes Cove is typical of one of many diverse natural habitats of *N. virens*. A Vitrodyne V-1000 microtensile tester was used to measure force and displacement as a 0.025-m diameter cylindrical probe was lowered into the sediment at 5 x 10^{-4} m s^{-1}, close to the speed of pharynx eversion. We found little difference in the response over velocities from 5 x 10^{-5} to 5 x 10^{-3} m s^{-1}. The elasticity problem of a circular, rigid plate resting on a semi-infinite solid can be solved for the elastic modulus as

$$E = \sigma d \frac{1-\upsilon^2}{\Delta} I_p \text{ (Das 2001, his Eq. 8.53)},\qquad\qquad \text{(equation 4.2)}$$

where σ is stress [Pa], d the plate diameter [m], υ Poisson's ratio [dimensionless], Δ the resultant displacement [m], and I_p (= 0.79) the influence factor for the shape of the rigid plate.

For gelatin, E was calculated using Eq. (4.2) from displacements resulting from test tubes of known weights resting upright on the surface of aquaria used for experiments (aquaria being too large for the Vitrodyne tester). We also tested smaller containers of gelatin with the Vitrodyne tester (as described for sediment) for comparison.

4.3.4. Experimental setup

Gelatin, a birefringent material, was placed between two circularly polarizing filters of opposing polarizations, with a light source on one end and a camera on the other (Harris 1978, Full et al. 1995, Dorgan et al. 2005). When filters initially are lined up, no light passes. Stress in the material re-orients light in directions of maximal and minimal stress; that re-oriented light passes through the filter, showing up as a lighted region. Area and intensity of the resulting light and dark patterns are related to the state of stress in the material (Harris 1978).

The experimental setup (Figure 4.1) comprises a Just Normlicht (Weilheim/Teck, Germany) Smartlight 5000 photographic light table covered with first a green color filter (Rosco CalColor #4430, Rosco Laboratories Inc., Stamford, CT), and then a right-handed, circular polarizing filter (3M HNCP 37% R.H. S-10 x 0.030 in from Edmond Optics, Barrington, NJ). In front of the filter was a 20.8-L glass aquarium of double-strength (2X) seawater-gelatin (28.35 g L^{-1}). A CCD videocamera (Basler A622f, Exton, PA) (camera 1) with 6X close-focus zoom lens (Edmund Optics #52-274, Barrington, NJ) opposed the light table to record in lateral view images of the worm (defined as the y-z plane) at 7.5 frames per second (fps). On the lens were a 52-mm, green (061) color filter, then a 52-mm, left-handed (standard), circular polarizing filter. Because the Rosco color filter is a gelatin sheet, it was placed between the light and the polarizer; placing it between the polarizers would show stress in the color filter, interfering with images. An identical camera (camera 2) and lens at 90 degrees recorded the dorsal (or ventral) view of the worm (defined as the x-z plane) at 3.75 fps. A smaller light table (Porta-

Figure 4.1. Diagram of experimental setup. Two light tables are shown as yellow blocks on opposite sides of the aquarium (light yellow block in center) from the cameras. Camera 1 recorded the lateral view of the worm and camera 2 recorded the dorsal or ventral view. Schemes of the 2-D views of each camera are shown with corresponding axes, and the orientation of the worm in the crack is shown in the aquarium. Between the light table and the aquarium are a colored filter and a right-handed, circular polarizing filter with a left-handed, circular polarizing filter and another color filter between the aquarium and the camera. The circular polarizing filter is shown here as a linear polarizing filter with a quarter-wave retarder; actual filters combine the two components. Filters on the far side of the cameras completely covered the light tables with no other light passing through, and the filters on the camera side were attached to the lenses. Cameras were run from separate computers with LabView software. The defined coordinate system is used in all relevant figures.
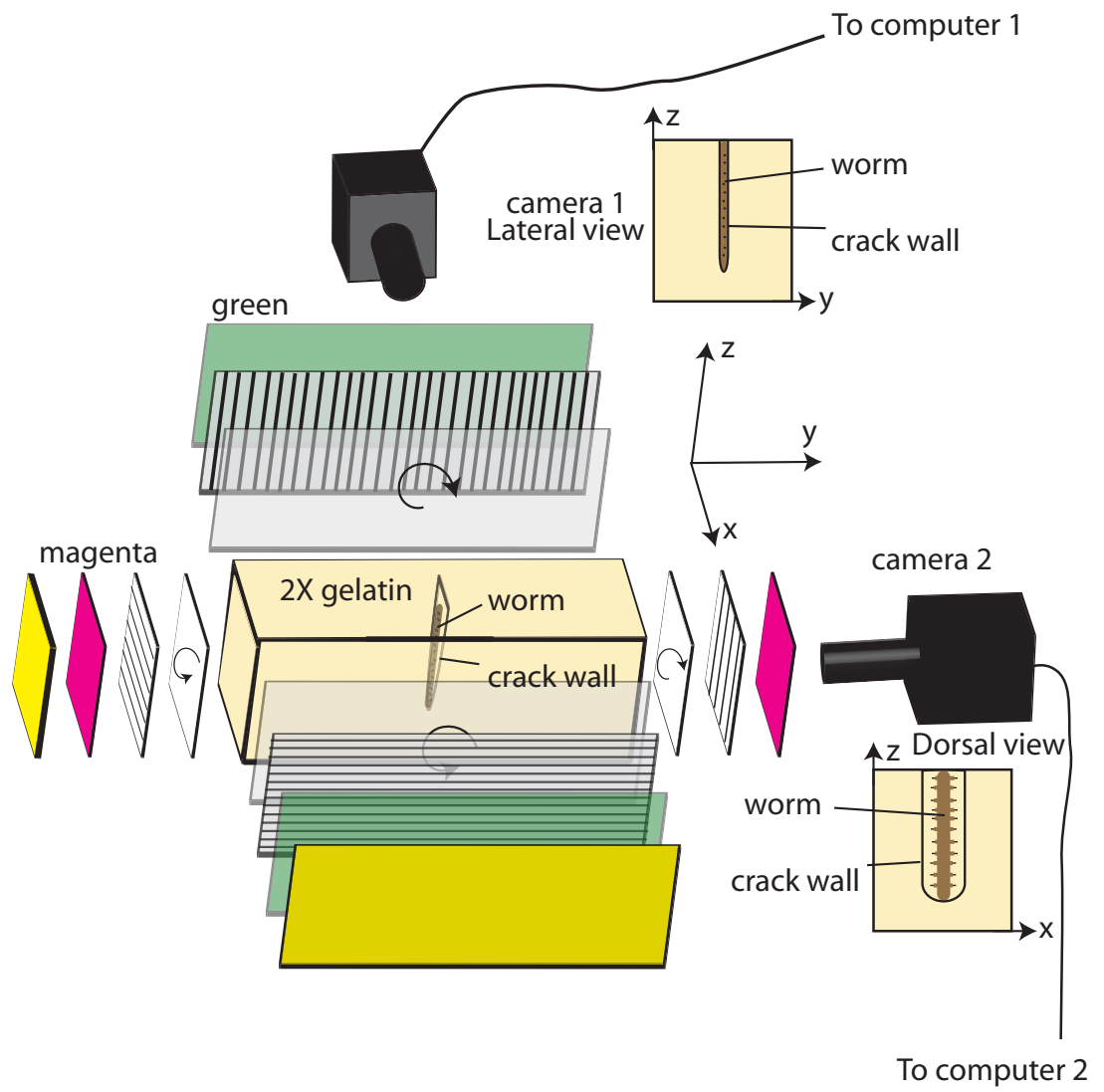
trace/Gagne 10 x 12 in) opposed camera 2 and was covered by a magenta filter (Rosco CalColor #4790), then a right-handed, circular polarizing filter. On the camera lens were a 52-mm, magenta (CC30M) filter, then a left-handed (standard), circular polarizing filter. The color filters partitioned the light spectrum between the two cameras, avoiding interference from the orthogonal light source. Cameras were attached to separate computers, and videos were recorded digitally and analyzed using LabView software (version 7.1.1, National Instruments, Austin, TX, USA).

We used circularly rather than linearly polarizing filters (cf. Full et al. 1995) because circular polarizers show a larger lighted region (cf. Sharples 1981). Circular polarizers combine a linear polarizer with a quarter-wave retarder (Figure 4.1). Our images show a single patch of light resulting from a force, and the area of the light field is proportional to the force.

Experiments were conducted in a cold room at 11°C. The only light sources were the photographic light tables, which were completely covered with the filters. Food-grade gelatin (www.bulkfoods.com) was made with seawater boiled to reduce viable bacteria and set overnight (12-36 h) in the cold room.

4.3.5. Calibration

Each tank of gelatin was calibrated using test tubes resting upright on the surface with volumes of water added (0.2 – 4.0 mL) as known weights. Aperture and zoom of the camera lens were set before each calibration and kept constant throughout experiments. Images were captured for each weight, and force regressed against number of pixels lighter than a threshold value for each tank (Figure 4.2; see appendix B).
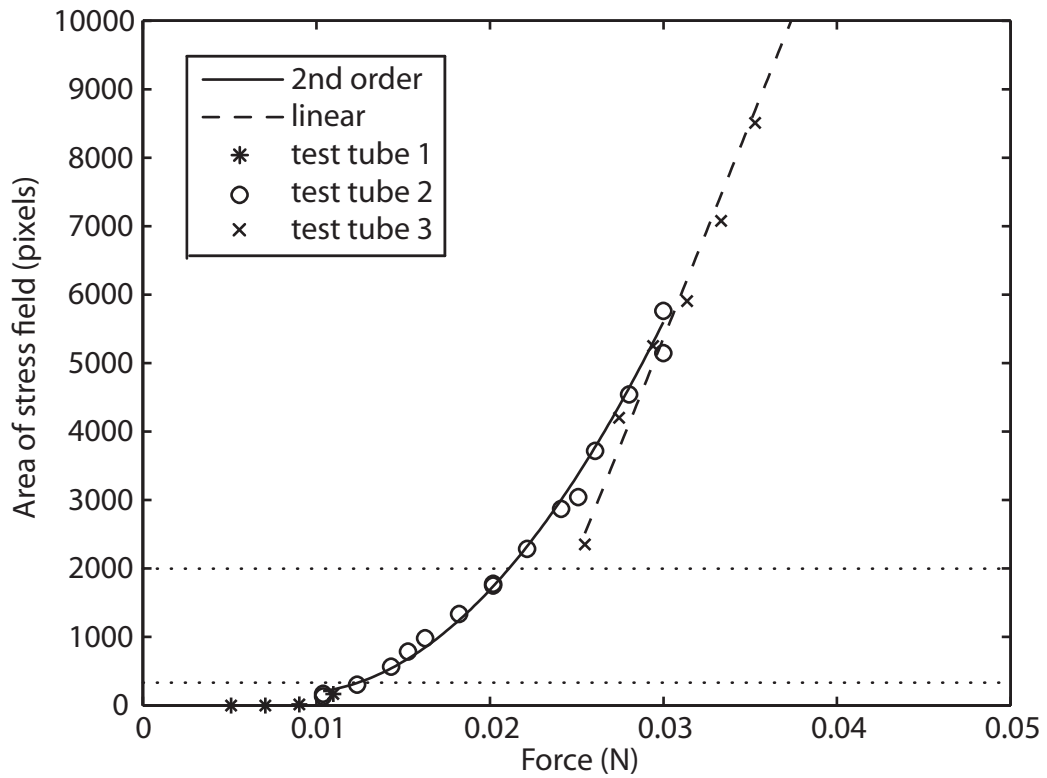
Figure 4.2. Calibration curve using three different test tubes (with water added) of known weights. Test tubes have the same diameter (0.01135 m), but were cut to different heights to reduce their weights, 0.52 (*), 1.1 (o), and 2.6 (x) g. A linear relationship exists for the larger test tube (x), but does not extend into the range of pixel areas around worms, indicated by the horizontal dotted lines. We instead used a second-order polynomial fit through the medium-sized test tube (o) that covered the range of observed pixel areas around worms ($r^2 = 0.997$, n = 11).

Thresholds were chosen for each tank to be as high as possible while lighting an area of $\geq$ 300 pixels on each side of the worm's everted pharynx. Photoelastic fringes, lines separating light from dark regions, indicate contours in the stress field. Because we worked with small stresses, we saw only primary fringes. There is a linear relationship between force and area of the primary compression fringe (Harris 1978, Full et al. 1995), but in our system that linear relationship holds for only a limited range of areas, with smaller stresses showing quadratic size changes. The observed area of the primary compression fringe is a 2-D projection of a 3-D stress field, and the order of the relationship is expected from mechanics to fall between linear (resulting from a large, distributed load) and quadratic (resulting from a point load). The range of pixel areas around worms falls mostly below the linear range, and a second-order polynomial was fitted (see appendix). We first digitally removed the light intensity gradient near the surface of the gelatin due to stress caused by evaporative shrinkage by subtracting an image taken after the test tube was removed, then adding a background pixel value. The background pixel value was an average of pixel values in an undisturbed dark region in the middle of the aquarium and was constant for all images used in a calibration. Images were analyzed with LabView.

Width of the test tube (0.01135 m) was chosen to make diameter of contact of the test tube with the gelatin surface (0.0053-0.0079 m, depending on weight) close to mean width and length of the worms' everted pharynges (0.0067 and 0.0068 m, respectively). The curved bottom of the test tube gave a distinct patch of light more similar in shape to the patches around the worms than did flat, rigid cylinders in preliminary tests. Test-tube

width provided a scale in the images to attach a length to the pixel dimension. Experimental validation of the calibration method is presented in appendix B.

4.3.6. Video analysis for kinematics

After calibration, a crack was initiated perpendicular to the view of camera 1 with forceps, and a worm emplaced. If worms pulled back out of the crack, they were gently replaced until they started burrowing. The macro lenses used have fixed focal lengths, so cameras were moved to keep worm distance from the camera constant.

We used only videos of the lateral view of the worm in which the plane of the crack was perpendicular to the lens of camera 1 (parallel to the x-z plane cf. Figure 4.1). Body twisting, diagnosed as a widening of the crack tip anterior to the worm, caused video rejection. If the worm moved toward or away from camera 1 (greater than 30° from vertical as observed with camera 2), light regions were too large (because some body stress lined up with the stress from the everted pharynx), and videos were rejected. To restrict wall effects, we used only videos in which worms were > 0.05 m away from all aquarium walls. At 0.05 m, the effect of the wall on K_I is approximately 10%, calculated by comparison to the exact solution for an edge crack in a finite-width plate.

Segments of video (3.75 fps) fitting the above criteria and the additional criterion that the camera was not moved (worm moved parallel to both camera planes) were used to measure frequency of pharynx eversion, distance moved between pharynx eversions, and resultant velocity. LabView was used to measure coordinates of the anterior tip of the worm, the crack tip, and width of the pharynx.

4.3.7. Force measurements

Frame grabs around each pharynx eversion fitting the above criteria were converted to binary images, and pixels above threshold counted in LabView. Compressional stresses on dorsal and ventral sides of the pharynx were analyzed separately because a separate force was applied to each crack wall. Thresholded images show on each side primary compression fringes produced by the pharynx, tension at the crack tip and, in some images, internal body pressure just posterior of the everted pharynx (Figure 4.3). The 'kidney-bean' shaped tensile stress fringe agrees qualitatively with stress patterns at crack tips under stresses perpendicular to the plane of the crack. To measure force exerted by the everted pharynx, we included only pixels in the region of compressive stress. In some cases, compressive and tensile stress fringes were indistinguishable, and these images were rejected. Forces were calculated from number of pixels through the calibration curve.

Projected planar area of the pharynx could be measured directly from the corresponding images from camera 2 only when the worms were moving straight down in the aquarium (in an x-z plane). For consistency, we instead measured pharynx width from camera 2 and length from camera 1 and approximated planar area as an ellipse. Internal pressure of the pharynx was calculated as the average of the dorsal and ventral forces divided by the planar area of the everted pharynx.

Internal body pressure was calculated from lighted areas of high stress around dilated segments of the body (that could be seen moving anteriorly as a peristaltic wave). Light regions were smaller and less intense than around the pharynx, so lower thresholds were used on the same images from the calibration. The area exerting the force was
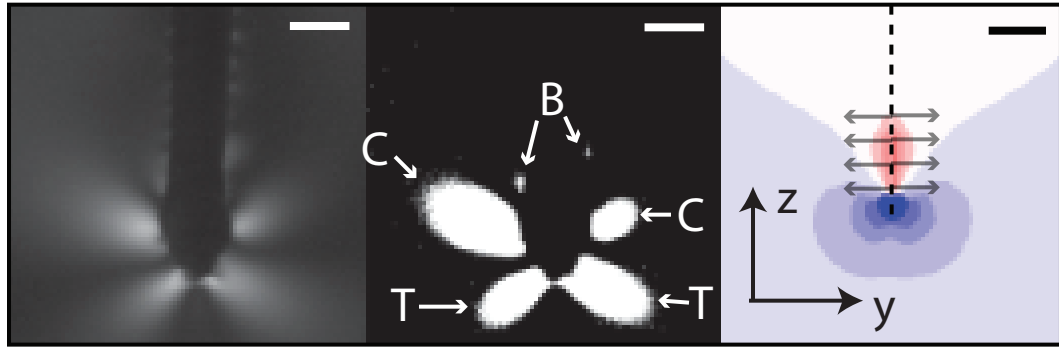
Figure 4.3. Video frame of pharynx eversion and corresponding thresholded image (frames from camera 1, the y-z plane). In the thresholded image, the small upper patches of light are posterior of the pharynx and result from body stress (B). The lower patches that join in the middle indicate tensile stresses (T) at the crack tip. Tensile stresses are shown in blue in the image of stress contours resulting from modeled stresses along the crack tip (right frame). Central patches in the thresholded image indicate compressive stress (C) from the force of pharynx eversion, and are the only pixels included in force calculations. Compressive stress is shown in red in the modeled image (scale bar = 0.005 m).

calculated as the planar area of one peristaltic wavelength, the product of the width of the worm (from camera 2) and the length of the region exerting the stress, measured as the distance along the worm between two regions (measured from the middle of the contact area of each). Internal pressure was calculated as the force divided by this area. Most of the visible stress was in the anterior of the body; very little stress was visible in the posterior. Stress was rarely visible in the absence of a clear peristaltic wave. Because we measured only visible stress, our measurements are closer to stress maxima than to averages.

4.3.8. Finite element modeling of the worm

Internal body pressure and pharynx pressure were used as inputs for finite element modeling of worm shape in gelatin with the program franc2d (Cornell Fracture Group, Cornell, NY). Franc2d is a two-dimensional, finite element modeling program designed for fracture that calculates both displacements resulting from applied stresses and stress intensity factors at crack tips. Because a worm burrows in 3-D and the model is only 2-D, we developed two models for two different views of the worm: lateral (y-z plane) and anterior (x-y plane). Both models ran in plane strain mode, which assumes that the thickness of the material was large (i.e., not a thin plate) and that all loads, geometric parameters, and solution fields were independent of the through-thickness coordinate. They can only approximate actual 3-D configuration of the burrowing worm, but results discussed later show that a 2-D analysis provides important insights into burrowing mechanics.

We first developed the lateral-view model, a rectangular geometry with the dimensions of the front (camera 1) view of the aquarium. Preliminary models of only the worm's pharynx greatly underestimated displacements, but modeling the worm's body (approximately the length of worms in gelatin during experiments) as well as the pharynx produced displacements much closer to those observed. An edge crack starting at the top surface extending half-way down the aquarium (0.1 m) represents the worm's burrow. Positions of the bottom and sides of the rectangle were fixed, assuming that the gelatin in the aquarium is stuck to the glass walls and does not move, as observed in experiments. Average stress exerted by the pharynx was applied to the crack walls from the crack tip to a point 0.00725 m behind the crack tip (the length of the crack wall needed to get a final displaced pharynx length of 0.00667 m; see results). Calculated internal body pressure was applied along the rest of the crack wall to 0.014 m from the top surface (model 1). Preliminary model trials showed that applying body stress all the way to the top lifted the top surface of the modeled tank much higher than observed in the aquarium of gelatin, likely because gravity is not included in the model. Because observed body stresses were visible only in the worms' anterior regions, the model was also run with linearly decreasing body stress (model 2), from the measured maximum body stress to the maximum stress that the worms could exert without producing visible stresses (intercept of the calibration curve). Because of the plane strain assumption, the model ignores lateral crack edges, potentially overestimating displacements.

To evaluate the importance of lateral crack edges as constraints on displacements, we developed an anterior model. A rectangular geometry was used with dimensions of the top of the aquarium. An interior crack of length 0.0066 m (the width of the worm)

represents the anterior view of the worm's burrow (model thickness equals length of worm). Bottom, top, and sides of the rectangle were fixed, as they represent the four sides of the aquarium. Calculated internal body pressure was applied to the crack walls. With stress kept constant over the original crack length, crack tips were extended by Δa and resultant maximum displacements (δ_{max}) calculated.

Stress intensity factors were calculated for the lateral model. The median value of three different methods of calculating K_I using franc2d was compared to the critical stress intensity factor for gelatin, 50 to 220 Pa m$^{1/2}$ (Johnson et al. 2002).

Stiffness in gelatin (E_{gel}) was then increased to that of sediment (E_{sed}), and Poisson's ratio (ν) was decreased from 0.45 to 0.3. Although gelatin is incompressible and has ν close to 0.5, we used a slightly lower value (0.45) to accommodate displacements in a plane strain model. Poisson's ratio for soils varies widely (from 0 to 0.5) depending on the soil type, confining pressure, and saturation state (Lade 2001). Saturated soils are incompressible, but observations of burrowing animals indicate that on these small spatial scales, forces result in compression of the solid-phase sediment by dewatering of the polymer-sediment matrix (explaining the presence of permanent burrows in sediments). Although Poisson's ratio for incompressible, saturated sediments is technically 0.5, the linear elastic model does not take into account dewatering on small spatial scales and longer time scales that result in small, permanent deformations (see results). Using a lower value of Poisson's ratio is not technically correct, but is a reasonable way to approximate nonlinearities using a simple linear model and worked well in our model validation experiments (see appendix B). We also calculated forces for a Poisson's ratio of 0.45 for comparison. We multiplied stresses measured in gelatin by

E_{sed}/E_{gel} to calculate approximate stresses that the worms need to apply in natural sediments to have the same body shape. Increased stiffness requires proportionally higher stresses to obtain similar displacements. These stresses were input into the model and resulted in larger displacements because Poisson's ratio had been decreased (increasing compressibility). We then reduced the stresses until displacements matched observed body thicknesses in gelatin. Pharyngeal stresses were then converted back to forces by multiplying by planar pharynx area. Stress intensity factors were calculated and compared to critical stress intensity factors for sediment, 280 to 490 Pa m$^{1/2}$ (Johnson et al. 2002). This modeling method was tested for a known system, and results are presented in appendix B.

4.4. Results

4.4.1. Measurement of material properties

Elastic moduli of muddy sediments (calculated from Eq. 4.2) were variable, $E_{sed} = (27 \pm 10) \times 10^3$ Pa (mean $\pm$ s.d.; n = 8). Although we used large cores (0.15 m diam.), there may be some wall effects, with overestimation of E. Removal of the core, however, caused sediment to settle considerably and expand radially. Because sediment was disturbed by the removal of the core and absence of constraint from surrounding sediments is more artificial than the constraining walls of the core, we did not use data from unconstrained cores. Values of E_{sed} decreased when the core was removed (from 1.57 to 1.05 x 10^4 Pa in one sample) as expected. We also removed surface layers from the unconstrained core and found that E increased with depth (from 1.05 to 1.61 x 10^4 Pa

at 0.01 m depth and 2.04 x 10^4 Pa at 0.03 m in one sample), but stayed near the range of variability observed across cores.

Elastic modulus for gelatin was $E_{gel} = (1.9 \pm 0.3)$ x 10^3 Pa (mean $\pm$ s.d.; n = 4). We also measured E in smaller (0.10 m diam., 0.10 m deep) containers of gelatin with the Vitrodyne V-1000 tester and found higher values of E (= 5.6 x 10^3 Pa) that we attribute to wall effects from the necessarily smaller container.

Representative loading-unloading curves (Figure 4.4) for mud and gelatin show elastic behavior for both materials. Gelatin is clearly linearly elastic, whereas the sediment curve shows lower resilience as well as a small plastic deformation following initial loading. Subsequent loadings remain elastic, however, and show slightly less loss of stored energy.

4.4.2. Video analysis and force measurements in gelatin

Mean distance traveled between pharynx eversions was 0.0073 ± 0.0018 m ($\pm$ s.d.; n = 6). Average time between pharynx eversions for worms that moved without stopping was 9.5 ± 3.8 s (n = 6), for an average velocity of (8.7 ± 3.5) x 10^{-4} m s^{-1} (n = 6) (Table 4.1). Worms sometimes stopped moving, but would often continue again after the tail was gently touched. Most worms exhibited consistent frequencies of pharynx eversions and distances traveled, and this behavior was similar for most worms observed (including the many samples eliminated because forces could not be measured). However, we observed one worm that traveled at approximately twice the velocity of average worms and did so with very few pharynx eversions. Unfortunately, this worm
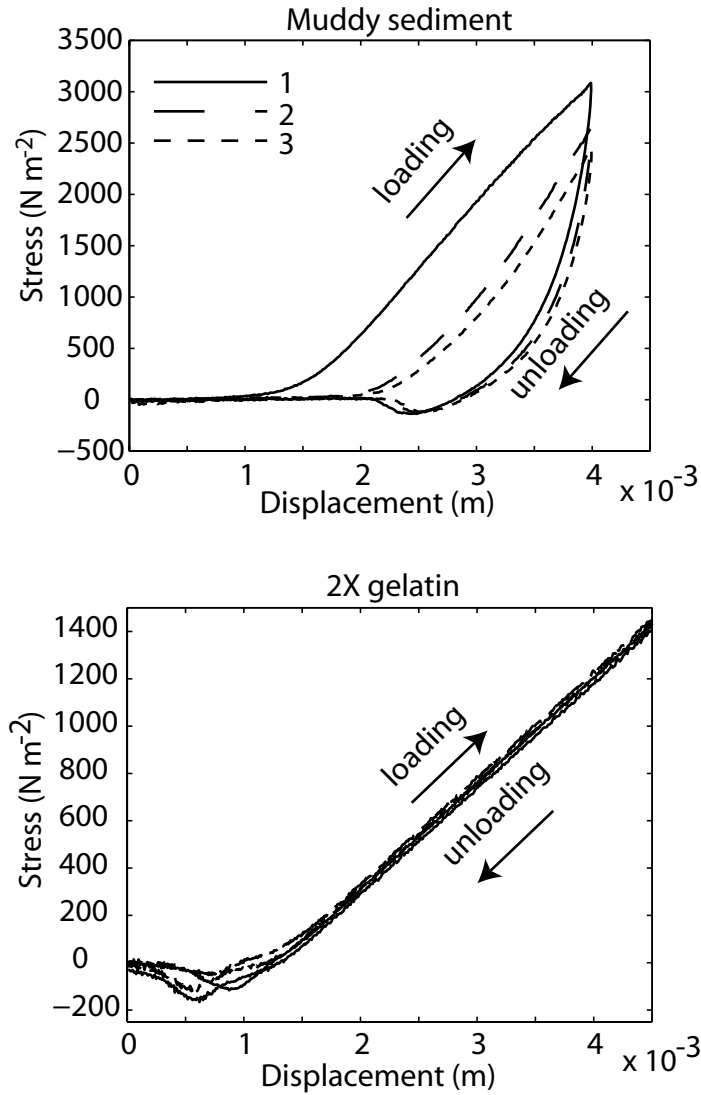
Figure 4.4. Loading-unloading curves for muddy sediment and gelatin showing linear elastic behavior for both materials. Force was measured as a 0.0254-m diam. cylindrical probe was lowered onto the surface of the material using a Vitrodyne-V1000 Universal Tester. Both materials exhibit linear elastic loading, although sediment shows a low resilience and a small plastic deformation after the first loading, visible as an approximately 0.5×10^{-3} m shift to the right from the initial loading curve to the second loading curve (also visible as a slight compression of the surface sediment, not shown). Subsequent loadings show minimal deformation.

Table 4.1. Kinematic data for individual worms. Time between pharyngeal eversions, distance traveled between each eversion, and resulting velocity is presented for individual worms (mean ± 1 s.d.).

Wet weight (g)	Time between eversions (s)	Distance traveled (mm)	Velocity (mm s^{-1})	N
5.1	5.7 ± 0.6	5.5 ± 0.8	0.96 ± 0.05	2
5.4	15.6 ± 2.6	7.6 ± 1.4	0.49 ± 0.09	3
5.5	7.6	10.2	1.3	1
6.9	6.9 ± 1.5	7.6 ± 0.8	1.1 ± 0.2	6
13.1	8.7	7.7	0.88	1
13.2	12.2 ± 1.7	5.3 ± 0.6	0.45 ± 0.08	5

was not oriented with the plane of the crack in line with camera 1, so forces and body width could not be measured.

A typical worm moves forward, extending the crack, then begins pharynx eversion while continuing forward and extending the crack. The crack tip does not extend beyond the anterior of the pharynx as it is being everted and moving in the anterior direction (Figure 4.5). The pharynx reaches its most anterior point before full eversion (Figure 4.5A). As the pharynx moves back and reaches its maximum width, the crack tip is visible. Between eversions, the worm moves its head from side to side within the plane of the crack, extending it laterally with the palps (see suppl. movie). Antennae often extend to and probe the crack tip, tracing its edge.

Forces exerted by the everted pharynx were measured for 6 worms, 5 of which exerted forces between 0.014 and 0.016 N (Table 4.2). The 6th worm exerted much smaller forces, 0.007 N, but pharynx width, length, and thickness were smaller than in other worms. Because we were looking for a maximum force exerted and it appeared that the sixth worm was not fully everting the pharynx (jaws not visible), we rejected that data point. Mean force exerted by the other 5 worms was 0.015 ± 0.001 N. Average pharynx area was $(3.7 \pm 1.1) \times 10^{-5}$ m^2 (Table 4.2). The 6 worms used had mean weight of 8.2 ± 3.9 g.

4.4.3. Finite element modeling results for gelatin

Displacements in the lateral model (Figure 4.6) are much closer to the shape (thickness) of the worm than displacements in the anterior-view model (Figure 4.7A), which are over an order of magnitude smaller than the thickness of the worm. Extending

106

Figure 4.5. A) Plot of worm movement, crack extension, and pharynx width over time for a representative worm. The position of the anterior end of the worm's head and the tip of the crack and the width of the pharynx (lateral view) were recorded from video frames at 3.75 frames s^{-1}. In one burrowing cycle, the worm begins to move forward, extending the crack, then everts its pharynx. Before the pharynx is fully everted, the worm's head and the crack tip reach the most anterior point, then the anterior end of the pharynx moves back as the pharynx everts completely. The worm then moves laterally within the crack (not shown) with little anterior movement before beginning to move forward again to repeat the cycle. One pharynx eversion is shown in greater detail in the lower graph. B) Sequence of images from one pharynx eversion as indicated by corresponding labels on (A). For each row, the left image is a lateral view (from camera 1, y-z plane) showing the stress fields, the center image is a thresholded copy of the left image, and the right image is the corresponding image from the dorsal view (from camera 2, x-z plane). Because the cameras were not run from the same computer, the images from the two cameras are nearly, but not perfectly, synchronous (scale bar = 0.005 m).

A

Worm movement and crack extension
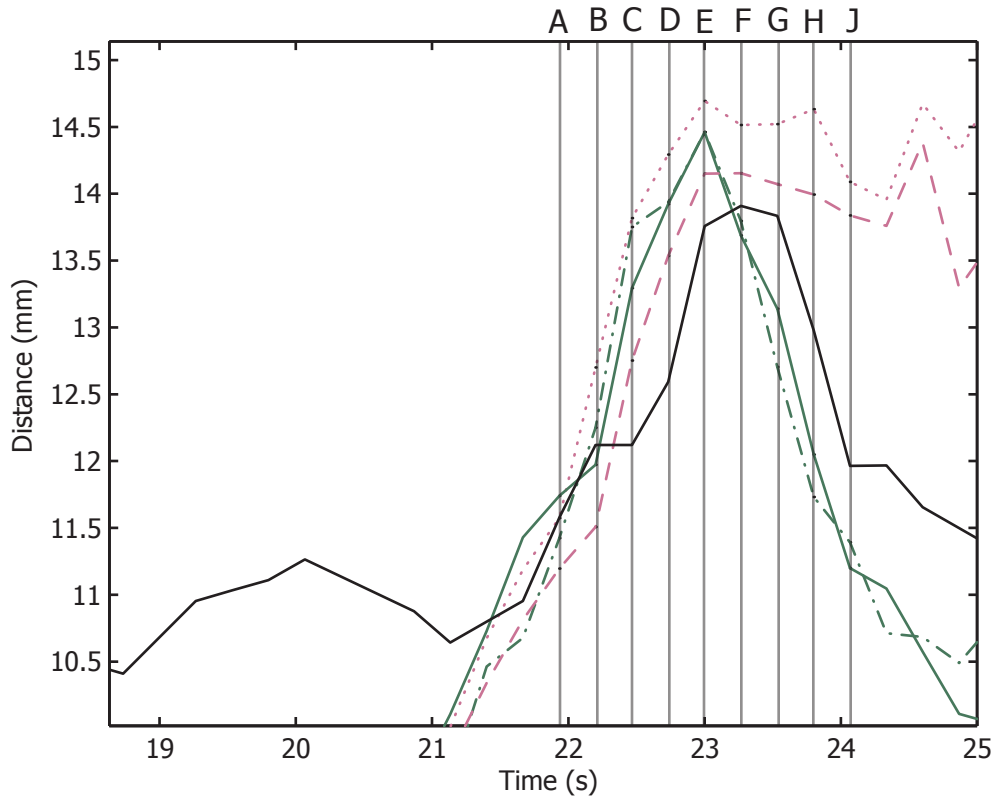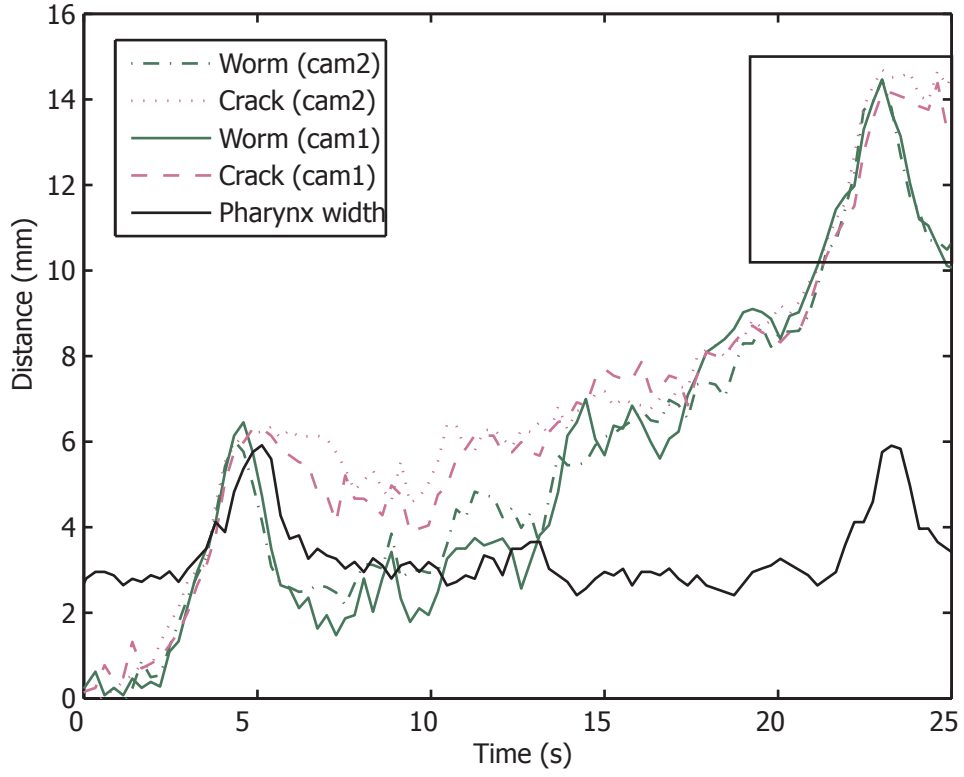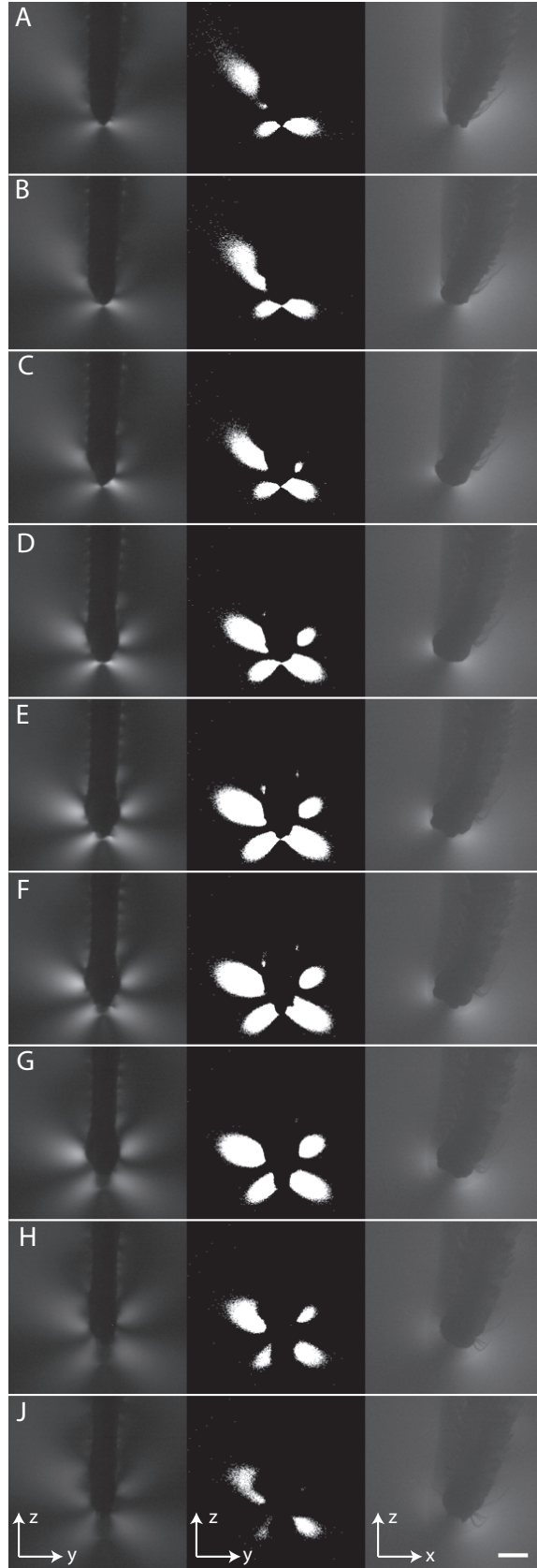
Table 4.2. Force measurements for individual worms. Force exerted, pharynx area, weight, and velocity is presented for individual worms (mean ± 1 s.d.).

Wet weight (g)	Force exerted (x 10^{-3} N)	Pharynx area (x 10^{-5} m^2)	Velocity (mm s^{-1})
5.1	6.8 ± 6 (n = 3)	2.1 ± 0.2 (n = 3)	0.96 ± 0.05 (n = 2)
5.4	16 ± 4 (n = 14)	3.3 ± 0.1 (n = 7)	0.49 ± 0.09 (n = 3)
5.5	14 ± 3 (n = 4)	3.0 ± 0.3 (n = 4)	1.3 (n = 1)
6.9	15 ± 2 (n = 15)	5.0 ± 0.3 (n = 7)	1.1 ± 0.2 (n = 6)
13.1	14 ± 2 (n = 10)	4.3 ± 0.3 (n = 5)	0.88 (n = 1)
13.2	16 ± 7 (n = 18)	4.4 ± 0.2 (n = 9)	0.45 ± 0.08 (n = 5)

Figure 4.6. Franc2d lateral model, a 2-D model of the y-z plane of the 3-D experiments. The displaced finite element mesh from model 2 (378 Pa pharynx stress, 92 Pa, linearly decreasing to 60 Pa, body stress) is shown in solid lines, and the original geometry with the crack is shown by dotted lines. The displaced mesh shows the shape of the worm in gelatin and the head region is enlarged below. The surface of the displaced mesh is slightly raised, a result of the displacements along the crack walls (scale bar = 0.005 m, magnification factor = 1).
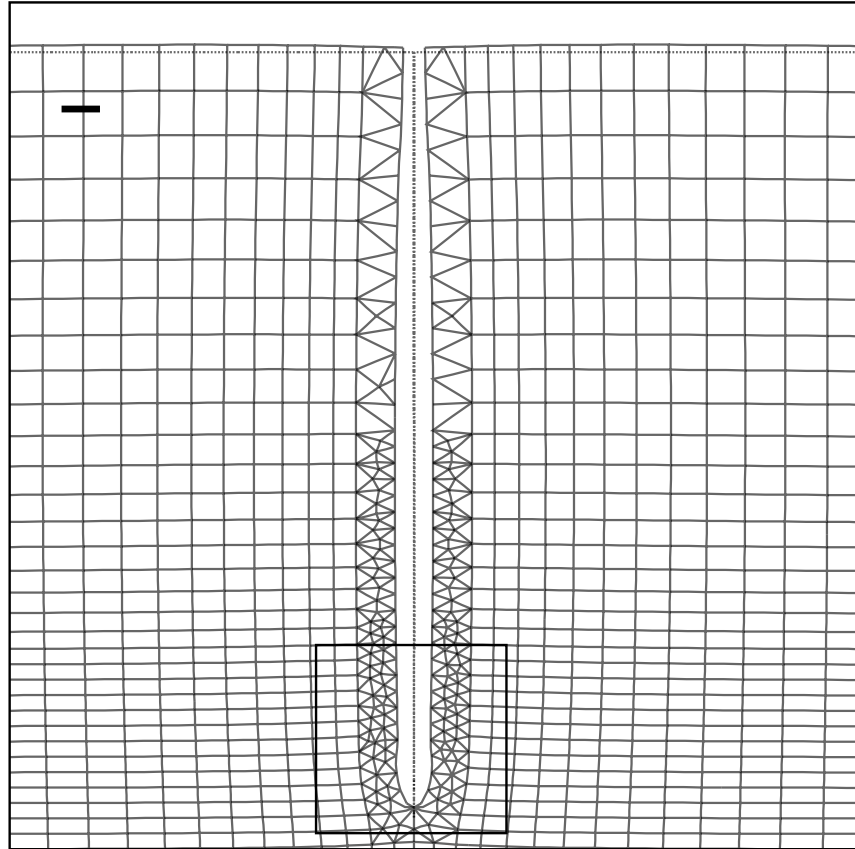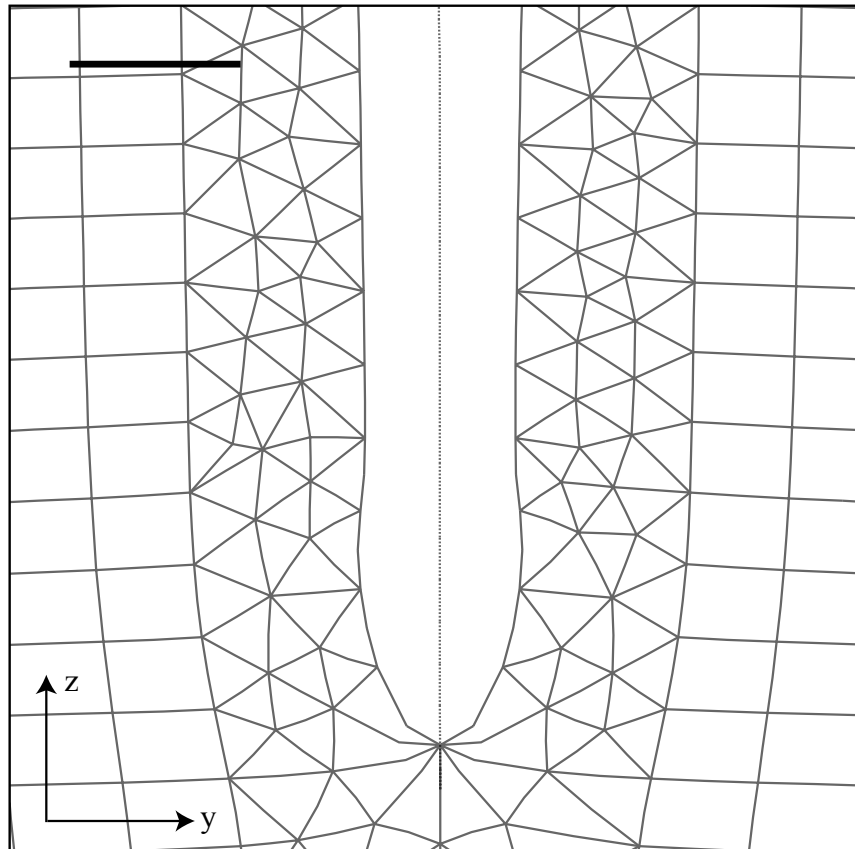
Figure 4.7. Franc2d anterior model, a 2-D model of the x-y plane of the 3-D experiments. A) Grey outline of deformed mesh is shown with maximum displacement (δ_{max}) and half-length of crack (a) indicated (scale bar = 0.001 m, magnification factor = 1). B) Change in maximum displacement in the anterior model as the crack is extended Δa at each tip. The dotted line at 0.0047 m indicates the measured distance from the worm's body to the lateral edge of the crack (data not shown).
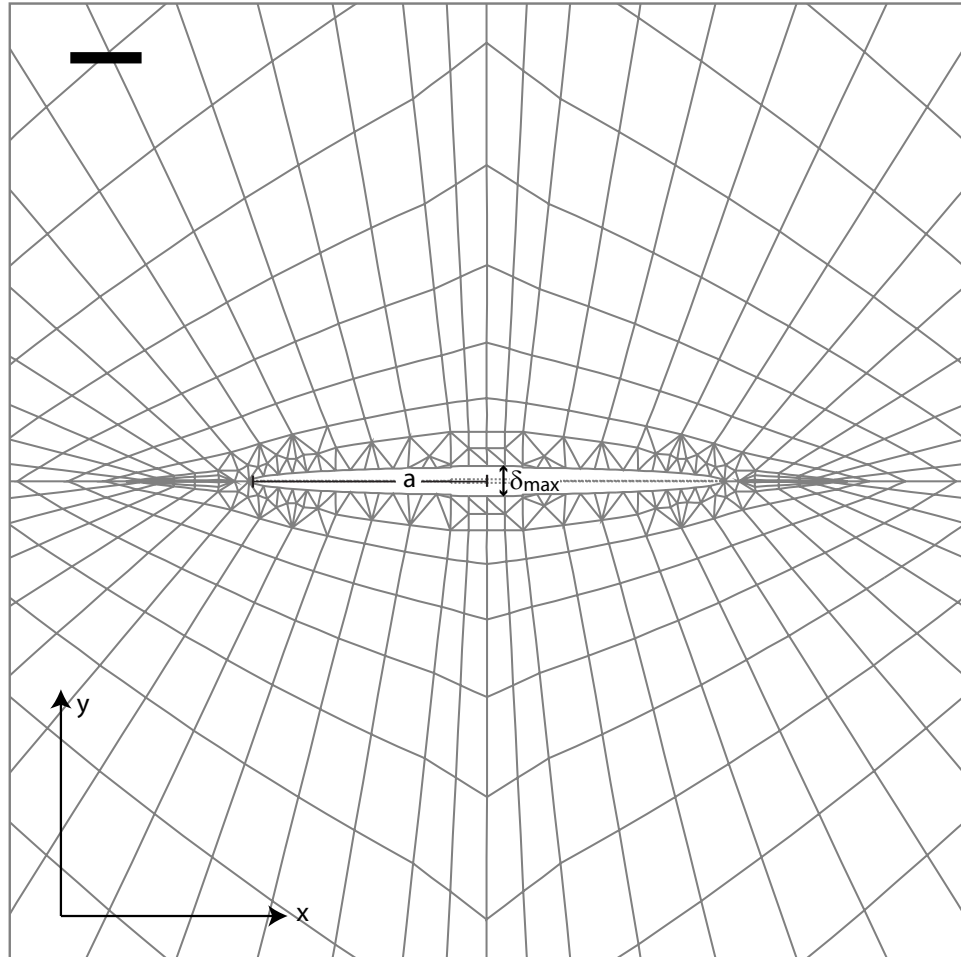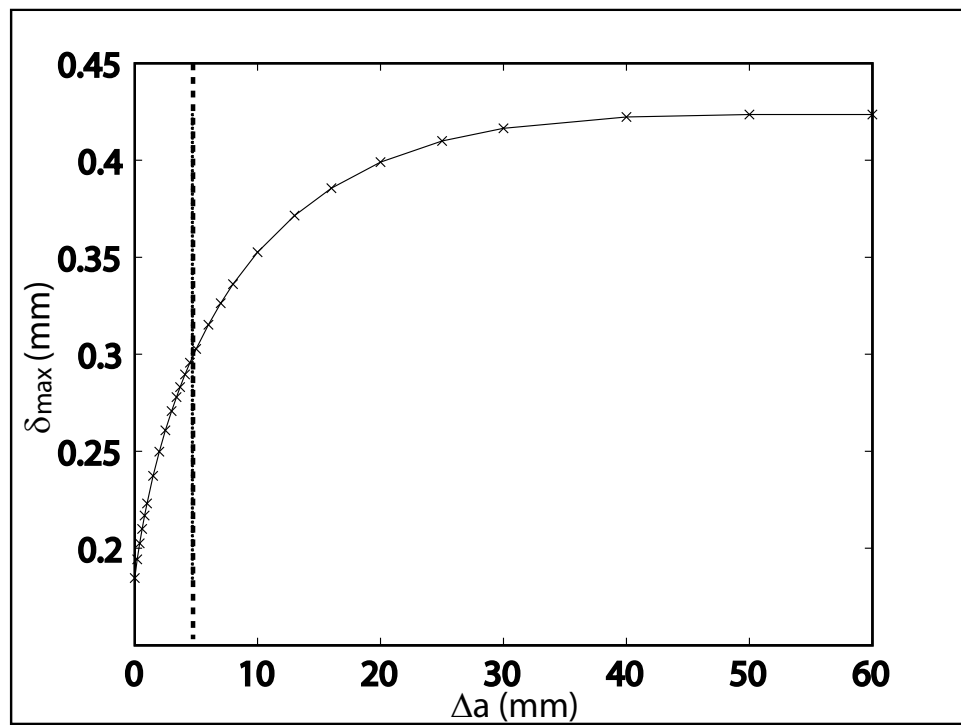
crack tips by Δa while leaving applied stresses constant increases modeled thickness, but maximum displacement reaches an asymptote after increasing by a factor of only 2 to 2.5, still much smaller than observed displacements (Figure 4.7B).

The two dimensions included in the 2-D lateral-view model are length and dorsoventral thickness, with the assumption that changes in the lateral direction, specifically the lateral crack edges, are unimportant in constraining the shape of the worm. We tested that assumption using the anterior model, in which lateral edges are present and maximum displacement increased as the lateral constraint was removed by extending crack width (cf. Figure 4.7B). The observed distance between the lateral edge of the worm's body and the lateral edge of the crack (visible in the right panels of Figure 4.5B) was 0.0047 m. At $\Delta a = 0.0047$ m, maximum displacement was 0.70 times that as Δa approached infinity, the assumption in the lateral model (cf. Figure 4.7B). Because the anterior model suggests that lateral edges were constraining thickness of the worm's body, we ran lateral models with constant (model 1) and linearly decreasing (model 2) body stresses reduced by this constraint factor of 0.70 (models 3 and 4). Decreasing body stress by the constraint factor resulted in decreased body displacements and slightly decreased pharynx displacements (Figure 4.8, Table 4.3).

Thicknesses of everted pharynges for observed worms are larger than the modeled displacements in the lateral-view model. We ran another model, extending the length over which the pharynx stress was applied from the average to the maximum observed pharynx length (model 5). Modeled pharynx thickness was larger than in the other models, but still smaller than observed thicknesses (Figure 4.8).
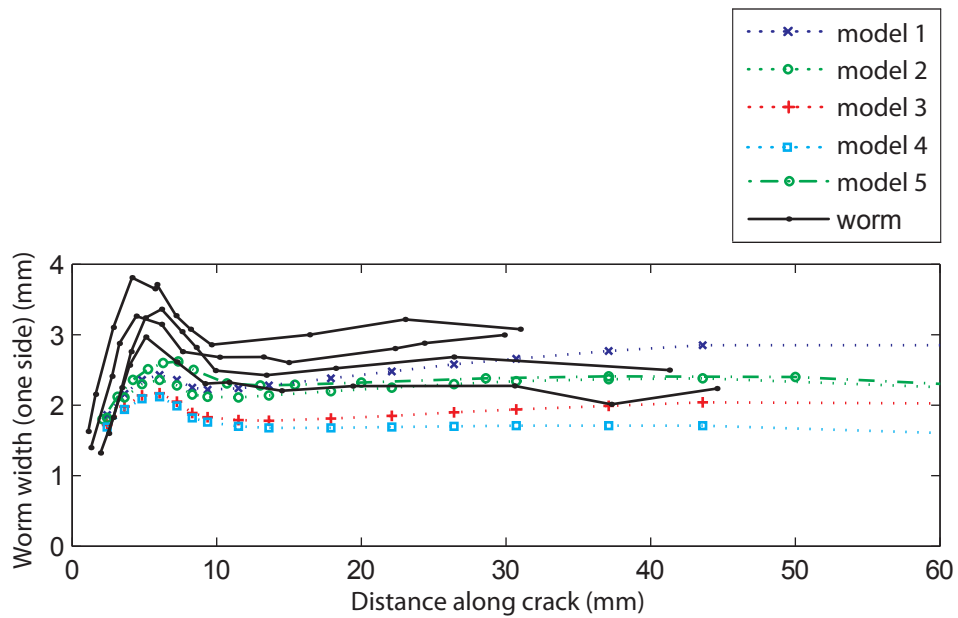
Figure 4.8. Worm width for different models and real worms (black). All five models have an applied pharynx stress of 378 Pa. Model 1 (blue dotted) has constant body stress of 92 Pa, model 2 (green dotted) has body stress linearly decreasing from 92 to 60 Pa, model 3 (red dotted) has constant body stress corrected for the lateral constraints to 64 Pa, model 4 (cyan dotted) has body stress corrected for the lateral constraints to 64 linearly decreasing to 42 Pa. In models one through four, pharynx stress is applied from the crack tip to 0.00725 m, resulting in a pharynx displacement equal to the average pharynx length observed, 0.00667 m. Model 5 (green dashed) has the same stresses as model 2, but the pharynx stress extends to 0.00839 m, resulting in pharynx displacement equal to the maximum pharynx length observed, 0.00779 m (Table 4.4).

Table 4.3. Stresses applied for the five finite element models with resulting maximum pharynx thicknesses and stress intensity factors.

Model	Pharynx length (mm)	Pharynx stress (Pa)	Body stress distribution	Body stress (Pa)	Maximum pharynx thickness (mm)	K_I (N m$^{-3/2}$)
1	6.67	378	Constant	92	2.43	62
2	6.67	378	Linearly decreasing	92 to 60	2.36	61
3	6.67	378	Laterally constrained	64	2.17	58
4	6.67	378	Laterally constrained, linearly decreasing	64 to 42	2.12	57
5	7.78	378	Linearly decreasing	92 to 60	2.62	64

Stress intensity factors for the five models (Table 4.3) ranged from 57 to 64 Pa $m^{1/2}$, within the range of critical stress intensity factors for gelatin, 50 to 220 Pa $m^{1/2}$ (Johnson et al. 2002). This result supports the use of the simplified lateral model, and more importantly validates the mechanism of burrowing by crack propagation as mechanically feasible. Worms are capable of generating stress intensities that can drive crack growth.

4.5. Discussion

4.5.1. Finite element modeling results for gelatin

Modest discrepancy between observed and (lateral) modeled displacements is reasonable considering simplified, 2-D, plane-strain approximation of the 3-D observations and considerable variability in material properties included in the model. In the model, stresses are applied perpendicular to the crack, whereas stresses applied by the worm as the pharynx everts likely have radial components. Stresses in other directions could not be included in the model, which is run in a single step. The worm pushes the pharynx forward, which could explain why observed pharynges are thicker than model predictions. Also, in the model, constant stress is applied over the entire pharynx area, but the force may be applied over a smaller area than the measured planar pharynx area and is unlikely to be evenly distributed over that smaller area. More focused modeled stresses would result in a more pronounced displacement peak. Variation in measured E for gelatin could explain some of the discrepancy, and there are likely other sources of error in approximating a 3-D process with a 2-D model. One specific example is the use of Poisson's ratio (ν) of 0.45 instead of 0.5, the value for an incompressible material. An

incompressible material in plane strain with fixed walls cannot deform because there is nowhere for the deformed material to go; setting $v = 0.5$ unsurprisingly caused the program to crash. Using a lower value of Poisson's ratio suggests, incorrectly, that the gelatin is compressible, but is necessary for the 2-D model to work at all; this compressibility in the model roughly equates with gel expansion upward in the real aquaria.

An alternative explanation is that error lies not in the modeling assumptions, but in measured forces input into the model. It is possible that the force measured from compression fringes may be slightly underestimated because the compressive stress fields might be affected by the tensile stress field at the crack tip. We believe that this error, if present, is very small because the compressive stress regions are small and usually appear to be clearly isolated from the tensile stress fields. It seems much more likely that the discrepancy comes from the simplifying assumptions of the model rather than experimental error.

Given potential sources of error in the model, displacements in all five models are reasonably close to observed values, and modeled stress intensity factors fall within the range of K_{Ic} for gelatin, adding support to model representations of experimental results. Unfortunately, results from the five models (Figure 4.8, Table 4.3) were not close enough to observed worm shapes, which themselves showed extensive variability, to determine which model is most appropriate. All five use the same value of pharynx stress; although body stress does affect pharynx width, differences are not critical in using the model to convert forces exerted in gelatin to those in natural sediments. If we assume that the discrepancy between modeled and observed worm shapes results from simplifying

assumptions in the model, it is reasonable to further assume that the same discrepancy will occur in modeling a worm in natural sediments. It follows that any of the models could be used to convert forces from gelatin to natural sediments as long as the shape of the worm in the sediment model matches that in the gelatin model.

4.5.2. Calculation of forces exerted in natural sediments

We selected model 2, with unconstrained, linearly decreasing body stress to calculate force exerted by the pharynx in natural sediments. We increased E from E_{gel} (= 1.9 kPa) to E_{sed} (= 27 kPa), decreased ν from 0.45 to 0.3, then calculated new stresses by multiplying stresses in the gelatin model by E_{sed}/E_{gel}. Pharyngeal stress was increased from 378 to 5305 Pa and body stress from 92 (linearly decreasing to 60) to 1291 Pa (linearly decreasing to 842). Applying the new stresses to the model resulted in larger displacements than in the gelatin model because of increased compressibility (from the change in Poisson's ratio), and stresses were scaled down to obtain a similar worm shape (Figure 4.9). Stresses applied in the final model were 4408 Pa for the pharynx and 1073 Pa (linearly decreasing to 700) for the body. We then multiplied pharyngeal stress by average pharynx area, 3.7×10^{-5} m^2, to calculate force exerted to propagate a crack in natural sediments, 0.16 N.

We followed similar methods to obtain the force for $\pm$ 1 s.d. of the elastic modulus for sediments, $(2.7 \pm 1.0) \times 10^4$ Pa. The forces needed to match the modeled displacements for $E = (1.7$ and $3.7) \times 10^4$ Pa are 0.10 and 0.22 N, respectively. We also calculated the force required for $E = 1.39 \times 10^5$ Pa to be 0.83 N, as measured in deeper sediments (Johnson et al. 2002). We followed the same procedure without changing
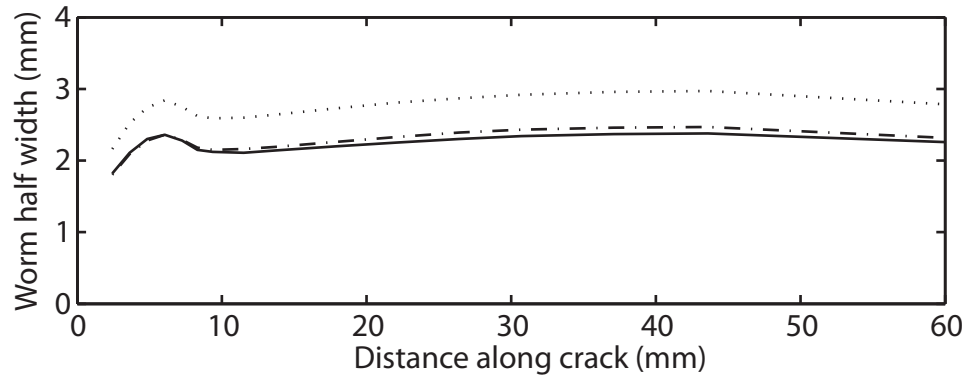
Figure 4.9. Worm width for model 2 in gelatin and in natural sediment with calculated stresses. The solid line is the worm width in gelatin (green dotted line in Fig. 4.8), with pharynx stress of 378 Pa and body stress 92 Pa, linearly decreasing to 60 Pa. The stresses were increased in natural sediments by E_{sed}/E_{gel} to a pharynx stress of 5305 Pa and body stress 1291 Pa, linearly decreasing to 842 Pa (dotted line). Because the change in Poisson's ratio was not considered, the calculated stresses resulted in higher displacements. Stresses were reduced by the ratio of the displacements in gelatin to the displacements from the first stresses applied in sediment, to pharynx stress 4408 Pa and body stress 1073 Pa, linearly decreasing to 700 Pa (dash-dotted line).

Poisson's ratio, and calculated a force of 0.20 N for $E = 2.7$ x 10^4 Pa, within the range of variability of E.

Burrowing forces and mechanics depend on mechanical properties of sediments, not only on each of E and K_{Ic}, but also their ratio. The force in sediment depends directly on E, assuming that the shape of the worm remains constant. An increase in E requires a larger force to obtain the same displacement. However, exerting a larger force makes the crack propagate more easily by increasing the stress intensity factor, K_I, above the critical value, K_{Ic}. Because we assume constant displacement and stress exerted depends on E, resulting stress intensity factors depend on the value of E. For $E = (1.7, 2.7, \text{ and } 3.7)$ x 10^4 Pa, $K_I = (4.7, 7.4, \text{ and } 10.2)$ x 10^2 Pa m$^{1/2}$, respectively, compared to K_{Ic} of 2.8 to 4.9 x 10^2 Pa m$^{1/2}$ for sediments (Johnson et al. 2002). Stress intensity factors within or above the range of critical values for sediments support the mechanism of burrowing by crack propagation in sediments as well as in gelatin.

The larger values of K_I are intriguing, although further research is needed to determine if they are significantly higher than K_{Ic}. One possible explanation is that our assumption of constant body shape is inaccurate; if worms are flatter in muddy sediments, less stress would be exerted, resulting in a lower K_I. More likely, our assumption of linear behavior of sediments is inaccurate over longer intervals (relevant to body stresses). Applied body stress may be lost to frictional dissipation, creep, or plastic deformation rather than amplified at the crack tip.

Infrasound measurements have shown that activities of individual animals in muddy sediments can be detected as pressure waves up to 0.5 m away (Wethey & Woodin 2005). Such pressure signals, which also depend on the mechanical properties of

sediments, could be used as an independent measure of burrowing forces if mechanics and heterogeneity of sediments were well enough known.

Burrowing forces further depend on body size: radial forces exerted by earthworms scale with (body mass)$^{0.43}$ (Quillin 2000). We did not consider allometry of burrowing forces but expect smaller worms to exert smaller forces than the large nereidids used in this study.

4.5.3. Burrowing mechanics

Crack growth can be characterized as stable or unstable; stable crack growth is associated with displacement-driven fracture (e.g., a wedge driven into a piece of wood, creating a crack opening as thick as the wedge), whereas unstable crack growth is associated with load-driven fracture (e.g., the two sides of the splintered wood are pulled with constant force, and as soon as the force exceeds a critical value, the wood breaks in two) (Anderson 1995). Crack extension as the worm moves forward agrees with descriptions in the fracture mechanics literature of stable, wedge-driven crack propagation. The entire body acts as a long wedge, and pharyngeal eversion thickens the wedge at the tip of the crack where it has greatest effect. Poor fit of the anterior model to the observed thickness of the worm in gelatin as well as poor fit of a preliminary lateral model in which only the pharynx was modeled suggest that the body acts as a (relatively) unconstrained wedge. The worm moves from side to side in the burrow between pharyngeal eversions, extending the crack laterally. This behavior is likely important in removing this lateral constraint, allowing greater displacements of the medium along the body with less stress than if crack walls were closer to the worm. Worms are able to

move forward without eversion, both over short distances in periods between pharyngeal eversions and over longer distances. This mode is consistent with observations of other worms that burrow by crack propagation without pharyngeal eversion (e.g., *Leitoscoloplos fragilis* (Polychaeta; Orbiniidae), *Heteromastus* sp. (Polychaeta; Capitellidae), and *Saccoglossus kowalewskii* (Hemichordata); K. M. Dorgan & P. A. Jumars, unpublished). Stable, wedge-driven fracture by worms is also consistent with the wedge shape of hard-bodied burrowers such as clams and urchins.

4.5.4. Implications for burrowing energetics

Energetic costs of burrowing have been considered much higher than for other forms of locomotion (Trevor 1978, Hunter & Elder 1989). Previous estimates, however, were also calculated from force measurements rather than measured directly through calorimetry or indirectly through oxygen consumption. External energy was calculated from measured forces, distances over which those forces were applied (force x distance = work), and the animal's velocity. Multiplying external energy by an energetic efficiency yields a net cost of transport. In previous studies, forces were often measured against rigid walls, overestimating them (e.g., 0.56 and 0.67 N radial forces exerted by *Polyphysia crassa* and *Priapulus caudatus* measured by Hunter & Elder (1989), compared to our calculation for *Nereis* of 0.16 N). In addition, because mechanics of burrowing and of the medium were not understood, distances over which the forces were applied were assumed to be distances the animal moved (Trevor 1978) rather than much smaller distances perpendicular to the direction of motion.

We originally thought that the primary problem with the use of external energy to calculate net cost of transport for burrowing, once forces and distances were accurately measured, was that we did not know energetic efficiency. However, our modeling work suggests that measuring external energy use is much more complicated. Force exerted by the everted pharynx and distance perpendicular to direction of movement can be multiplied to estimate work, but modeling shows that neglecting body stress underestimates displacements and results in stress intensity factors below critical for fracture. Furthermore, the worm must also exert propulsive forces parallel to the direction of motion in order to move forward in the burrow. Although it is possible to calculate total external work from applied stresses using franc2d (by integrating along the length of the crack), the model assumes a linear elastic material without loss of stored energy or creep over time. Sediment does behave linearly on short time scales, but the body of the worm applies pressure longer than does the pharynx, and the linear assumption is unlikely to hold over those longer periods. Attempts to link forces exerted by burrowing animals to energetic costs of burrowing (e.g., Hunter & Elder 1989, Trevor 1978) are complicated by the nonlinear and poorly understood potential energy storage and loss behaviors of sediments that need additional modeling and measurement attention at spatial and temporal scales of burrowing.

Chapter 5

WORMS AS WEDGES: EFFECTS OF SEDIMENT MECHANICS ON BURROWING BEHAVIOR

5.1. Chapter Abstract

Recent studies document that muddy marine sediments demonstrate linear elastic response to load and deformation on temporal and spatial scales relevant to animal movement, and that burrowers move in such sediments by fracture. Opening mode crack growth (Mode I) in linear elastic solids depends on three mechanical properties, fracture toughness, stiffness, and Poisson's ratio. Cracks propagate in mode I when the stress intensity factor (K_I) at the crack tip exceeds the material's fracture toughness (K_{Ic}). We prepared a series of clear gels that varied in stiffness and fracture toughness. The polychaete *Nereis virens* altered its body shape and behavior across these gels in order to elongate its burrow. We modeled burrow elongation as stable, wedge-driven crack growth, and calculated that K_I values at the tips of the burrows reach K_{Ic} values of most gels without pharynx eversion, and exceed K_{Ic} when the pharynx was everted. In materials with higher fracture toughnesses, worms everted their pharynges to become thicker and blunter wedges, as predicted from simple wedge theory. On the other hand, in stiff materials with low toughness, worms moved their heads from side to side to extend crack edges laterally, relieving elastic forces compressing them and allowing them to maintain body shape more easily. The mechanism of burrowing by crack propagation is utilized across a range of material properties found in natural muds, and variation in these properties strongly influences burrowing behaviors. These results highlight the importance to understanding of bioturbation of quantifying mechanical properties of

muds and variations in those properties on spatial and temporal scales relevant to burrowers, as different sediment mechanics likely influence particle mixing by altering burrowing behaviors.

5.2. Introduction

Burrowing animals are ecosystem engineers, altering sediment structure by moving through, ingesting and egesting the sediment (cf. Meysman et al. 2006). Extensive literature documents dependence of benthic community structure on sediment properties, primarily grain size and organic content (e.g., Gray 1974, Ramey and Snelgrove 2003). Recently, we have identified the sediment mechanical variables that determine the capability of animals to burrow in muds by means of crack propagation (Dorgan et al. 2005, Dorgan et al. 2006). Here we begin an examination of the potential feedbacks between sediment mechanics and behavior by asking whether worms alter their burrowing behaviors as those sediment mechanical variables assume different values.

Sediments exhibit dramatically different material properties, ranging from granular materials such as clean monodisperse sands to linear elastic materials such as certain muddy sediments. Differences in material properties result in differences in burrowing behavior in different sediments (Dorgan et al. 2006). The polychaete *Nereis virens* burrows through muddy marine sediments by crack propagation (Dorgan et al. 2005), and this mechanism is likely widespread in muds (Dorgan et al. 2006). The burrow is a planar crack (shaped much like a tongue depressor) that extends laterally as well as anteriorly away from the worm, which is compressed dorsoventrally by the elastic

walls of the burrow (Dorgan et al. 2005). The worm exerts a dorsoventral force against the burrow walls and the resulting stress in the sediment is amplified at the crack tip. The crack extends when the stress intensity factor, K_I, a measure of the stress amplification at the crack tip, exceeds the critical stress intensity factor, K_{Ic}, a material property of the elastic solid that is measured experimentally and describes the fracture toughness of the material.

Linear elastic fracture mechanics theory considers three material properties for two-dimensional problems in which the material is isotropic and the crack is loaded only in mode I, the crack opening mode: elastic modulus or stiffness (E), critical stress intensity factor or fracture toughness (K_{Ic}), and Poisson's ratio (ν). The stiffness (force L^{-2}) relates stress, σ (force L^{-2}), and strain, ε (elongation (L)/original length (L)), as $\sigma = E\varepsilon$ in a linear elastic, isotropic material undergoing uniaxial deformation. Poisson's ratio (dimensionless) is defined as the negative of the constant of proportionality between longitudinal and transverse strain under uniaxial stress. For incompressible materials, Poisson's ratio is equal to 0.5; lower values of ν indicate higher compressibility. Mode I stress intensity, K_I (force L$^{-1.5}$), is the coefficient of the dominant term in the series expansion of the stress field at a crack tip under mode I loading and is used to compare stresses at cracks of varying configurations under varying loading conditions. The crack propagates when K_I exceeds the critical value, K_{Ic}, the fracture toughness. Another way of stating the fracture criterion is that when energy release rate, G (energy L^{-2}), exceeds resistance of the material, R (energy L^{-2}), the crack grows. If energy release rate increases as the crack grows, growth is unstable (e.g., shattered glass), whereas if energy release rate decreases as the crack grows, growth is stable and stops when energy release

rate falls below material resistance. In general, displacement- or wedge-driven fracture is often stable, whereas load-driven fracture is often unstable. Relevant fracture mechanics have been recently reviewed (cf. Dorgan et al. 2006, Mach et al. 2007, Dorgan et al. in press) and can be found in engineering texts (e.g., Anderson 1995).

According to linear elastic fracture mechanics (LEFM) theory, the ratio of fracture toughness (K_{Ic}) and stiffness (E) determines the shape of bubbles that grow by fracture in elastic media (Johnson et al. 2002, Boudreau et al. 2005). Growth of bubbles in muddy sediments has been modeled using LEFM (Johnson et al. 2002, Boudreau et al. 2005), and LEFM has been applied to burrowers as well (Dorgan et al. in press). This ratio, K_{Ic}/E, is also important to burrowers and has been assumed to affect burrow shape and consequently burrowing behavior. Forces exerted by *Nereis virens* were measured in seawater gelatin, used as an analog for muddy sediments because the ratios of K_{Ic}/E are similar (Johnson et al. 2002, Dorgan et al. in press). Finite element modeling was used to convert forces measured in gelatin to those exerted by *N. virens* in natural sediments. Calculated forces are much lower than those previously measured (cf. Hunter and Elder 1989) and are directly proportional to the stiffness (E) of the material, which varies considerably in muds. Not only does E vary among sediments and with depth in sediments, but K_{Ic} varies extensively as well, and these variations and their dependence on properties such as grain size, porosity and organic content are poorly understood.

To address the question of whether variations in mechanical properties of muddy sediments, specifically in the ratio K_{Ic}/E, affect burrowing kinematics, we developed transparent polymer gels with different fracture toughnesses and stiffnesses and observed and quantified burrowing behavior of *Nereis virens* in the different media. From fracture

mechanics theory, the shape of a wedge that extends a crack stably also depends on the ratio of K_{Ic} to E; the higher K_{Ic}/E, the thicker and blunter the wedge (Sih 1973). We predicted that the shapes of burrowing worms would depend on this ratio and modeled worms as wedges to calculate K_I.

Stiffness and fracture toughness, material properties of elastic solids such as marine muds, are used to develop a dimensionless "wedge" number. The wedge number compares the work of fracture to extend the burrow and the work to move forward and deform an elastic medium. The Reynolds number, which incorporates fluid parameters of density and viscosity in a ratio of work against inertia to work against viscosity, has provided great insight to differences in swimming behaviors in animals moving at different Re. An analogous tool for burrowing behavior, as developed here, has only recently been possible with advances in understanding of sediment mechanics (e.g., Johnson et al. 2002).

5.3. Materials and Methods

5.3.1. Animals

Specimens of *Nereis virens* (~ 6-8 cm length) were collected from an intertidal mud flat in Edgecomb, ME, at low tide and kept under flowing seawater until use in experiments.

5.3.2. Relevant fracture mechanics theory and predicted implications to burrowing behavior

We observed in our kinematic analysis of *N. virens* burrowing in gelatin that the crack extends anteriorly only when the worm is moving forward, i.e., the worm's body is a wedge driving the crack growth (Dorgan et al. in press). The analytical solution for the stress intensity factor at the tip of a stable crack produced by a 2D wedge of arbitrary profile (Figure 5.1) is

$$K_I = \frac{E\sqrt{2a}}{2\sqrt{\pi}(1-v^2)} \int_a^\infty \frac{f'(z-b)}{\sqrt{z(z-a)}} dz \, , \, a > b \text{ (Sih, 1973).} \qquad \text{(equation 5.1)}$$

As shown in Figure 5.1, y = ± f(z - b) is the wedge profile, or worm thickness, *b* is the distance between the crack tip and the tip of the wedge. The distance between the crack tip and the contact with the wedge, *a*, is calculated based on the assumption that crack growth is stable. Equation (5.1) can be used to calculate the stress intensity generated by a worm of known shape. (N.B.: To obtain Eq. (5.1), the equation for k_I given by Sih (1973; section 1.2.9, p. 4) was multiplied by $\sqrt{\pi}$ to conform with modern notation for K_I. In addition, the equation was rewritten in terms of *E* and *v*. The coordinate system was changed from *x-y* to *y-z* to correspond with the 3D coordinate system used for experiments (the same as in Dorgan et al. in press) in which the z-axis is vertical.) Considering a worm as a wedge, *b* is the distance between the anterior end of the worm and the front of the burrow, and (*a* - *b*) is the distance between the anterior end of the worm and the dorsoventral contact of the body with the crack wall. The wedge is symmetrical about the z-axis, whereas the dorsal and ventral sides of a worm are not equal; however, when the worm is moving straight, the shape is approximately

131
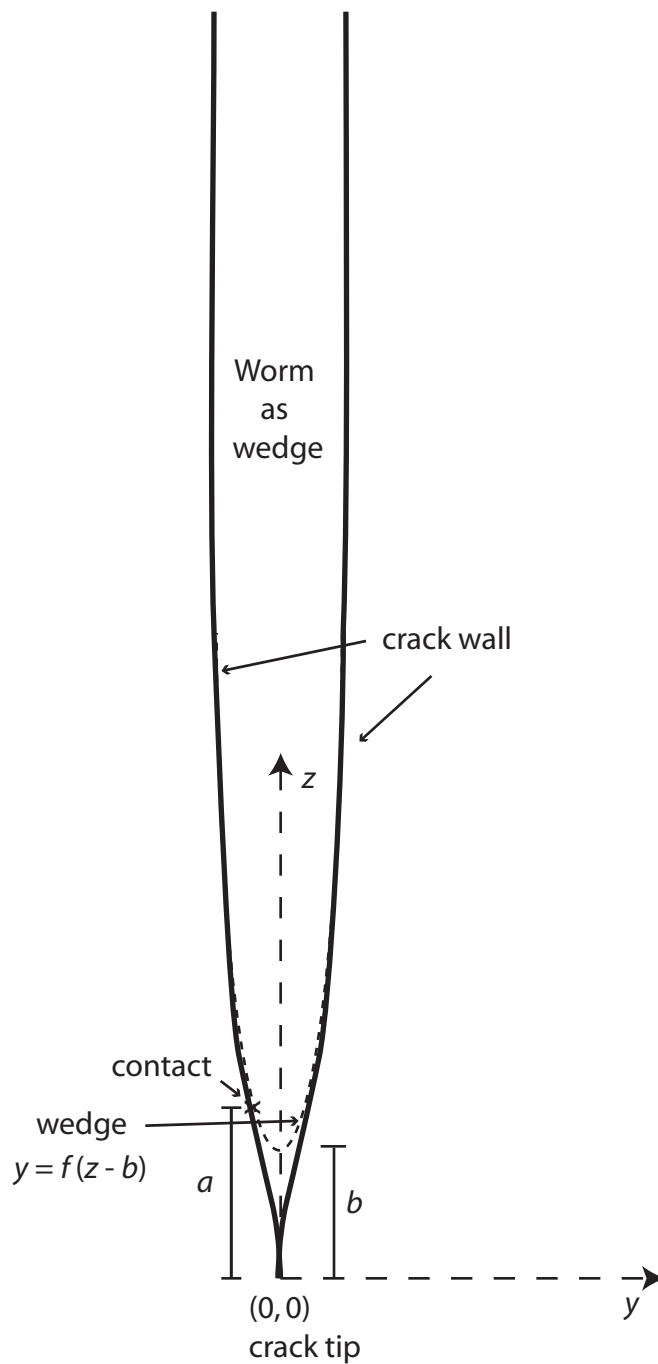
Figure 5.1. Wedge of arbitrary profile (dotted line) extending a crack (solid line) by stable crack growth. The schematic can be interpreted as a worm burrowing downward. The wedge profile is given by $y = \pm f(z - b)$, where b is the distance between the crack tip and the anterior end of the worm, and a is the distance between the crack tip and the contact of the wedge with the crack wall (adapted from Sih 1973).

symmetrical (cf. Dorgan et al. 2005). In addition, the wedge is assumed to be infinitely long, whereas worms clearly are not. The anterior part of the wedge contributes much more to K_I than the posterior part; as z increases (toward the posterior of the worm), the term, $\sqrt{(z(z-a))}$ increases and the slope of the worm's body approaches zero. The posterior region of the worm therefore contributes little to K_I.

It is possible to obtain b from video, either by direct visualization of the crack tip or by assuming that when the worm is moving forward, $b = 0$, and when the anterior end of the worm moves backward, b is the distance between the anterior end and the previously farthest anterior point of advance. However, neither a nor $(a - b)$ can be easily obtained from video analysis of worms burrowing.

To solve the problem of one equation (Eq. 5.1) and two unknown variables (a and K_I), another equation was needed. Equation (5.1) was derived from the combination of two equations (containing three unknowns; Barenblatt 1962),

$$h - \int_a^\infty f'(z-b)\sqrt{\frac{z-a}{z}}dz = \frac{K_I\sqrt{2\pi a}(1-v^2)}{E} \quad \text{(his eq. 6.10)} \quad \text{(equation 5.2)}$$

and

$$h = \int_a^\infty f'(z-b)\sqrt{\frac{z}{z-a}}dz \quad \text{(his eq. 6.8).} \quad \text{(equation 5.3)}$$

Here, h, the third unknown, is the half thickness of the wedge at infinity. Since we can measure h (the half thickness of the worm's body) from video, we now have two equations (Eqs. 5.1 and 5.2) and two unknowns (a and K_I). (N.B.: To obtain Eq. (5.2), 'K' in equation 6.10 (Barenblatt 1962) was multiplied by $\sqrt{(\pi/2)}$ to conform with modern notation for K_I. In Eqs. (5.2) and (5.3), the y-z coordinate system replaces the x-y coordinate system used by Barenblatt (1962).) Solving Eq. (5.2) for K_I gives

$$K_I = \frac{E}{\sqrt{2\pi a}(1-v^2)}\left(h - \int_a^\infty f'(z-b)\sqrt{\frac{z-a}{z}}dz\right) \qquad \text{(equation 5.4)}$$

K_I and a were obtained by solving Eqs. (5.1) and (5.4), a system of integral equations in a and K_I, iteratively. A simple iterative scheme suffices in which an initially small value of a is increased until Eqs. (5.1) and (5.4) yield values of K_I that agree to within a tolerance of 2 Pa m$^{0.5}$. The average of the two K_I values is then taken as the solution. This simple solution approach is possible because elasticity theory guarantees a unique solution to Eqs. (5.1) and (5.4) (Timoshenko and Goodier 1970).

We have shown that a 2D, plane strain, finite element model of the lateral view of *Nereis virens* burrowing in gelatin is a reasonable approximation for the 3D geometry of the worm when it is extending a crack-shaped burrow (Dorgan et al. in press). This same approximation is made in applying the 2D wedge equation. The assumptions in applying a 2D plane strain model are that the dorsoventral thickness of the worm is constant over the entire lateral width of the worm, and that the width is large enough that the stress field around the body is unaffected by the lateral edges of the crack and is instead constant through the width of the worm. In other words, a 2D, dorsoventral cross-section through the middle of the worm (showing an anterior to posterior profile of thickness and applied stresses) adequately represents the displacements and stress field across the entire width of the worm. In gelatin, *N. virens* moves its head from side to side, extending the crack laterally, and we have suggested that this behavior is important in enabling approximation of the burrow as a 2D plane strain geometry because it moves the effect of the lateral edge of the crack away from the worm, making the stress field around the worm more constant across the width of the worm.

Application of the wedge equation was tested by using measured shapes of large nereidids burrowing in gelatin, for which K_I was calculated from measured forces through finite element modeling (data from Dorgan et al. in press). From the finite element model, K_I varied from 57 to 64 Pa m$^{0.5}$ (Dorgan et al. in press), and from the wedge equation (Eqs. 5.1 and 5.4), K_I was 54 Pa m$^{0.5}$. K_{Ic} for gelatin is 50-220 Pa m$^{0.5}$ (Johnson et al. 2002). These two methods differ substantially: the finite element modeling method calculates K_I from the stresses applied, whereas the analytical wedge equation calculates K_I from the applied displacements using the material stiffness. The similar results from the two methods indicate that the analytical wedge equation is as applicable as previously used finite element analysis. Use of photoelastic stress analysis to measure forces exerted by burrowing worms, as required for application of the finite element method (cf. Dorgan et al. in press), is limited to large worms that exert large forces burrowing in clear materials. The wedge equation enables calculation of K_I for small worms burrowing in more opaque materials and thus expands greatly the range of materials for which mechanical analysis is feasible.

Another advantage of using an analytical solution rather than finite element modeling to calculate K_I is the ability to make predictions from the equations. From Eq. (5.1), the stress intensity factor increases in direct proportion to the stiffness of the material, following intuition because the stiffer the material, the larger the stresses that must be exerted on the crack faces by the wedge to maintain displacements compatible with the wedge profile. In other words, the ratio K_I/E is determined by the shape of the wedge. The aspect ratio of bubbles is proportional to the ratio, K_{Ic}/E, and we expected the shape and even behavior within the burrow also to depend on this ratio. This

135

assumption is consistent with the wedge equation; if K_{Ic}/E increases, the aspect ratio of a bubble increases and a wedge will have to change shape to have a higher K_I/E to reach the critical value. Bubbles that grow by fracture essentially act as oblate spheroidal wedges, so the dependence of bubble and wedge shapes on the same ratio is unsurprising. Wedges with steeper slopes, i.e., blunter fronts, particularly near the point of contact with the crack wall (at $z = a$, cf. Figure 5.1), will generate higher stress intensity factors. From Eq. (5.4) comes the intuitive prediction that a thicker wedge (larger h) will have a higher stress intensity factor, just as a bubble with a larger aspect ratio exerts a higher K_I (cf. Johnson et al. 2002).

Considering worms as wedges, we can make both qualitative and quantitative predictions about how burrowing behavior depends on the mechanical properties of sediments. As K_{Ic}/E increases, the stress intensity factor (normalized to E) from the wedge shape must increase in order for the crack to propagate. The most obvious way to increase the stress intensity factor is through pharynx eversion, which increases the thickness of the wedge near the crack tip as well as the slope of the anterior end near the contact with the crack wall. Although the worm is physiologically constrained to a range of body shapes, its hydrostatic skeleton enables some variation in body thickness and in the shape of the anterior region. For example, driving the body forward into the crack would increase the thickness and the slope of the head region. Both body thickness and slope (of the head) at the point of contact (the distance a from the crack tip) are expected to be larger in materials with greater fracture toughness-to-stiffness ratios. The null hypothesis was of no change in body shape with solid mechanical properties of the sediment, tested against the one-tailed alternative of thicker and blunter shape as K_{Ic}/E

increased. We also predict that the stress intensity factors calculated from lateral views of burrowing worms will differ in gels with different fracture toughnesses and will be close to the critical stress intensity factors for the gels in which they are burrowing.

5.3.3. Gels

Five polymer gel recipes were developed that appeared homogeneous (i.e., no precipitate or obvious heterogeneity), were transparent enough to see worms clearly in a 500-mL aquarium, and in which worms were able and willing to burrow (Table 5.1). The five recipes were selected to be approximately isosmotic with seawater and non-toxic. Gels were all kept in a cold room at 11˚C during experiments. First, we used gelatin (www.bulkfoods.com), 28.35 g (L seawater)$^{-1}$. Gelatin appeared stiffer than in previous experiments (Dorgan et al. 2005, Dorgan et al. in press) due to wall effects in smaller aquaria, although the concentrations were the same. Gelatin was mixed in 500 mL seawater and brought to a boil, mixing continually.

For the second gel, gelatin (28.35 g (L seawater)$^{-1}$) was mixed with 5 g (L seawater)$^{-1}$ ι-carrageenan (FMC Biopolymer, Philadelphia, PA), added to seawater and stirred for 20 min to fully hydrate the carrageenan, then brought to a boil. Gelatin is synergistic with ι-carrageenan but not κ-carrageenan (Philips and Williams 2000), and the mixture of gelatin and ι-carrageenan is qualitatively similar but more transparent than the more commonly used mixture of κ- and ι-carrageenan; ι-carrageenan gels are less stiff and tougher than κ-carrageenan gels, and mixing the two varieties in differing proportions yields gels with intermediate properties (Philips and Williams 2000). This gel started to set almost immediately and was poured into aquaria within a minute after

Table 5.1. Gel recipes.

Material	Gelatin	Gelatin/ ι-carrageenan	Gelatin/agar	κ-carrageenan/ glucomannan	Gelatin/LA gellan gum
Ingredients	28.35 g L^{-1} gelatin	28.35 g L^{-1} gelatin 5.0 g L^{-1} ι-carrageenan	28.35 g L^{-1} gelatin 5.0 g L^{-1} agar	4.8 g L^{-1} κ-carrageenan 1.2 g L^{-1} glucomannan	14.18 g L^{-1} gelatin 1.5 g L^{-1} LA gellan gum
Hydration		Stir for 20 min	Stir for 12 min	Stir for 20 min	Hydrate in tap water

138

being removed from heat. (Waiting too long resulted in a heterogeneous gel.) To prevent cracking the glass, aquaria were placed in a container of hot water and allowed to heat up before the hot liquid was added.

For the third gel, gelatin (28.35 g (L seawater)$^{-1}$) was mixed with 5 g (L seawater)$^{-1}$ agar (www.bulkfoods.com), added to seawater and stirred for 12 min to fully hydrate the agar, then brought to a boil.

For the fourth gel, 4.8 g (L seawater)$^{-1}$ κ-carrageenan (FMC Biopolymer, Philadelphia, PA) was mixed with 1.2 g (L seawater)$^{-1}$ glucomannan (or konjac mannan, Starwest Botanicals, Cordova, CA), added to seawater, stirred for 20 min. to fully hydrate the carrageenan, then brought to a boil. Addition of glucomannan to κ-carrageenan, a stiff, brittle gel, results in a much tougher gel (Philips and Williams 2000). We initially tried higher concentrations of this mixture as well as higher proportions of glucomannan but worms were either unable to burrow or moved too slowly and stopped too frequently to obtain useful data. We therefore consider this gel to be near a limit of fracture toughness for *Nereis virens* of the size range used in experiments.

For the fifth gel, gelatin (14.18 g L^{-1}) was mixed with 1.5 g L^{-1} low acyl (LA) gellan gum (Kelcogel F, CP Kelco U.S., Chicago, IL) and added to tap water and stirred and brought to a boil. Once the solution boiled, salts were added to make 35 psu artificial seawater. The LA gellan gum does not hydrate in the presence of salts, instead forming a precipitate and settling, but salts are needed for cross-linking and are added after hydration.   LA gellan gum is a stiff, brittle gel that is synergistic with gelatin (Philips and Williams 2000).

Aquaria were built with glass sides (enabling use of polarizing filters) and plexiglass bases with inside dimensions of 0.072 m wide x 0.072 m deep x 0.10 m high. This size was chosen so the worms could be seen clearly in the most opaque gel, the κ-carrageenan and glucomannan mixture. Small holes were drilled in the centers of the plexiglass bases for fracture toughness measurements and were covered with silicone sealant before gels were added.

5.3.4. Mechanical testing of gels

5.3.4.1. Elastic modulus

A Vitrodyne V-1000 microtensile tester was used to measure force and displacement as a probe was lowered onto the surface of the gels in the aquaria (some replicates were in round beakers of the same surface area and height as the aquaria). Finite element analysis provides the calibration factor for computing E from the measured force-displacement response. Several replicate measurements (N = 4-8) were taken using two different probes (0.0126 m and 0.0047 m radii), and results were averaged. Stiffness measurements were not conducted in the cold room, but gels were kept as close to 11˚C as possible.

Although an analytical solution exists for the elastic modulus as a function of displacement and force exerted by a rigid cylinder resting on the surface (cf. Dorgan et al. in press), that solution assumes that the material is a semi-infinite solid (i.e., no wall effects). Because the aquaria are small (0.072 m x 0.072 m x 0.1 m deep), the walls do affect the apparent material stiffness. To account for the wall effect, we instead modeled the probe on the surface of an aquarium using the finite element modeling program,

franc2d (Cornell Fracture Group). Displacements of 0.002 m were applied along the radius of each of the two probes in a 2D axisymmetric model and the model was used to obtain stress as a function of r. Although the aquaria are rectangular, the axisymmetric model required the geometry to be approximated as a cylinder. We chose a radius, r = 0.0395 m, to give equal surface areas between the modeled and actual aquaria (close to radius 0.04 m of beakers). A line plot of stress along the probe contact was obtained from franc2d, and the stress was integrated over the area of the probe to calculate the force exerted. Because we obtained surface stresses on the bottom face of the probe, σ_i, at n discrete points, r_i, in the finite element model, we used a summation

$$F = \sum_{i=1}^{n} \sigma_i (\pi(r_{i+1}^2 - r_i^2)),$$
(equation 5.5)

rather than integration to find the total force applied to the probe.

The force required to displace the probe 0.002 m is a linear function of stiffness. This procedure was repeated for three values of stiffness to ensure linearity, and a linear regression between calculated force and the three values of stiffness was obtained. (Because calculated force depends directly on stiffness, the three points fell on the same line.) This regression was then used to convert forces measured with the Vitrodyne tester at 0.002 m displacement to stiffnesses of the gels.

5.3.4.2. Fracture toughness: Method 1

Fracture toughness was measured by injecting a bubble into the gel, measuring bubble pressure, and using the solution for the stress intensity factor for a penny-shaped crack with internal pressure. This solution, from the principle of superposition, is equal to the solution for a penny-shaped crack with far-field stress,

$$K_I = \frac{2}{\sqrt{\pi}} \sigma \sqrt{a_{bub}} \qquad\qquad \text{(equation 5.6)}$$

where a_{bub} is the principal radius (half-length) of the bubble, and σ is the far-field stress (Sih 1973).

Water was injected through a (25G) needle inserted through the hole in the bottom of the aquarium to form a bubble (Figure 5.2). The needle was attached to, on one side of a valve, a syringe to initiate the bubble, and on the other side, a pressure transducer (that measured the internal pressure of the bubble) and a syringe dispenser. The setup was attached to a micromanipulator used to insert the needle into the gel. Because we expected that the pressure needed to initiate a bubble would be greater than the upper limit of the transducer, the bubble was started with the valve to the transducer closed. Then, once the bubble formed, the valve was switched and the bubble was grown in increments with the dispenser. Two CCD cameras recorded the shape of the bubble from 90° angles and were lined up to capture views perpendicular, respectively, to the major and minor axis of the oblately spherical bubble. Photographic light tables were placed on opposite sides of the aquarium from the cameras, and the cameras and lights had crossed polarizing filters to more easily visualize the bubble (cf. Dorgan et al. in press). For more opaque materials, the polarizers were lined up to allow more light to pass through the gel. The bubble made a penny-shaped crack with the plane oriented roughly 10-15° from vertical.

The pressure peaked when water was added, and as the bubble started to grow the pressure decreased toward an asymptote (Figure 5.3A). This constant pressure, P_{tot}, reached after the bubble stopped growing, was used to obtain σ_c. Because the bubble was vertical, a pressure gradient existed between the crack tip at the top of the bubble and the

Figure 5.2. Schematic of bubble injection. A needle is inserted through a hole (covered with silicone glue) in the bottom of an aquarium of gel with the valve closed to the pressure transducer. A bubble is initiated with the lower syringe to protect the pressure transducer from the relatively high pressures needed to initiate the bubble. Once the bubble forms, the valve is switched and the bubble is grown incrementally with the syringe dispenser. Two cameras set up at 90° capture images each time the bubble is grown (once growth stops and pressure stabilizes). A hydrostatic pressure gradient exists between the crack tip and the needle (where the baseline pressure is measured), and that difference is removed during analysis.

bubble side view
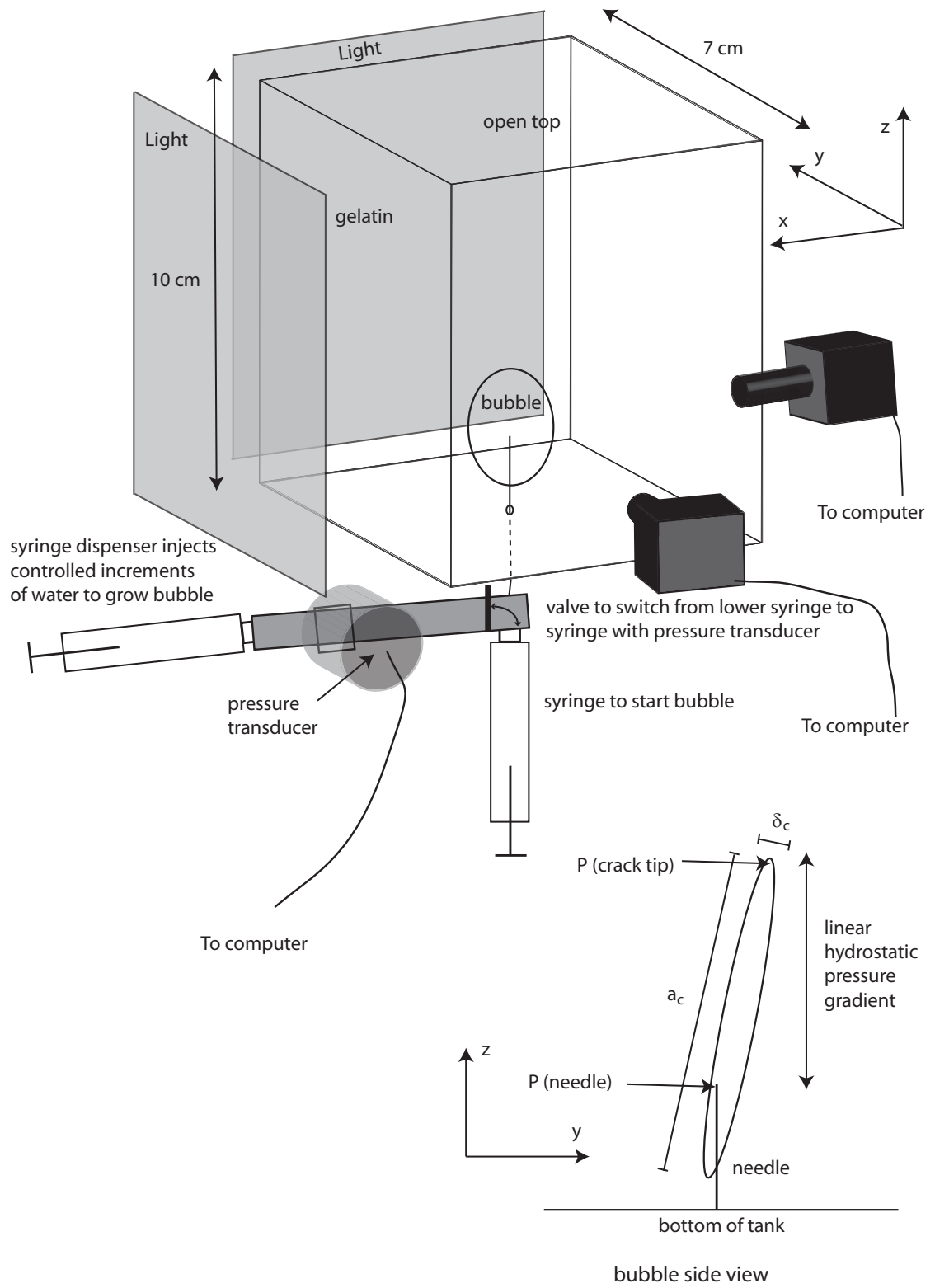
Figure 5.3. Pressure record during bubble injection in (A) gelatin and (B) κ-carrageenan/ glucomannan. A) In gelatin, a flat baseline (b) follows an initial peak (p) created by adjustment of the needle; then the valve is closed, causing the pressure to increase. The bubble is injected while the valve is closed, and when the valve is opened, the pressure increases rapidly. A small amount of water is added immediately (the peak before the first x) to ensure that the pressure in the bubble is at σ_c, and when the pressure levels out, images are captured and the pressure is recorded, from which the hydrostatic pressure and baseline are subtracted to obtain σ_c. A peak occurs each time the bubble is grown, and a pressure recording is taken each time the pressure levels out (indicated with x's). The needle is then removed and a second baseline (b) is recorded (to be averaged with the initial baseline). Corrected pressures (σ_c) are indicated with *'s. B) In κ-carrageenan glucomannan, air rather than water was used for injection The initial baseline (b) is lower than for the water bubble because the water does not extend up the needle. The valve is closed after the baseline is obtained, then the bubble is initiated. When the valve opens, the pressure peaks, then decreases due to creep. The valve is closed, and the bubble grown. When the valve opens again, another pressure peak occurs. In this bubble injection, the baseline did not drop as low as the original baseline, so only the first baseline was used.

gelatin bubble injection

κ−carrageenan glucomannan bubble injection

146
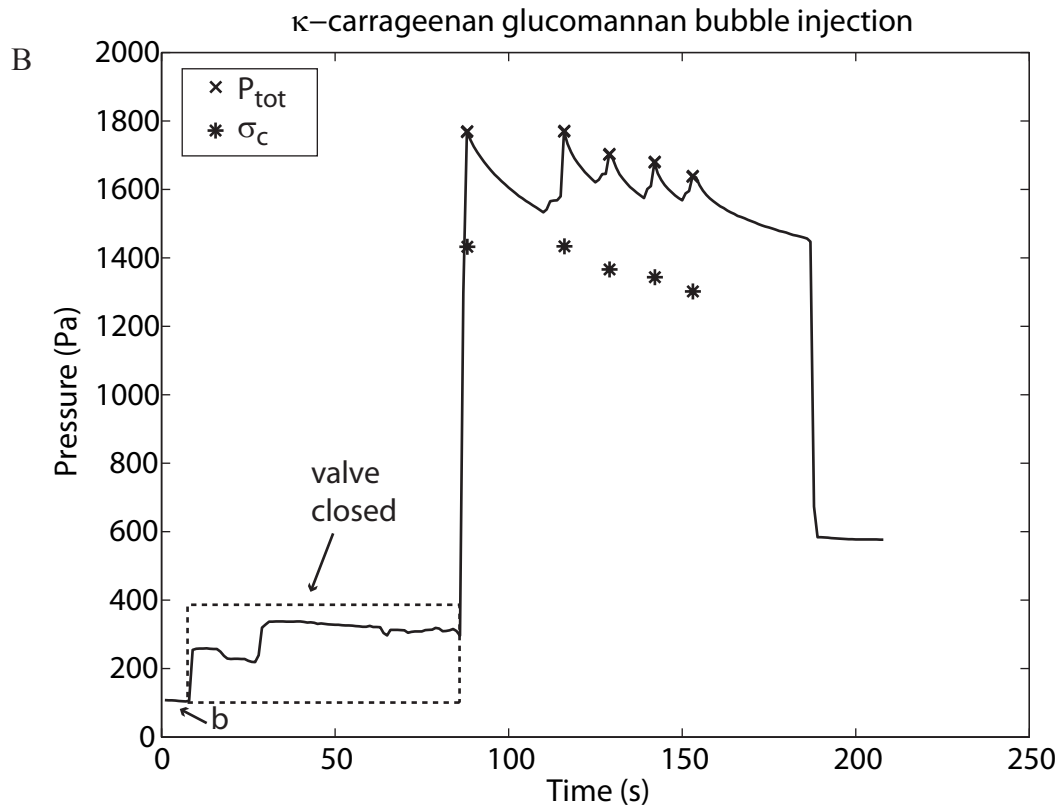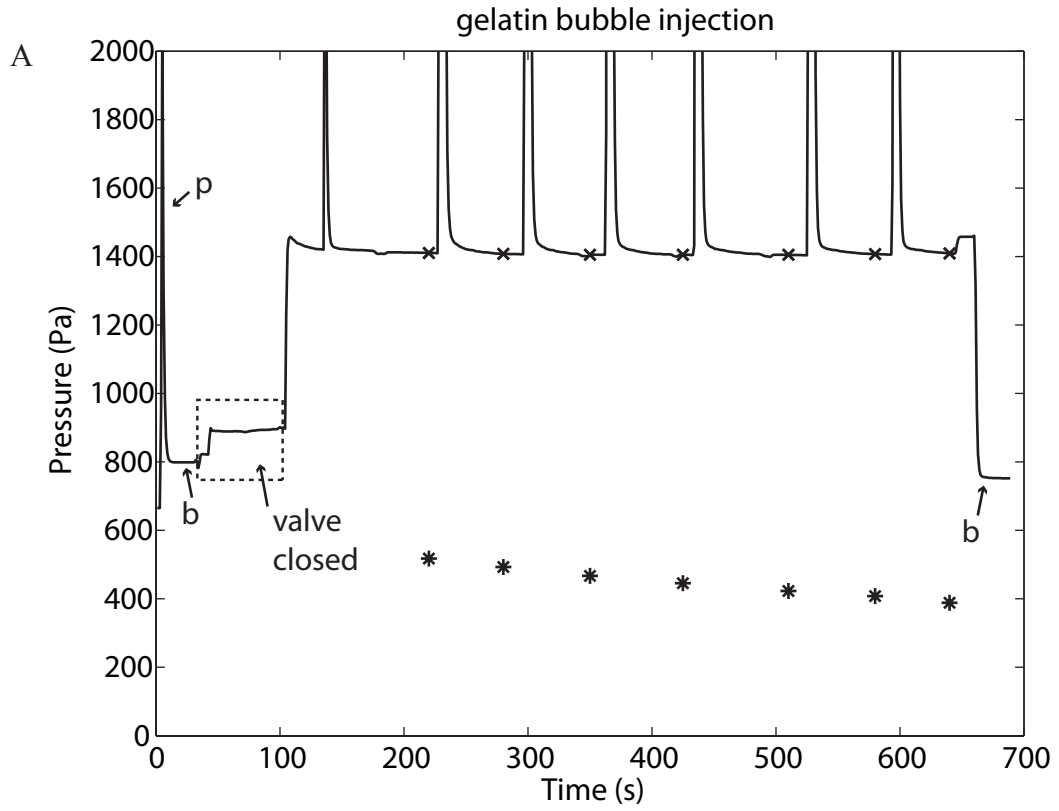
needle; the pressure difference, P_{hydro}, calculated from the height difference (cf. Figure

5.2), was subtracted from the pressure transducer reading. A baseline pressure, P_{base},

recorded both before the needle was inserted and after the needle was removed (labeled

'b' in Figure 5.3A), was also subtracted from the pressure transducer reading.

Occasionally, the pressure did not drop as low as the initial baseline pressure after the

needle was removed, possibly due to a clog in the needle, in which case only the initial

baseline was used. The critical pressure,

$$\sigma_c = P_{tot} - P_{hydro} - P_{base} \qquad\qquad \text{(equation 5.7)}$$

was used to calculate K_{Ic} from Eq. (5.6). K_{Ic} was calculated as the slope of the linear

regression between $\sqrt{a_{bub}}$ (x-axis) and $(\sqrt{\pi})/(2\sigma_c)$ (y-axis). The regression was forced

through the zero intercept.

In the κ-carrageenan/glucomannan gel, the water-filled bubble could not be seen

even with the polarizing filters. Because the length of the bubble was necessary to

calculate K_{Ic}, we used air instead of water to create an easily visualized bubble. For air

bubbles, the vertical pressure gradient is very small ($P_{hydro} \approx 0$) and only the baseline

pressure was subtracted. Bubbles did not grow in initial experiments in which air was

added with the dispensing syringe (cf. Figure 5.2), likely because the material was too

tough. We instead used only the lower syringe (used only to initiate bubbles in other

materials) to add air to grow the bubble, turning the valve to measure the pressure with

the pressure transducer as quickly as possible after adding air. Because pressure was not

measured as air was added to the bubble, the pressure peak observed in the other gels was

not captured. Instead, the pressure peaked when the valve opened, then slowly decreased

at a fairly constant rate, during which time the bubble did not grow (in other materials,

the bubble slowly extended as the pressure dropped) (Figure 5.3B). We believe that the

drop in pressure was due to creep because as the pressure dropped, an imprint of the

previous bubble (thicker than the extended part) slowly disappeared. We considered the

initial maximum pressure when the valve was opened to the pressure transducer to be P_{tot},

but this value slightly underestimates σ_c because of the drop in pressure that occurred

between the time the bubble stopped growing and the valve was opened. Calculated K_{Ic}

for this gel is therefore likely slightly underestimated using method 1.

5.3.4.3. Fracture toughness: Method 2

Fracture toughness was also calculated from the aspect ratios of the bubbles. The

two cameras were oriented to view the bubble injected in method 1 straight on (the head

or tail of the 'penny') and at 90° (to measure thickness). The aspect ratio was calculated

from the bubble thickness and length. The aspect ratio of the bubble, a penny-shaped

crack, is

$$\frac{\delta_c}{a_c} = \frac{2(1-v^2)K_{Ic}}{\sqrt{\pi}Ea_c^{\frac{1}{2}}}$$
(equation 5.8)

δ_c is the displacement or half-thickness of the bubble and a_c is the half-length of the

bubble (labeled on Fig. 2). (Eq. (5.8) is similar to Johnson et al. (2002) Eq. 19, corrected

based on Fett (1982); confirmed by personal communication with B.P. Boudreau). K_{Ic}

was calculated for each aquarium as the average of K_{Ic} values for bubbles in which both

length and thickness could be clearly seen in images.

Because of the creep in the κ-carrageenan/glucomannan, the thickness of the bubble may have been overestimated, leading to overestimation of K_{Ic} (compare to underestimation by method 1 in this gel).

5.3.5. Experimental design for burrowing experiment

After the bubble injection, a worm was added to the aquarium and placed in a crack made with forceps, similar to previous experiments (Dorgan et al. 2005, Dorgan et al. in press). Video was recorded with cameras on two sides of the aquarium (cf. Figure 5.2) once worms began burrowing. Segments of video were selected for both dorsal (or ventral) and lateral view analyses (Figure 5.4). For a video segment to be used, the worm had to be burrowing within the plane of view of the camera rather than moving toward or away from the camera (at less than 30° from vertical with respect to the view from the other camera). Other criteria for selection were that the camera was not moving and the worm was in focus.

After a worm burrowed, it was preserved in formalin, and later the width of the 4th setiger was measured from the ventral side of the worm. This width was used to calculate normalized pharynx and body thicknesses to compare among worms burrowing in different gels. Preserved body lengths and wet weights were also measured. ANOVA for differences in mean length, width, and weight of worms in each gel ensured that worms of similar size were used in the different materials.
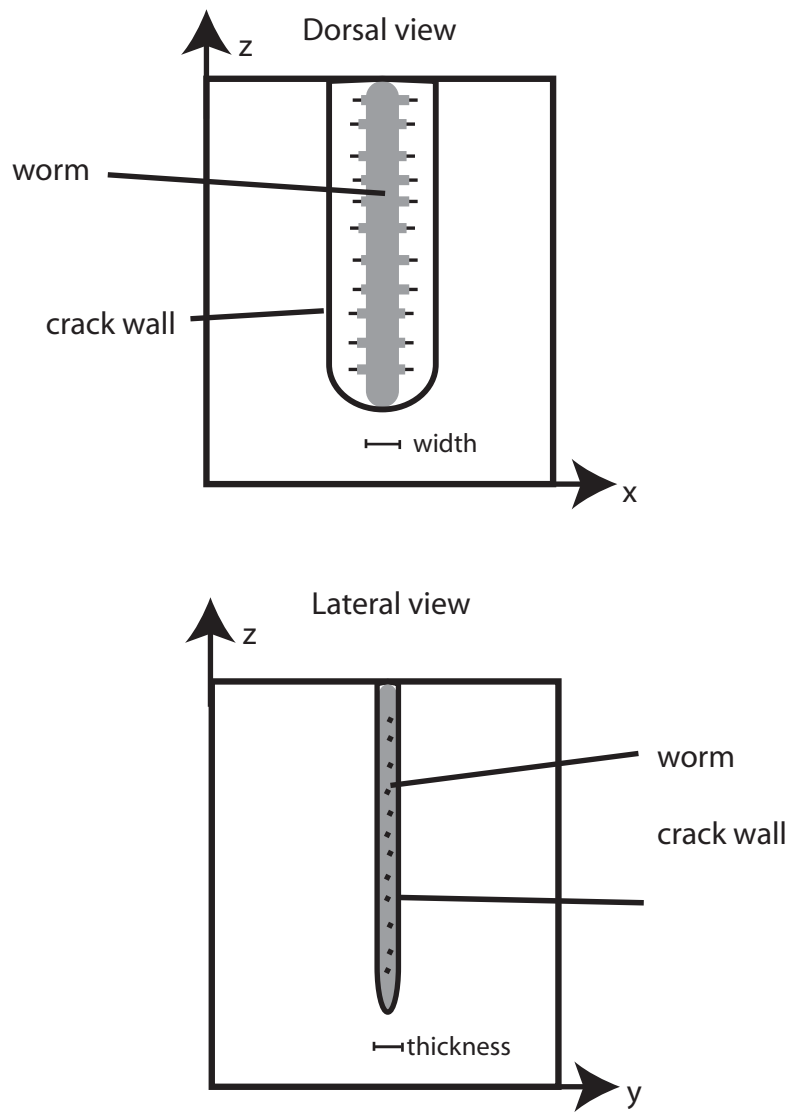
Figure 5.4. Schematic of the coordinate system used in analysis. The lateral view image shows the worm as a wedge, except the z-axis is used instead of the x-axis (as in Fig. 5.1) to indicate that in most cases, the worm was burrowing downward in the aquarium.

5.3.6. Video analysis: dorsal/ventral view

Dorsal view video segments were used to measure velocity, time and distance traveled in each cycle of lateral head movement and pharynx eversion, and the lateral distance moved by the anterior end of the worm. The lateral distance is an indication of how far the burrow extends laterally away from the worm and hence an indication of relief of stress from elastic rebound of the material.

For segments of video showing a direct dorsal view, the x-z coordinates of the center of the anterior end of the worm were obtained for a sequence of frames. A second-order polynomial was fitted through the x-z coordinates to separate forward progress from lateral head movements. Distance traveled for each frame was calculated as the length of the polynomial curve from the initial frame. Lateral movements of the anterior end of the worm over time were calculated as the residuals from the best-fit polynomial.

Video segments were then classified into one of the following behavioral categories: (1) periodic, side-to-side head movements without pharynx eversions, (2) pharynx eversions with irregular or no head movements, or (3) pharynx eversions with periodic, side-to-side head movements. Further analysis differed for the three categories of behavior. Most worms exhibited only one of the three behavioral categories; one worm burrowing in gelatin/agar exhibited more than one behavior in sequences long enough for analysis and was included in both behavior categories.

For video segments in which the worm exhibited periodic, side-to-side head movements without pharyngeal eversions, we calculated the period of head movement, lateral distance of head movement, forward distance traveled per cycle of head movement, and velocity. The period of head movement (s cycle^{-1}) was determined by first removing

the best-fit second order polynomial then finding the peak in the Fourier-transformed, polynomial-detrended data. The inverse of the peak frequency is the period of head movement. Video segments of less than three complete cycles were excluded. Average lateral distance of head movement was calculated as the average of the peaks of the residuals, doubled to obtain the full amplitude. Only peaks between two zero intercepts were included (for example, if the worm's head was initially on the left side, an initial left peak was excluded and measurement started with the first right peak). Lateral distance of head movement was normalized for comparison of worms among gels by dividing by the width of the worm (m/m). Velocity was calculated as the slope of the best-fit line of distance traveled as a function of time. Distance traveled per cycle was calculated as the product of the period of the cycle and the velocity. When more than one video segment was analyzed for a worm, weighted averages of periods and lateral distances of head movements, forward distances per cycle and velocities were calculated for that worm based on the number of cycles of head movement in each video segment.

For video segments in which the worm exhibited pharynx eversions with irregular or no head movements, the period of pharynx eversions, distance traveled between eversions, and resulting velocity were calculated. Pharynx eversions resulted in peaks in a plot of distance traveled as a function of time (because the pharynx rapidly extended anteriorly, then was retracted, decreasing the distance traveled). The period of pharynx eversions was calculated as the time between those peaks, and the distance traveled per cycle was calculated as the distance between peaks. Velocity was then calculated as the distance per cycle divided by the period of the cycle. Because period, distance, and

152

velocity were all calculated from individual cycles, the average for each worm was simply the average of the observations.

For video segments in which the worm exhibited pharyngeal eversions with periodic side-to-side head movements, the period of pharynx eversions, distance traveled per cycle, and velocity were calculated as for the worms exhibiting pharynx eversions without periodic head movements. In addition, we calculated the period and lateral distance of head movements. Because the head movements alternated with pharynx eversions, calculating periods from Fourier-transformed residuals did not work. Instead, the period and distance traveled were measured directly for individual cycles of head movement from plots of forward distance traveled as a function of time. The calculated distances and periods of head movements exclude the pharynx eversion part of the cycle, whereas distances and periods of pharynx eversions include the head movement part of the cycle.

5.3.7. Video analysis: lateral view

Lateral-view video segments were used to calculate K_I using the wedge equation. For video segments in which the worm everted its pharynx, sequences of frames around the pharynx eversion were analyzed, whereas for video segments without pharynx eversion, individual frames were analyzed. Stress intensity factors (K_I) and points of contact with the crack wall (a) were calculated from measured worm thicknesses by solving Eqs. (5.1) and (5.4) in Matlab 7.4.0 (R2007a; The Mathworks, Inc., Natick, MA, USA). The slope of the anterior region at the point of contact was also calculated. For sequences of images around a pharynx eversion, the peak K_I was identified.

For segments of video showing a direct lateral view, individual frames were captured, and for each frame thicknesses were measured at 10 different distances from the anterior of the worm with LabView. The 10 distances at which thicknesses were measured were not identical because the lengths of worms visible in frames differed and distances were chosen to cover the entire visible length. The shape of the worm was determined by interpolating from those 10 thicknesses using a cubic spline function in Matlab. The thickness of the worm (the average of the posterior two data points) was extended out to 0.02 m length for consistency in comparing data from frames with thicknesses measured at different distances.

Normalized pharynx thickness, normalized body thickness, distance to contact with crack wall (a), and the slope at contact were averaged for each material for comparison among gels. Pharynx thicknesses were measured as the maximum thickness along the anterior 0.002 m of the worm. For this comparison, pharynx and body thicknesses were normalized to worm size by multiplying by the average width of all worms and dividing by the width of the individual worms. (Real thicknesses were used to calculate K_I and a.)

5.4. Results

5.4.1. Animals

Worms used in experiments had preserved length of 3.4 ± 0.5 cm (mean $\pm$ s.d., N $= 37$), width of the 4th setiger of 1.7 ± 0.2 mm, and wet weight of 107 ± 41 g. Worm size did not differ significantly among the five gels (F-values for an ANOVA test for

differences in means were $F_{4,34} = 0.44$, $F_{4,34} = 0.45$, and $F_{4,34} = 0.96$ for length, width, and wet weight, respectively, with corresponding p values of 0.78, 0.77 and 0.44).

5.4.2. Gel mechanics

Stiffnesses were similar for gelatin (7100 ± 372 Pa; mean ± S.D., N = 8), gelatin/ι-carrageenan (6880 ± 1464 Pa, N = 5), and κ-carrageenan/glucomannan (8258 ± 1218 Pa, N = 6) (Table 5.2). Gelatin/agar was significantly stiffer (16855 ± 1671 Pa, N = 6) than other materials (although the difference between gelatin/agar and gelatin was not significant), and gelatin/LA gellan gum was least stiff (3615 ± 1121 Pa, N = 4), although not significantly so.

Results from both methods of measuring fracture toughness place the gels in the same order of increasing toughness, and numbers were fairly similar between the two methods (Table 5.2). K-carrageenan/glucomannan is significantly tougher than the other gels, and from method 2, gelatin/agar is significantly tougher than gelatin/LA gellan gum. Gelatin/ι-carrageenan has similar fracture toughness to gelatin, gelatin/agar has a slightly higher toughness, and gelatin/LA gellan gum is slightly less tough. Method 1, using measured internal pressures of bubbles, resulted in fairly high r^2 for regressions for gelatin ($r^2 = 0.69\text{-}1.00$ for N = 4-16) and gelatin/ι-carrageenan ($r^2 = 0.40\text{-}1.00$ for N = 2-6), moderate r^2 for gelatin/agar ($r^2 = 0.41\text{-}0.59$ for N = 5-8), and low r^2 for κ-carrageenan/glucomannan ($r^2 = 0.08\text{-}0.29$ for N = 2-5) and gelatin/LA gellan gum ($r^2 = 0.06\text{-}0.41$ for N = 2-6). The low r^2 for κ-carrageenan/glucomannan was unsurprising considering the problems with obtaining this measurement (discussed in methods). Method 1 was expected to underestimate K_{Ic}, whereas Method 2 was expected to

Table 5.2. Stiffnesses (E) and fracture toughnesses (K_{Ic}) of the five gels.

Material	Gelatin	Gelatin/ ι-carrageenan	Gelatin/agar	κ-carrageenan/ glucomannan	Gelatin/LA gellan gum	ANOVA results
E (Pa)	7100 ± 372[a,b] (N = 8)	6880 ± 1464[a] (N = 5)	16855 ± 1672[b] (N = 6)	8258 ± 1281[a] (N = 5)	3615 ± 1121[a] (N = 4)	F(4,35) = 6.61 p = 0.0005
K_{Ic} (Pa m$^{0.5}$) (Method 1)	58.1 ± 8.2[a] (N = 3; r^2 = 0.69-1.00 for n = 4-16*)	58.7 ± 4.2[a] (N = 3; r^2 = 0.40-1.00 for n = 2-6)	84.7 ± 5.5[a] (N = 5; r^2 = 0.41-0.59 for n = 5-8)	161.9 ± 37.3[b] (N = 5; r^2 = 0.08-0.29 for n = 2-5)	43.0 ± 2.3[a] (N = 4; r^2 = 0.06-0.41 for n = 2-6)	F(4,20) = 19.93 p < 10^{-6}
K_{Ic} (Pa m$^{0.5}$) (Method 2)	65.4 ± 9.5[a,b] (N = 3)	69.4 ± 2.4[a,b] (N = 2)	112.1 ± 12.6[a] (N = 4)	257.4 ± 9.1[c] (N = 4)	35.5 ± 3.2[b] (N = 3)	F(4,20) = 37.65 p < 10^{-8}
K_{Ic}/E (m$^{0.5}$) (Method 1)	0.0082 ± 0.0016	0.0085 ± 0.0024	0.0050 ± 0.0008	0.0196 ± 0.0076	0.0119 ± 0.0043	
K_{Ic}/E (m$^{0.5}$) (Method 2)	0.0092 ± 0.0018	0.0101 ± 0.0025	0.0067 ± 0.0014	0.0312 ± 0.0059	0.0098 ± 0.0039	

* N = number of gels tested, n = number of increments of bubble growth (i.e., points in regression)

156

overestimate K_{Ic}, and true K_{Ic} likely falls between the results from the two methods, 161.9 ± 37.3 Pa (mean ± S.D., N = 5) and 257.4 ± 9.1 Pa (N = 4), respectively. In the gelatin/LA gellan gum, the bubble sometimes grew down or to the side as well as growing upward in the aquarium, possibly because the fracture toughness was low, allowing the crack to extend easily. This variability may have contributed to the low r^2 in this material.

Stiffnesses and fracture toughnesses of gels were lower than measured E and K_{Ic} of natural sediments, but the ratios of K_{Ic}/E of the gels fall within the range for natural sediments (Figure 5.5A). Stiffness and fracture toughness data for natural sediments are extremely limited; both properties have been measured in sediment cores from Cole Harbour, Nova Scotia, Canada (Johnson et al. 2002, Boudreau et al. 2005), and stiffness has also been measured in sediment cores from Lowes Cove, ME (Dorgan et al. in press). This limited sample size and geographic range clearly make extrapolation to all muddy sediments questionable, but these are the only existing data. Among the gels, the ratio K_{Ic}/E is similar for gelatin, gelatin/ι-carrageenan, and gelatin/LA gellan gum (Figure 5.5B). Gelatin/agar has a lower K_{Ic}/E and κ-carrageenan/glucomannan has a higher K_{Ic}/E than other gels.

5.4.3. Burrowing mechanics: Dorsal view analyses

Three different behaviors were observed in video segments in the five different gels (Figure 5.6, Tables 5.3, 5.4). Most of the worms in gelatin and gelatin/LA gellan gum extended their burrows by moving their heads from side to side and did not evert their pharynges (Figure 5.6A). In gelatin, one worm everted its pharynx once, but only

Figure 5.5. Fracture toughness (K_{Ic}) calculated with method 1 plotted against stiffness (E). Error bars indicate standard deviations. A line from the origin through the K_{Ic} of gelatin separates tougher (above) from stiffer (below) materials. A, Gels (open circles) are compared to natural muds (closed circles). Stiffnesses of natural muddy sediments were measured on the surface of sediments from Lowes Cove, ME (2.4 x 10^4 Pa; Dorgan et al. in press) and in sub-surface sediments from Cole Harbour, Nova Scotia, Canada (1.4 x 10^5 Pa; Johnson et al., 2002). Fracture toughness has only been measured in sediments from Cole Harbour (280 to 490 Pa m$^{0.5}$; Johnson et al. 2002), and this range is indicated for both measured stiffnesses. The dashed line indicates that stiffnesses in natural sediments likely span the range between the two data points. B, Fracture toughness plotted against stiffness for only the gels used in this study (note different axes).

159
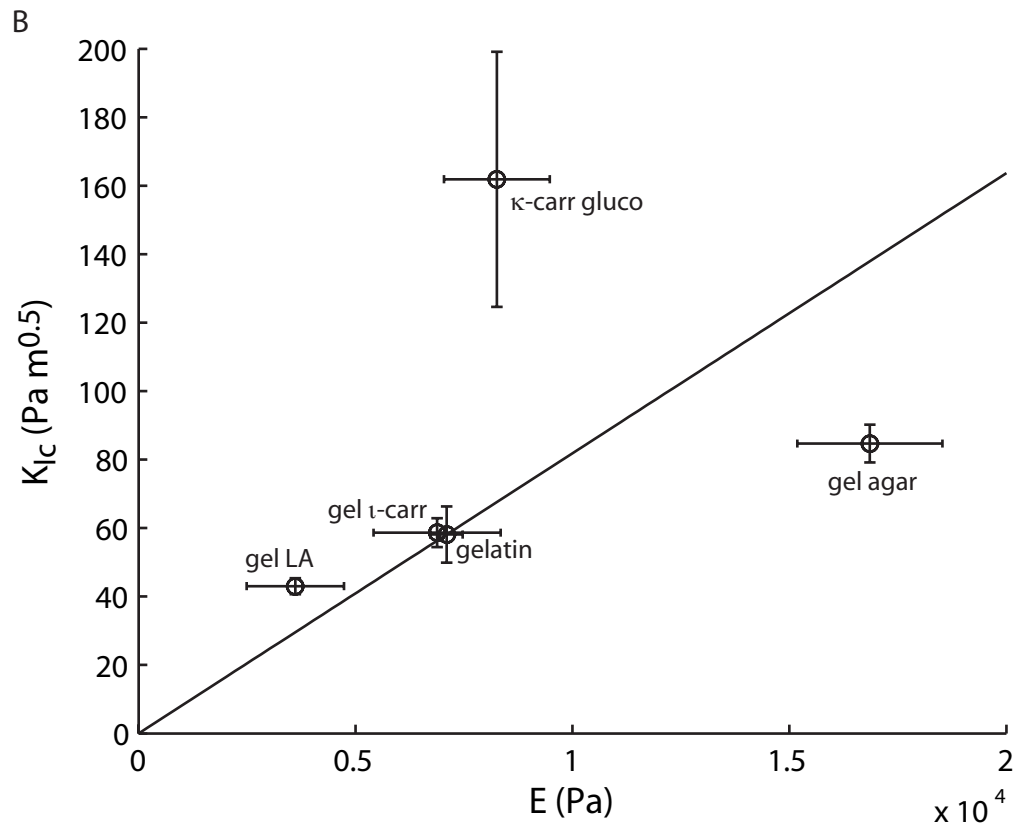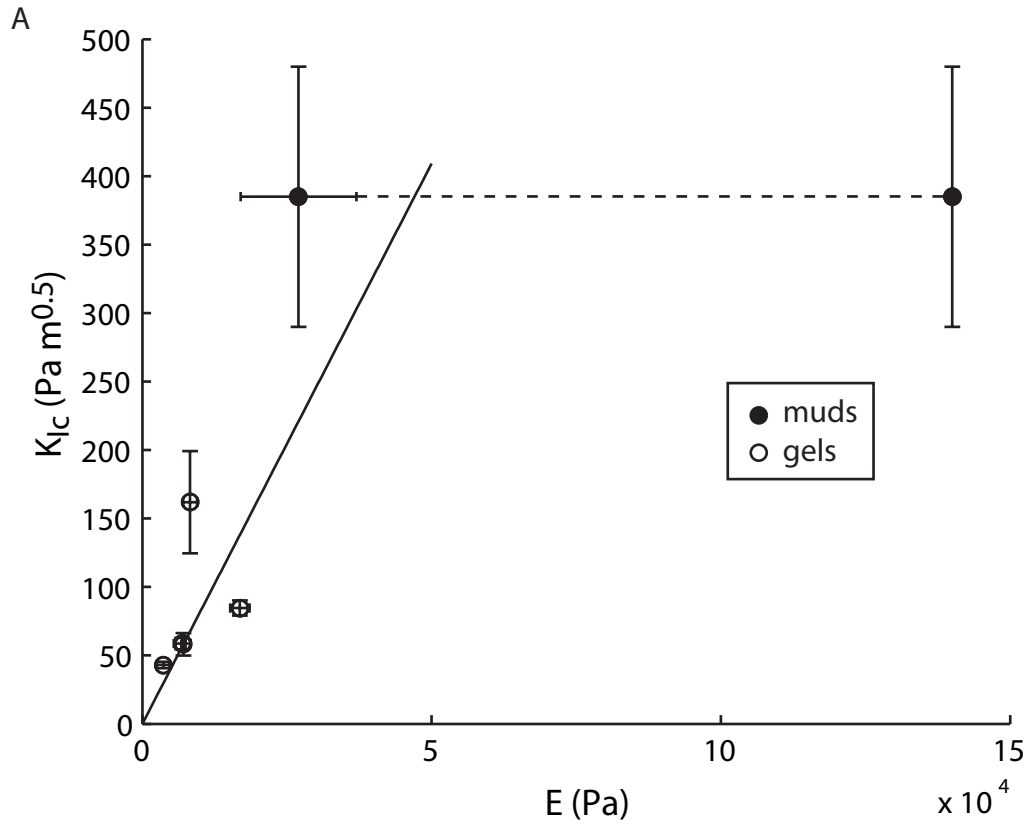
Figure 5.6. Distance moved, recorded from dorsal-view video segments. The solid line is the forward distance taken from a best-fit line through the *x-z* coordinates of the anterior end of the worm. The dot-dash line is the lateral distance moved by the anterior end of the worm. The residuals from the best-fit line were added to a best-fit line through the distance data (the slope of which is the worm's velocity) to superimpose the lateral head movement on top of the forward distance moved. Times of observed pharynx eversions (*) are plotted along the best-fit line. A) Representative worm burrowing in gelatin. The sinusoidal lateral head movement can be seen clearly from the dotted line. The worm was moving straight ahead at a constant velocity, which is shown by the near linearity of the solid line of distance vs. time. There are no pharyngeal eversions. B) Representative worm burrowing in agar by alternating pharynx eversions and head movements. The pharynx eversions are shown as peaks in the plot of forward distance (the forward distance increases quickly when the pharynx is everted, then decreases when the pharynx is retracted). Between pharyngeal eversions, the head moves from side to side, visible in the dotted lateral distance plot. C) Representative worm burrowing in κ-carrageenan/ glucomannan. Again pharynx eversions are visible as peaks in the forward distance plot. The lateral distance plot is linear, showing no periodic head movements.

A — gelatin

B — gelatin / agar

legend:
- forward distance
- best−fit
- lateral distance
- * eversion

C — κ−carrageenan glucomannan

Table 5.3. Data from analysis of dorsal-view video of worms with no pharynx eversion. Normalized lateral distance of head movement was calculated from the full amplitude of the residuals from the best-fit, 2nd order polynomial (because the worm often moved in a curved path) through the x-z coordinates of the anterior end of the worm. The lateral distance of head movement was normalized by dividing by the width of the worm measured at the 4th setiger.

Material	Gelatin	Gelatin/ι-carrageenan	Gelatin/agar	κ-carrageenan/glucomanna	Gelatin/LA gellan gum	ANOVA results
Occurrence of side-to-side head movement	6/6	3/5	2/4*	0/6	5/6	
Normalized lateral distance (dimensionless)	0.59 ± 0.10	0.44 ± 0.24	0.78 ± 0.11		0.62 ± 0.30	F(3,12) = 0.97 p = 0.44
Period (s)	2.48 ± 0.43[a]	3.37 ± 0.37[a,b]	5.14 ± 1.45[b]		3.88 ± 0.85[b]	F(3,12) = 7.93 p = 0.0035
Velocity (mm/s)	0.55 ± 0.13[a]	0.26 ± 0.08[b]	0.15 ± 0.04[b]		0.25 ± 0.12[b]	F(3,12) = 11.04 p = 0.0009
Forward distance (mm/s)	1.31 ± 0.10[a]	0.88 ± 0.20[b]	0.75 ± 0.01[b]		0.90 ± 0.24[b]	F(3,12) = 8.58 p = 0.0026

* One worm exhibited side-to-side head movements in one video segment and periodic pharynx eversions in another video segment so was included in both analyses.
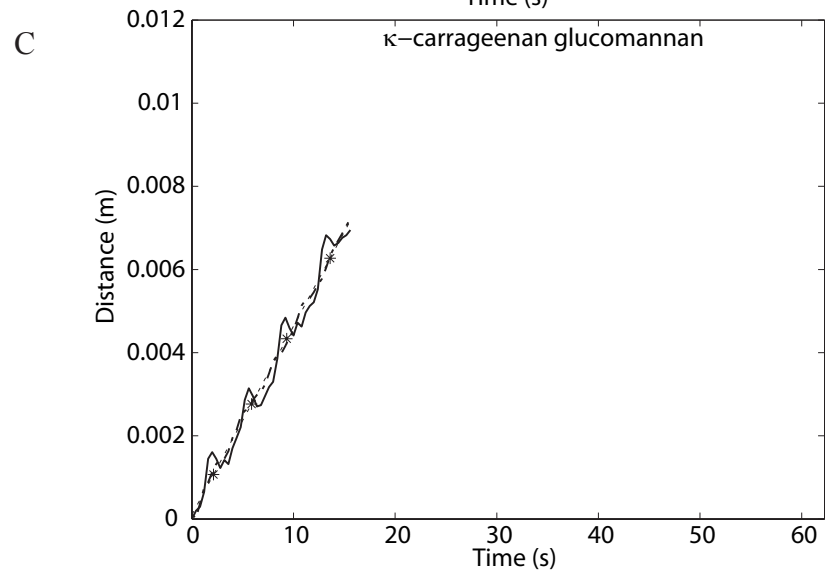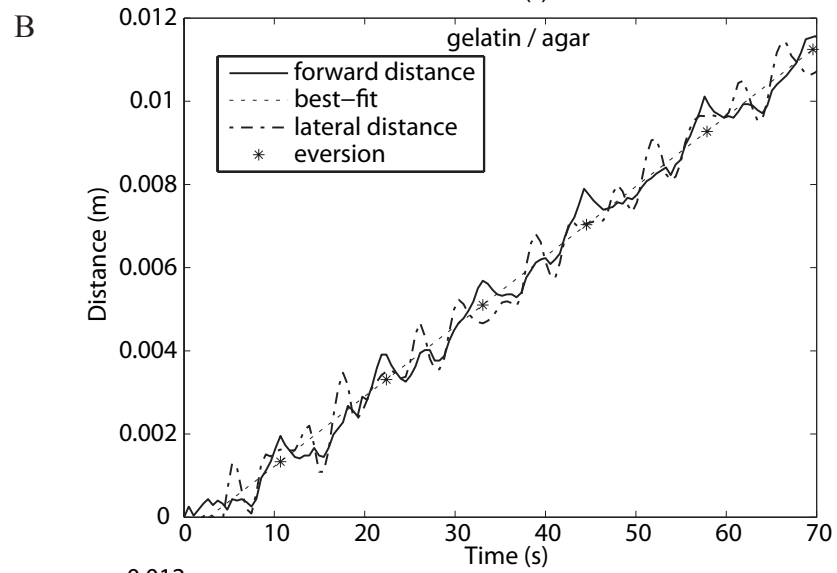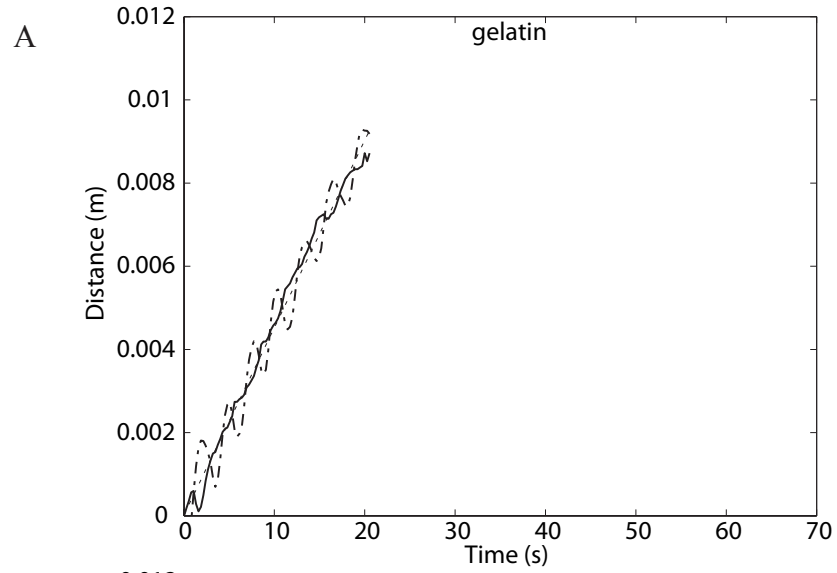
Table 5.4. Data from analysis of dorsal-view video of worms that everted their pharynges. Normalized lateral distance of head movement was calculated from the full amplitude of the residuals from the best-fit, 2nd order polynomial (because the worm often moved in a curved path) through the x-z coordinates of the anterior end of the worm. The lateral distance of head movement was normalized by dividing by the width of the worm measured at the 4th setiger. The two categories of behavior in which the pharynx was everted were combined to make the table more concise. None of the worms burrowing in κ-carrageenan/glucomannan moved their heads laterally, whereas all worms burrowing in other materials did.

Material	Gelatin	Gelatin/ ι-carrageenan	Gelatin/agar	κ-carrageenan/ glucomannan	Gelatin/LA gellan gum	ANOVA results
Occurrence of pharynx eversions	0/6	2/5	3/4*	6/6	1/6	
Period of eversion cycle (s)		9.12 ± 3.13	9.31 ± 3.64	7.99 ± 3.69	7.6	$F_{(3,8)} = 0.16$ p = 0.92
Forward distance (mm cycle^{-1})		1.45 ± 0.21	1.53 ± 0.67	1.44 ± 0.46	4.1**	$F_{(2,8)} = 0.87$ p = 0.45
Velocity (mm s^{-1})		0.17 ± 0.08	0.15 ± 0.04	0.21 ± 0.07	0.54**	$F_{(2,8)} = 0.03$ p = 0.97
Period of head movement between eversions (s)		3.20 ± 0.52	4.22 ± 0.75	N/A***	2.8	$F_{(2,3)} = 2.26$ p = 0.25
Normalized lateral distance of head movement (dimensionless)		0.71 ± 0.05[a]	0.97 ± 0.04[b]	N/A***	0.66[a]	$F_{(2,3)} = 27.06$ p = 0.012

* One worm exhibited side-to-side head movements in one video segment and periodic pharynx eversions in another video segment so was included in both analyses.

** Not included in ANOVA. Inclusion results in $F_{(3,8)} = 8.88$, p = 0.0063 and $F_{(3,8)} = 10.06$, p = 0.0043 for forward distance and velocity respectively.

*** No worms in κ-carr/gluco exhibited periodic head movement between pharynx eversions.

the dorsal view was recorded and it was not included in the analysis of pharynx eversion behavior because there were not multiple eversions from which to calculate time and distance between eversions. In the gelatin/LA gellan gum gel, several worms everted their pharynges only once. One worm everted its pharynx multiple times, and that dorsal-view video was analyzed. Three out of five worms in the gelatin/ι-carrageenan gel did not evert their pharynges, instead burrowing by moving their heads from side-to-side.

Most of the worms burrowing in gelatin/agar (3/4) everted their pharynges and moved their heads from side to side between pharynx eversions (Figure 5.6B). Two out of five worms in gelatin/ι-carrageenan showed this behavioral pattern, as did one out of six worms burrowing in gelatin/LA gellan gum.

All of the worms burrowing in the κ-carrageenan/glucomannan gel everted their pharynges but did not move their heads from side to side to extend the burrow laterally (Figure 5.6C). For conciseness, data on pharynx eversion behavior for these worms are presented in Table 5.4 with the worms that everted their pharynges and moved their heads, but the behaviors were clearly different.

Velocities, forward distances traveled per cycle, and periods of cycles were compared among gels for each behavioral category (except for pharynx eversion with no head movement, which occurred only in the toughest gel). Worms in gelatin moved faster, had shorter periods of head movement and moved forward farther with each cycle of head movement than worms in the other materials. Worms in gelatin/agar moved slightly slower with longer periods and shorter distances moved in each cycle, although the differences were not significant. There were no significant differences in the velocities and velocity components for worms that everted their pharynges. The one

worm that everted its pharynx in gelatin/LA gellan gum moved forward farther in each cycle and consequently at a higher velocity than worms in other materials, but only one worm was observed in this material. We calculated ANOVAs both including and excluding this worm and found that inclusion of this datum resulted in significant differences among gels, whereas exclusion resulted in no significant differences (Table 5.4).

Comparison of lateral head movement among gels indicated that worms in gelatin/agar moved their heads farther from side to side than worms in the other materials, both between pharynx eversions (significant difference) and when the pharynx was not everted (difference was not significant). The normalized lateral distance was calculated for comparison among worms that differed in size as the full amplitude of the head movement, measured in the center of the anterior tip of the worm, divided by the measured width of the 4th setiger of the preserved worm. Normalized lateral distance is dimensionless, whereas normalization of thicknesses uses average worm width for dimensions of length.

5.4.4. Burrowing mechanics: Lateral view analyses

Because video segments of both dorsal and lateral views were not obtained for all worms, some worms were included in both dorsal and lateral analyses and some were included in only one. The numbers of worms exhibiting each of the three behaviors in the lateral view video segments (Tables 5.5, 5.6) are therefore similar but not exactly the same as those for the dorsal view segments (Tables 5.3, 5.4).

Table 5.5. Data from analysis of lateral-view video of worms with no pharynx eversion. Body thickness and pharynx thickness were normalized by multiplying by the average width of worms measured at the 4th segment divided by the width of the individual worm.

Material	Gelatin	Gelatin/ι-carrageenan	Gelatin/agar	κ-carrageenan/glucomannan	Gelatin/LA gellan gum	ANOVA results
Calculated K_I (Pa m$^{0.5}$)	57.6 ± 7.9	60.7 ± 5.2	116.4		34.7 ± 7.2	
K_{Ic} (Pa m$^{0.5}$)	58.1 ± 8.2*	58.7 ± 4.2*	84.7 ± 5.5* 112.1 ± 12.6**		43.0 ± 2.3* 35.5 ± 3.2**	
Normalized body thickness (mm)	0.75 ± 0.03	0.90 ± 0.17	0.68		0.80 ± 0.16	$F(3,9) = 1.07$ $p = 0.41$
$(a - b)$ (mm)	1.41 ± 0.22	2.09 ± 1.40	1.51		1.48 ± 0.33	$F(3,9) = 0.63$ $p = 0.62$
Slope at a	0.18 ± 0.05	0.19 ± 0.05	0.15		0.23 ± 0.06	$F(3,9) = 1.01$ $p = 0.43$
N	4	3	1	0	5	
t-test H$_a$: $K_I \neq K_{Ic}$	p = 0.94	p = 0.62			p = 0.06*, 0.86**	

* calculated using method 1

** calculated using method 2

Table 5.6. Data from analysis of lateral-view video of worms that everted their pharynges. Body thickness and pharynx thickness were normalized by multiplying by the average width of worms measured at the 4th segment divided by the width of the individual worm.

Material	Gelatin	Gelatin/ ι-carrageenan	Gelatin/agar	κ-carrageenan/ glucomannan	Gelatin/LA gellan gum	ANOVA results
Maximum K_I (Pa m$^{0.5}$)		114.6 ± 14.5	195.7 ± 8.8	127.2 ± 10.1	64.6	
K_{Ic} (Pa m$^{0.5}$)		58.7 ± 4.2*	84.7 ± 5.5* 112.1 ± 12.6**	161.9 ± 37.3* 257.4 ± 9.1**	43.0 ± 2.3* 35.5 ± 3.2**	
Normalized body thickness (mm)		0.825 ± 0.148[a,b]	0.589 ± 0.065[a]	0.904 ± 0.106[b]	0.754[a,b]	$F(3,9) = 8.02$ $p = 0.0065$
Normalized pharynx thickness (mm)		0.892 ± 0.036[a,b]	0.676 ± 0.078[a]	0.916 ± 0.106[b]	0.914[a,b]	$F(3,9) = 6.04$ $p = 0.016$
$(a - b)$ (mm)		0.478 ± 0.085	0.623 ± 0.098	0.500 ± 0.067	0.508	$F(3,9) = 2.35$ $p = 0.14$
Slope at a		0.631 ± 0.060	0.461 ± 0.103	0.568 ± 0.064	0.493	$F(3,9) = 2.62$ $p = 0.11$
N	0	2	4	6	1	
t-test H$_a$: $K_I \neq K_{Ic}$		$p = 0.0066$*	$p < 0.001$***	$p = 0.055$* $p < 0.001$**	$p = 0.0037$* $p = 0.015$**	

* calculated using method 1
** calculated using method 2
*** for both method 1 and 2

Calculated K_I values from worm thicknesses for worms that did not evert their pharynges were very close to K_{Ic} values for each of the four materials (Table 5.5). The normalized body thickness (multiplied by (average width of all worms measured)/(individual worm width)) of the worm in gelatin/agar was slightly lower than for worms in other materials, but as only one worm was included, this may not be a true difference.

Maximum K_I's for worms that everted their pharynges were higher than the K_{Ic}'s for gelatin/agar, gelatin/ι-carrageenan, and gelatin/LA gellan gum, but were lower than K_{Ic} for κ-carrageenan/glucomannan (Table 5.6). Changes in the shapes of the worms as the pharynx was everted and inverted are most apparent in gelatin/agar and least apparent in κ-carrageenan/glucomannan (shown in Figure 5.7 for representative worms in each material; no worms everted their pharynges in gelatin, so this material was excluded). Real thicknesses were used to calculate K_I (Figure 5.7A), but normalized thicknesses of both the body and the pharynx are presented for comparison among different gels (Figure 5.7B). Average normalized body and pharynx thicknesses at the maximum K_I were higher in κ-carrageenan/glucomannan and lower in gelatin/agar (Table 5.6, Figure 5.7B). Body and pharynx thicknesses were smaller and showed greater variability across a pharynx eversion cycle in gelatin agar. Thicknesses were larger and showed less variability in κ-carrageenan/glucomannan.

The distances from the anterior end of the worm to the dorsoventral contact with the crack wall ($a - b$), which were calculated simultaneously with K_I, did not differ significantly among gels, although were slightly greater in the gelatin/agar gel. The point of contact was approximately 0.5 mm from the front of the worm, consistent with

Figure 5.7. Lateral view thickness and calculated stress intensity factor over a pharynx eversion cycle in different gels. A) Worm thickness profiles over a cycle of pharynx eversion for representative worms in each material. The first profile is plotted with the crack tip at (0,0) and each subsequent profile is offset 0.5 mm further to the right. When the anterior of the worm was at a distance $b > 0$ from the crack tip, the tip of the profile starts at the distance b from the crack tip, which is always at the origin. The *'s indicate the point of contact of the worm with the crack wall, calculated from Eqs. (5.1) and (5.4), and x's are individual measurements of width from which profiles were interpolated. B) K_I (solid line), calculated from worm profiles shown in (A) are indicated with thick lines and x's. Normalized body thickness (h, dot-dash line) and pharynx thickness (dotted line) for the same worm are also indicated with thick lines and x's. Thin lines with no x's are calculated from a different worm in each material (other than gelatin/LA gellan gum, in which only one worm everted its pharynx) for which profiles are not shown. Pharynx thickness was calculated as the largest thickness between the crack tip at $y = 0.002$ m. Both thicknesses were normalized by multiplying by the average worm width divided by the individual worm width.
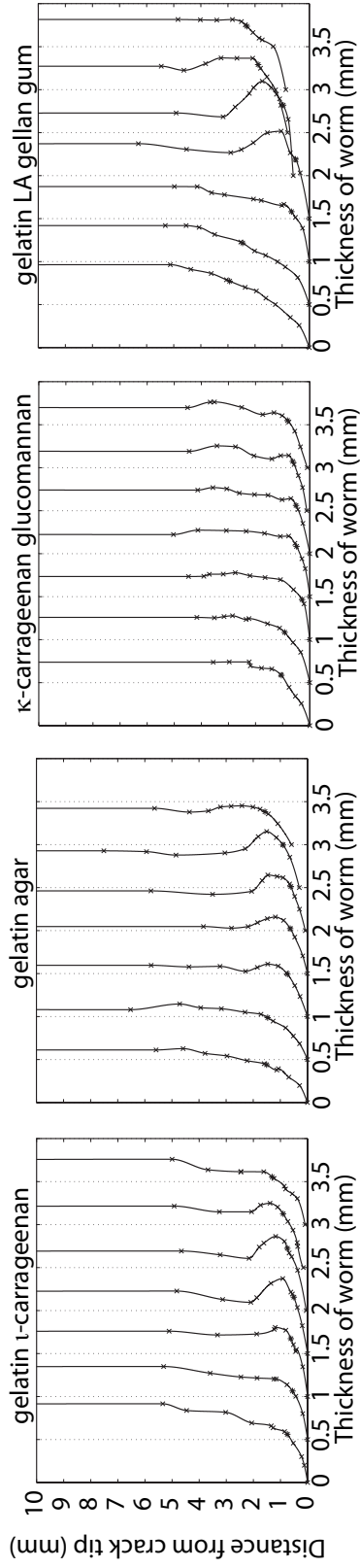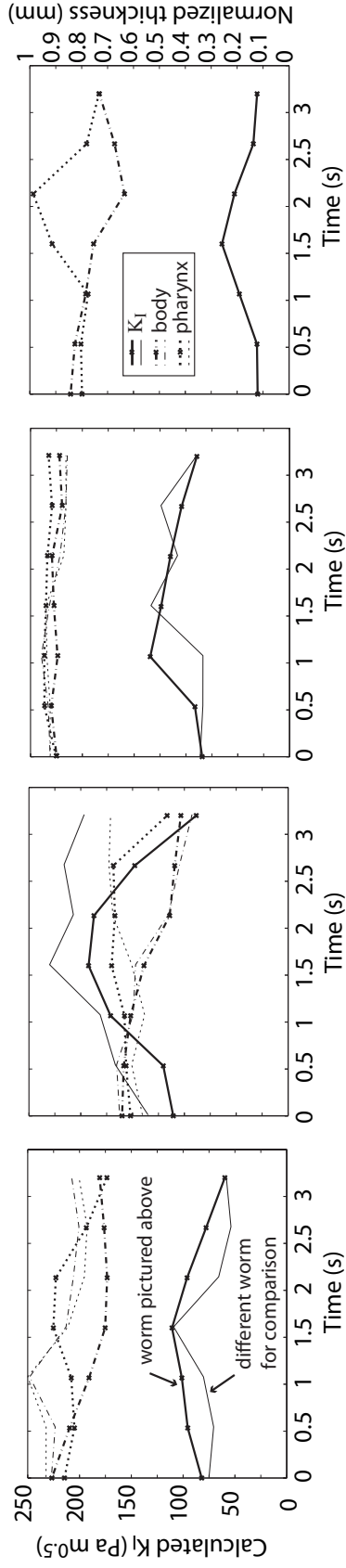
previous images of stress fields around worms, in which the compressive stress field around the pharynx begins approximately half way between the anterior end of the worm and the maximal thickness of the everted pharynx (cf. Dorgan et al. in press). The slope of the everted pharynx at the point of contact also did not differ significantly among gels.

5.5. Discussion

5.5.1. Differences in burrowing behavior

The three different behaviors exhibited by worms among the different gels can be explained by differences in mechanical properties of those gels. Side-to-side head movement reduces the effect of stiffness on the burrower by extending the crack edges away from the worm laterally. Worms in the stiffest (lowest K_{Ic}/E) material (gelatin/agar) moved their heads the greatest lateral distance, whereas worms in the toughest (highest K_{Ic}/E) material (κ-carrageenan/glucomannan) showed no head movement. Additionally, worms in the toughest material (κ-carrageenan/glucomannan) everted their pharynges and had thicker bodies than worms in other materials, as predicted.

Initially we were surprised that worms everted their pharynges in the stiff gelatin/ agar, as we expected that pharynx eversion would be unnecessary to extend the crack. The stress intensity factor close to the critical value for the one worm that did not evert its pharynx supports our prediction that the worms would not need to evert their pharynges to extend the crack, and indeed peak stress intensity factors greatly exceeded the critical values when the pharynx was everted. One possible explanation for this behavior is that the pharynx eversion extends the crack anteriorly to reduce the effect of stiffness on the anterior end of the worm. We have used finite element modeling to show that internal

pressure to maintain body shape decreases as the crack edge is extended laterally away from the worm (cf. Dorgan et al. in press). It follows that anterior crack extension should reduce pressure in the head region. We calculated the effect of anterior crack extension on pressure using a 2D, axisymmetric, finite element model and compared results to those from lateral crack extension modeled in 2D plane strain (Figure 5.8). Neither model is a good approximation of the worm, although comparison of model results with consideration of the assumptions of the two models does provide useful information. We showed that the 2D anterior view, plane strain model with measured stresses applied to the crack walls does not accurately predict body thickness of nereidids and suggested that removal of the lateral constraint allows the worm to use its body as a wedge to pry apart the sediment (Dorgan et al. in press). This deduction implies that when the lateral crack edge is very close to the worm, the model more accurately predicts displacements, and as the lateral crack edge extends away from the worm, modeled displacements will increasingly underestimate actual displacements. In other words, the internal pressure needed to maintain body shape as predicted by the model will be most accurate for small distances and will overestimate pressures as the crack extends away from the worm, underestimating the decrease in required pressure shown in Figure 5.8B and the benefit of extending the lateral crack edge in stiff materials. In contrast, the axisymmetric model likely overestimates pressures for small distances between the crack tip and the worm and is comparable or more accurate as the distance between the crack tip and the worm increases. The axisymmetric model is more constrained than the 3D worm because the axisymmetric model assumes that the anterior constraint applies 360° around the worm's head rather than the actual 180°. Greater constraint results in larger stresses to maintain a

Figure 5.8. Internal pressure required for the worm to maintain constant body shape (or displacement) as the crack extends away from the worm. A) A 2D plane strain model represents the lateral crack extension away from the body of the worm, and a 2D axisymmetric model represents the anterior crack extension. B) Internal pressure required for the worm to maintain constant body shape decreases as the crack extends away from the worm in both the plane strain and axisymmetric models. The plane strain model overestimates the required pressure and underestimates the decrease in pressure as the crack extends because it does not include the wedging effect in the 3rd dimension (cf. Dorgan et al., in press). The axisymmetric model also overestimates the required pressure because it is more constrained than the anterior of the worm, which is only constrained axially for 180° anterior of the worm rather than the whole 360° in the model.
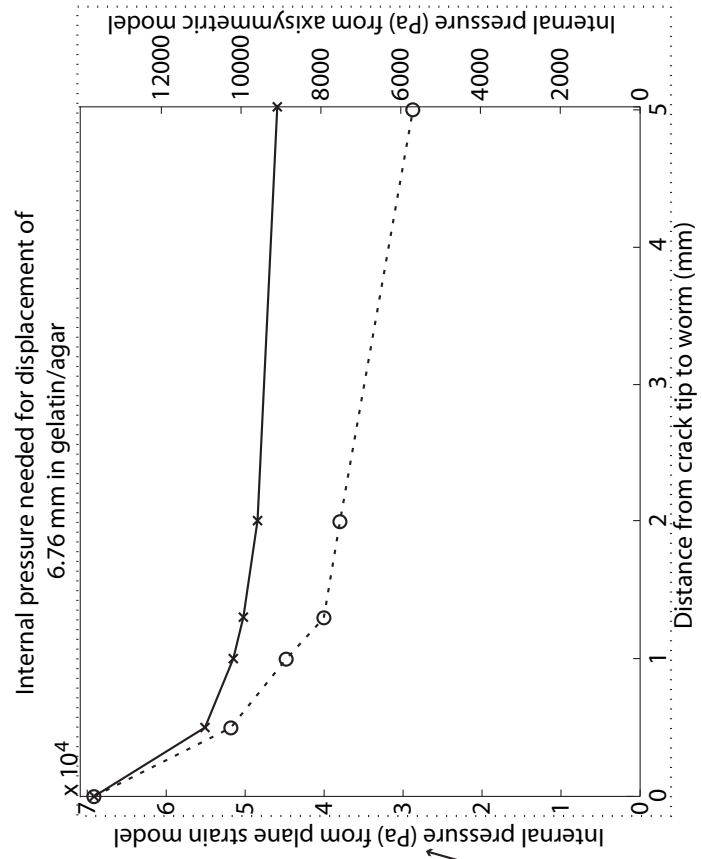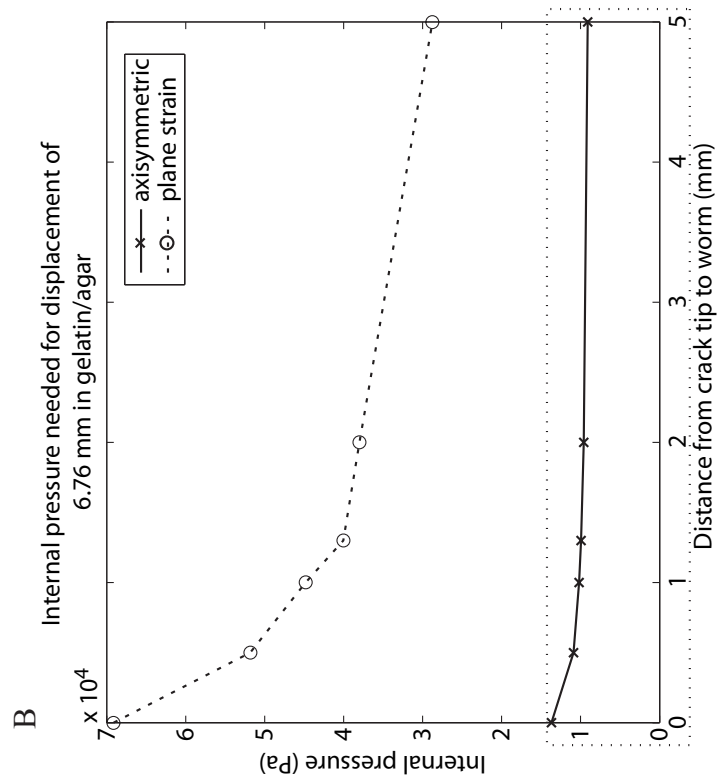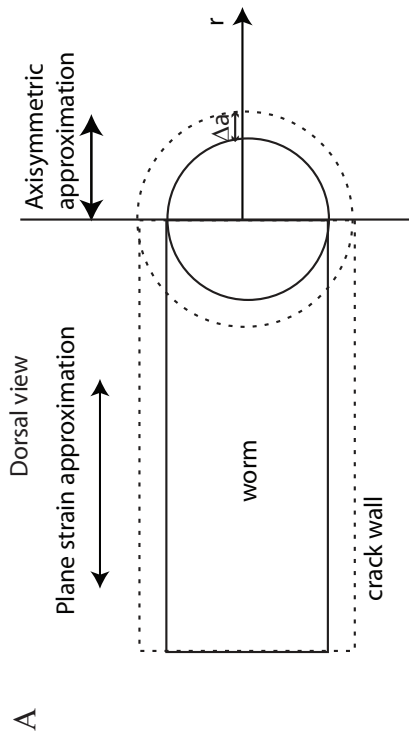
given displacement. As the crack extends, the constraint is removed, and the deviation of the model either does not change or decreases. This line of reasoning suggests that although anterior crack extension does decrease the internal pressure required, the effect is not as great as for lateral crack extension.

The high K_I relative to K_{Ic} during pharynx eversions in gelatin/agar, gelatin/ι-carrageenan, and gelatin/LA gellan gum implies that the crack extends anterior to the worm, which is difficult to see in the videos because the gelatin/agar (in which most pharynx eversions occurred) was translucent rather than completely transparent, and polarizers had been oriented to allow enough light to see the worm clearly. The crack is most easily visible when the polarizers are crossed, and becomes very difficult to see as the polarizers block less light. We had calculated K_I assuming that the crack extended only as far as the anterior end of the worm, as observed in previous experiments in gelatin (cf. Dorgan et al., in press). To calculate how far the crack would extend in front of the worm (since $K_I > K_{Ic}$), the stress intensity factor was calculated for increasing distance between the wedge and the crack tip (b in Eq. 5.1) until the stress intensity factor decreased to K_{Ic}. Calculated b for gelatin/agar is 1.3 ± 0.4 mm (mean $\pm$ S.D., N $= 4$), gelatin/ι-carrageenan is 1.4 ± 0.3 (N $= 2$), and gelatin/LA gellan gum is 1.2 (N $= 1$). These distances are very close to the forward distances moved by the worms in one pharynx eversion cycle (1.53 ± 0.67 (N $= 3$), 1.45 ± 0.21 (N $= 2$), and 4.1 (N $= 1$) mm respectively). These results suggest that pharynx eversion (rather than head movement) is the primary means of crack extension in these materials. We had predicted that pharynx eversion would not be necessary to extend the crack in stiffer materials, and this prediction was supported by K_I values close to K_{Ic} for worms not everting their pharynges.

The mechanics show that pharynx eversion behavior in stiff materials extends the crack out in front of the worm, in contrast to our previous results suggesting that the crack tip extends with (and no farther than) the anterior end of the worm (Dorgan et al. in press). Both behaviors are supported by mechanics and the increased use of pharynx eversion in the stiffest material suggests that extending the crack anteriorly may be advantageous in maintaining body shape. Anterior crack extension may also accommodate feeding along the wall of the burrow.

In the toughest material, the κ-carrageenan/glucomannan gel, none of the worms showed periodic, side-to-side head movement. Unfortunately, this gel was the most opaque, and the shape of the burrow could not be resolved (nor could the shape of bubbles, as discussed in methods). The lack of head movement suggests that the lateral edges of the crack were much closer to the worm than in other gels. This assumption is supported by observed close proximity of the antennae to the worm's body compared to their posture in gelatin. In gelatin, in which the crack shape is clearly visible, the antennae often trace the anterior to lateral edges of the crack. This toughest gel was the only one in our experiment for which the calculated stress intensity factor did not exceed, or even reach, the critical value for the material. However, use of the wedge equation is based on the 2D plane strain assumption. We have previously suggested that the reason the 2D approximation works for burrowing worms is that side-to-side head movement removes the lateral constraint (cf. Dorgan et al. in press). This assumption does not hold for this material, and it is therefore not surprising that results using the wedge equation do not make sense mechanically. The close proximity of the lateral constraint would allow the worm to build up higher internal pressures and exert more stress (cf. Figure 5.8B),

leading to a higher stress intensity factor than calculated in the 2D problem. However, the importance of the 3rd dimension in this case makes the problem much more complicated, and calculation of an accurate stress intensity factor would require 3D, finite element modeling.

In the tough κ-carrageenan/glucomannan gel, all worms exhibited the same behavior, whereas in the very stiff gelatin/agar gel, most but not all of the worms exhibited behavior characteristic of high stiffness. This difference may simply result from our choice of gels; the κ-carrageenan/glucomannan may be more extreme and therefore worms exhibit more consistent behaviors. Additionally, our sample sizes are too small to make conclusive statements about several of the behavioral differences. It seems plausible, however, that toughness would be a greater constraining factor on behavior than stiffness. Mechanically, if K_I does not exceed K_{Ic}, the crack will not grow. An increase in stiffness requires an increase in internal pressure to maintain body shape. Maintaining a higher internal pressure requires the worm to expend more energy, but only when the worm reaches its physiological maximum strength does a discrete change in its ability to move occur (assuming that there is a discrete physiological maximum strength). It follows that the greater the differences in burrowing energetics between the two behaviors observed in gelatin/agar, the sharper the transition between the two behaviors. Forces exerted by *Nereis virens* during pharynx eversion increase directly with sediment stiffness (Dorgan et al. in press). Smaller forces are required to deform a material smaller distances, so the forces exerted by *Nereis virens* burrowing by moving its head from side to side should be lower than during pharynx eversion. These smaller forces are exerted over smaller distances, but for longer periods, so external work done

may be similar. Research on burrowing energetics in different materials may help to explain the different behaviors.

On the other hand, differences in behavior of worms in gelatin and in gelatin/ι-carrageenan were observed even though neither stiffness nor fracture toughness differed significantly between the two materials. Addition of ι-carrageenan was expected to make the gel tougher and less stiff, and although the means followed the trend expected, the differences were small and not statistically significant, in part because of the large variability in stiffness of the gelatin/ι-carrageenan. Because this gel set very quickly, variability in mechanical properties may have resulted from small differences in the time between boiling and pouring into the aquaria. Although we tried to measure fracture toughness and stiffness for each aquarium used, initial attempts to measure stiffness by applying a weight to the surface of the gel and measuring displacement with a camera resulted in high variability (because camera-measured displacements were not precise enough). More precise stiffnesses were measured near the end of the experiments using the Vitrodyne tester. In addition, about half of our attempts to measure fracture toughness failed due to bubble leaking or contact of the bubble with the bottom of the tank (resulting from initiating too large a bubble). Without data on fracture toughness and stiffness for each aquarium and with small sample sizes, it is impossible to determine whether the differences in behaviors between gelatin and gelatin/ι-carrageenan and within gelatin/ι-carrageenan are statistically significant and if so result from variability in material properties.

There was considerable variation in the time for the worm to start burrowing, during which the worm either moved very little or repeatedly backed out of the initial

crack. These differences were difficult to quantify (and are not shown), in part because the behavior depended on how often the worm was re-inserted into the crack and poked with the pipet. Although velocity data were collected and are presented for each material (Table 5.3), the velocity likely depended on how much energy was expended by the worm before starting to burrow, which differed among worms and was not quantified. The higher velocities of worms in gelatin and the one worm that everted its pharynx in gelatin/LA gellan gum may reflect greater 'willingness' to burrow in these materials.

The three different behaviors appear to be used in three different mechanical regimes. The head movement without pharynx eversions seen in gelatin may represent a response to material of intermediate toughness and stiffness. Pharynx eversions with large side-to-side head movements may be characteristic of stiff materials, and pharynx eversions without head movements may characterize tough materials. These different behaviors suggest the need for a dimensionless number to characterize the material in which burrowing occurs.

5.5.2. Dimensionless "wedge" number

Components of external work for a worm to move forward in its burrow a distance Δx include work to extend the crack by fracture a distance Δx, work to deform the elastic material enough to make room for the worm's body, inertial work, and work done against friction. The energy of fracture, W_{Cr} (J), is

$$W_{Cr} = G_c(\Delta x)w_{crack} \qquad\qquad (\text{equation 5.9})$$

where G_c is the crack resistance (or critical energy release rate) (energy L^{-2}), Δx is the distance that the crack extends (L), and w_{crack} is the width of the crack (L). Fracture

occurs when the available energy for fracture, G, exceeds G_c, the amount of energy

released when the crack grows and a unit area of new crack is formed. This energy-based

fracture criterion is more convenient in calculating work of fracture than is the stress

intensity factor, K_I, as a criterion of fracture, and in plane strain, G is related to K_I

through stiffness and Poisson's ratio as

$$G = \frac{K_I^2(1-v^2)}{E} \text{ (Anderson, 1995).} \qquad \text{(equation 5.10)}$$

The work, W_{el}, to deform an elastic material with stiffness E in order to move forward Δx

follows a proportionality rule given by

$$W_{El} \propto Ehw_{worm}(\Delta x) \qquad \text{(equation 5.11)}$$

where h is the thickness of the worm (L), and w_{worm} is the width of the worm (L). Inertial

work can be ignored because burrowers move slowly (cf. Alexander 2003).

Friction can be ignored in this first-order approximation because frictional work is

roughly proportional to the work to deform the elastic material (the elastic restoring force

is the normal force, which is multiplied by a friction coefficient to obtain the friction

force). The frictional work would be added to the elastic work to obtain the work to move

forward, so assuming the friction coefficient and worm size to be constant, including the

frictional work would have the same effect as multiplying the elastic work by a constant.

In addition, we have suggested that work against friction may be less significant than

previously thought because worms move by peristaltic waves in which stationary, dilated

segments withstand most of the elastic restoring force, enabling narrower, extended

segments to move against relatively small frictional forces (Dorgan et al. 2006).

The work to burrow a unit distance is therefore the sum of the work of fracture

(Eq. 5.9) and the elastic work (Eq. 5.11),

$$\frac{W_{tot}}{\Delta x} = \frac{W_{Cr} + W_{El}}{\Delta x} = G_c w_{crack} + Ehw_{worm}.$$ (equation 5.12)

The ratio of these components of external work can be expressed as a dimensionless "wedge" number, *Wg,*

$$Wg = \frac{G_c}{Eh}\frac{w_{crack}}{w_{worm}}.$$ (equation 5.13)

The dimensionless wedge number is the ratio of the work of fracture to the work against the elastic restoring force of the sediment and is related to the ratio of K_{Ic} to E through Eq. (5.10) as

$$\frac{G_c}{Eh}\frac{w_{crack}}{w_{worm}} = \frac{K_{Ic}^2(1-v^2)}{E^2 h}\frac{w_{crack}}{w_{worm}}.$$ (equation 5.14)

If the wedge number is large, burrowing is essentially a fracture problem; if it's small, maintaining body shape should be a bigger problem than propagating the crack.

Observations of worms burrowing in gels with differing K_{Ic}/E (or G_c/E) show that worms exhibit behaviors that reduce a high wedge number or increase a low wedge number. The thickness of the worm (*h*) normalized to worm width varies as a function of (G_c/E). If G_c/E is small, the worm moves its head from side to side to increase the width of the crack relative to the width of the worm, increasing the second part of the wedge number. If G_c/E is large, the worm thickness is relatively large and the width of the crack does not extend much beyond the width of the worm (Figure 5.9). Side-to-side motion of the head has been noted in previous burrowing studies (e.g., Elder 1973, Hunter et al. 1983); here we posit one function for such motion and suggest its likely relation to material properties.
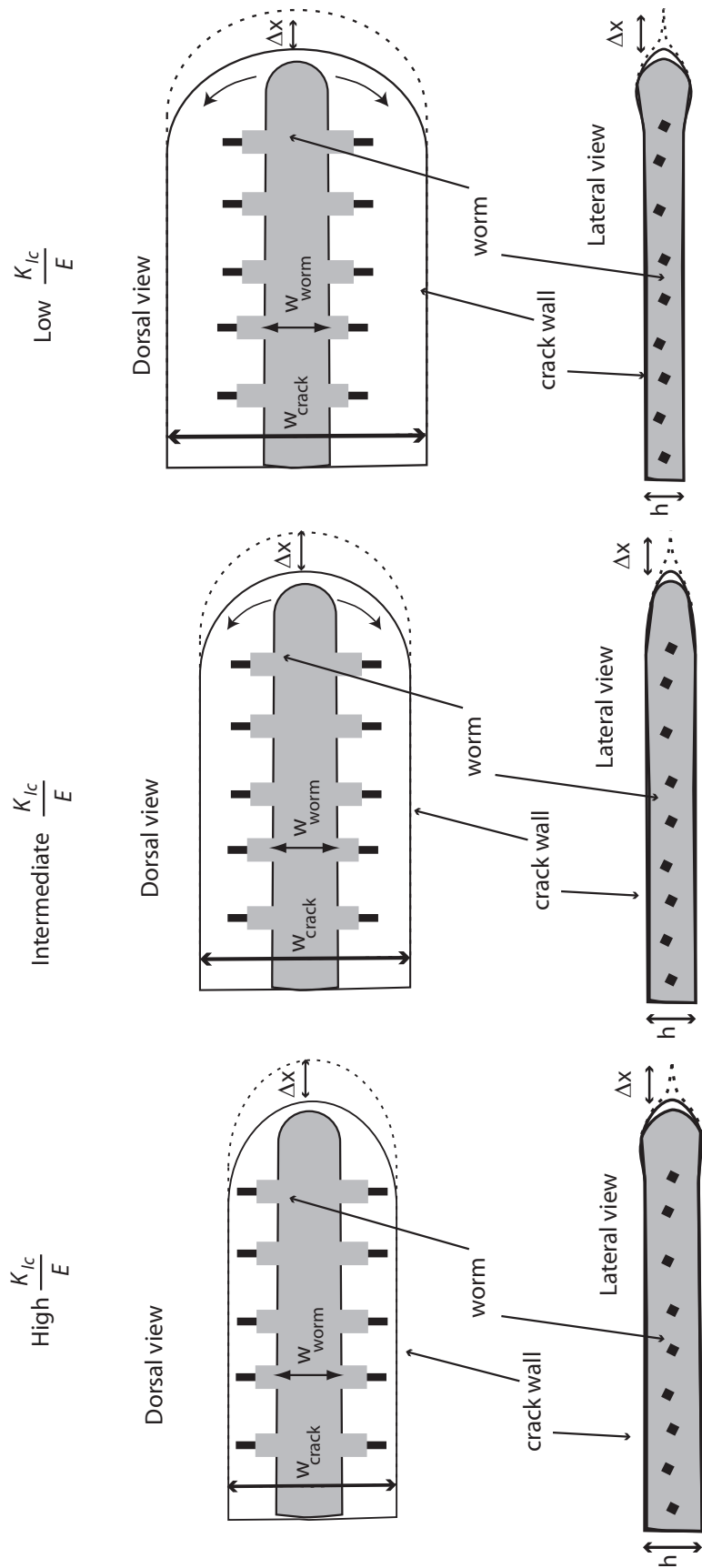
Figure 5.9. Scheme of differences in burrowing mechanics with wedge number. Worm width is indicated at the 4th setiger.

We observed obvious behavioral differences in gels with different ratios of K_{Ic}/E. The range of K_{Ic}/E values in natural sediments exceeds the range in these gels (cf. Figure 5.5), and is poorly understood. The rigid particles in natural sediments are expected to increase their stiffness, but may also cause stress softening (Koehl 1982), reducing the effect of stiffness on burrowers over time. Higher fracture toughnesses in natural sediments than gels might result from microcracking around particles. Clearly, more research on the mechanical properties of muds on spatial and temporal scales relevant to burrowers is needed to predict burrowing behaviors in natural sediments. Conversely, observations in transparent gels containing particles of the same refractive index would also clearly be worthwhile in an attempt to match mechanics of the simplified media to those of natural sediments.

Pharyngeal eversions are used for both burrowing and feeding; understanding how behavior depends on sediment mechanics may also lend insight into subsurface feeding behaviors. We showed that worms in the stiffer gels could effectively extend the burrow either by pharynx eversion or by driving the head forward in the crack. None of the worms were feeding while burrowing in the gels, effectively separating burrowing behavior from feeding behavior in our experiments. In natural sediments, worms may be feeding while everting their pharynges to extend the crack or may feed from the crack walls without extending the crack. Understanding burrowing mechanics can help identify when and at what frequency pharynx eversions are necessary for crack extension.

In natural sediments, these differences in behavior likely affect particle movements differently and therefore have implications for bioturbation. Particle mixing likely depends on the width of the crack, which varies with the ratio of fracture toughness

to stiffness. In materials with high stiffness, side-to-side motion may be a major driver of bioturbation during burrowing. These different behaviors may also be more or less effective in creating a permanent burrow after crack extension by fracture; intuitively, larger forces exerted during pharynx eversion and repeated application of forces through changes in body thickness would be more effective at deforming sediments plastically. In materials with high fracture toughness, the large forces needed to produce a crack may be sufficient to rearrange particles plastically at the crack tip. In order to predict how movement of sediment grains varies with worm behavior, more research on sediment mechanics is needed, specifically how sediment grains are released from the matrix under forces exerted by burrowers. Once these interactions are known, stratigraphic effects can be predicted through automaton modeling (e.g., Choi et al. 2002, Reed et al. 2006).

The differences in behavior with sediment properties observed also support making further investigations into how these burrowing-relevant mechanical properties of sediments depend on classically measured factors such as grain size, porosity and quantity and quality of organic material. If they do not, then new mechanical measurements need to be added to the arsenal in order to understand the strong feedbacks in organism-sediment interactions. Because bulk sediment behaves so much like an elastic polymer, it is clear that the polymeric matrix that binds muddy sediments warrants greater attention from both mechanical and chemical perspectives.

Chapter 6

CONCLUSIONS

The mechanism of burrow extension by crack propagation is mechanically efficient and appears to be widespread among burrowers in muddy sediments. Understanding of this mechanism raises questions about the reputed high energetic cost of burrowing and helps explain observed behaviors of worms and many other burrowing organisms and the effects of those behaviors on particle mixing.

Of the questions raised in the literature review of Ch. 3, I have subsequently shown that forces exerted by burrowers are lower than previously measured, likely due to wall effects in previous studies. I have also shown that the behaviors of worms can be understood from linear elastic fracture mechanics are affected by the mechanical properties of sediments in predictable ways. Relevant mechanical properties are the stiffness, or elastic modulus, E, and the fracture toughness, or critical stress intensity factor, K_{Ic}.

Some interesting questions with implications for bioturbation and energetics of locomotion remain. Although measured forces are lower than in previous studies, whether that decrease translates to lower energetic cost than suggested in previous studies is unknown and depends on more direct measures of energetic cost. The mechanisms by which crack propagation releases particles from the sediment matrix have great relevance to a mechanistic understanding of bioturbation. Additionally, the mechanisms by which a crack becomes a permanent burrow is unknown and has relevance both to understanding animal behavior and to resulting particle mixing.

REFERENCES

Abdalla, A. M., Hettiaratchi, D. R. P. & Reece, A. R. 1969. The mechanics of root growth in granular media. *Journal of Agricultural Engineering Research* **14**, 236-48.

Alexander, R. M. 2003. *Principles of Animal Locomotion.* Princeton, NJ: Princeton University Press.

Alexander, R. R., Stanton, R. J., Jr. & Dodd, J. R. 1993. Influence of sediment grain size on the burrowing of bivalves: Correlation with distribution and statigraphic persistence of selected Neogene clams. *Palaios* **8**, 289-303.

Aller, R. C. 1982. The effects of macrobenthos on chemical properties of marine sediment and overlying water. In *Animal-Sediment Relations*, P. L. McCall & M. J. S. Tevesz (eds), New York: Plenum Press, 53-104.

Aller, R. C. 1988. Benthic fauna and biogeochemical processes in marine sediments: the role of burrow structures. In *Nitrogen Cycling in Coastal Marine Environments*, T. H. Blackburn & J. Sorensen (eds), New York: Wiley, 301-38.

Anderson, T. L. 1995. *Fracture Mechanics: Fundamentals and Applications*. Boca Raton, FL: CRC Press.

Ansell, A. D. & Peck, L. S. 2000. Burrowing in the Antarctic anemone, *Halcampoides* sp., from Signy Island, Antarctica. *Journal of Experimental Marine Biology and Ecology* **252**, 45-55.

Ansell, A. D. & Trueman, E. R. 1968. The mechanism of burrowing in the anemone, *Peachia hastata* Gosse. *Journal of Experimental Marine Biology and Ecology* **2**, 124-34.

Atkinson, R. J. A. & Taylor, A. C. 1988. Physiological ecology of burrowing decapods. In *Aspects of Decapod Crustacean Biology*, A. A. Fincham & P. Rainbow (eds), Symposium of the Zoological Society of London 59, 201–26.

Barenblatt, G. I. 1962. The mathematical theory of equilibrium cracks in brittle fracture, In *Advances in Applied Mechanics* v. 7, H. L. Dryden & T. von Karman (eds.), Academic Press, 55-129.

Bellwood, O. 2002. The occurrence, mechanics, and significance of burying behavior in crabs (Crustacea: Brachyura). *Journal of Natural History* **36**, 1223-38.

Blair, N.E., Levin, L.A., DeMaster, D.J., & Plaia, G. 1996. The short-term fate of fresh algal carbon in continental slope sediments. *Limnology and Oceanography* **41**, 1208-19.

Boudreau, B. P., Algar, C., Johnson, B. D., Croudace, I., Reed, A., Furukawa, Y., Dorgan, K. M., Jumars, P. A., Grader, A. S. & Gardiner, B. S. 2005. Bubble growth and rise in soft sediments. *Geology* **33**, 517-20.

Boudreau, B. P., Choi, J., Meysman, F. J. R. & Francois-Carcaillet, F. 2001. Diffusion in a lattice-automaton model of bioturbation by small deposit feeders. *Journal of Marine Research* **59**, 749-68.

Bousfield, E. L. 1973. *Shallow-water Gammaridean Amphipoda of New England*. Ithaca, NY: Comstock Publishing Associates.

Broek, D. 1978. *Elementary Engineering Fracture Mechanics*. Alphen aan den Rijn, the Netherlands: Sijthoff & Noordhoff.

Brown, A. C. & Trueman, E. R. 1991. Burrowing of sandy-beach molluscs in relation to penetrability of the substratum. *Journal of Molluscan Studies* **57**, 134-6.

Chandler, H. W. 1984. The use of non-linear fracture mechanics to study the fracture properties of soils. *Journal of Agricultural Engineering Research* **29**, 321-7.

Chapman, G. 1949. The thixotropy and dilatancy of a marine soil. *Journal of the Marine Biological Association of the United Kingdom* **28**, 123-40.

Chen, Z. & Mayer, L. M. 1999. Sedimentary metal bioavailability determined by the digestive constraints of marine deposit feeders: Gut retention time and dissolved amino acids. *Marine Ecology Progress Series* **176**, 139-151.

Choi, J., Francois-Carcaillet, F. & Boudreau, B. P. 2002. Lattice-automaton bioturbation simulator (LABS): implementation for small deposit feeders. *Computers and Geosciences* **28**, 213-22.

Clark, R.B. 1964. *Dynamics in Metazoan Evolution*. London: Oxford University Press.

Cook, J. & Gordon, J. E. 1964. A mechanism for the control of crack propagation in all-brittle systems. *Proceedings of the Royal Society* **A252**, 508-20.

Dantu, P. 1957. Contribution àl'étude mécanique et ométrique des milieux pulvérulents. *Proceedings of the 4th International Conference on Soil Mechanics and Foundation Engineering*, 144–8.

Das, B. M. 2001. *Principles of Geotechnical Engineering*. Boston, MA: PWS Publishing Company.

Day, J. H. 1967. *A Monograph on the Polychaeta of Southern Africa. Part 2. Sedentaria.* London: British Museum (Natural History).

Diaz, R. J. & Cutter, G. R. J. 2001. In situ measurement of organism-sediment interaction: rates of burrow formation, abandonment, and sediment oxidation, reduction. In *Organism-Sediment Interactions*, J. Y. Aller et al. (eds), Columbia, South Carolina: University of South Carolina Press, 19-32.

Dorgan, K. M., Jumars, P. A., Johnson, B. D., Boudreau, B. P. & Landis, E. 2005. Burrow elongation by crack propagation. *Nature* **433**, 475.

Dorgan, K. M., Jumars, P. A., Johnson, B. D. & Boudreau, B. P. 2006. Macrofaunal burrowing: the medium is the message. *Oceanography and Marine Biology: An Annual Review* **44**, 85-141.

Dorgan, K. M., Arwade, S. R., & Jumars, P. A. In press. Burrowing in marine muds by crack propagation: kinematics and forces. *Journal of Experimental Biology.*

Duran, J. 2000. *Sands, Powders, and Grains: An Introduction to the Physics of Granular Materials*. New York: Springer.

Durelli, A. J. & Riley, W. F. 1965. *An introduction to photomechanics*. Englewood Cliffs: Prentice-Hall.

Dvorkin, J., Prasad, M., Sakai, A. & Lavoie, D. 1999. Elasticity of marine sediments: rock physics modeling. *Geophysical Research Letters* **26**, 1781-1784.

Edmonds, J., Cushing, J. M., Constantino, R. F., Henson, S. M., Dennis, B. & Desharnais, R. A. 2003. Park's Tribolium competition experiments: a non-equilibrium species coexistence hypothesis. *Journal of Ecology* **72**, 703-12.

Elder, H. Y. 1973. Direct peristaltic progression and the functional significance of the dermal connective tissues during burrowing in the polychaete *Polyphysia crassa* (Oersted). *Journal of Experimental Biology* **58**, 637-55.

Elder, H. Y. 1980. Peristaltic mechanisms. In *Aspects of Animal Movement*, H. Y. Elder & E. R. Trueman (eds), Cambridge: Cambridge University Press, 71-92.

Fauchald, K. & Jumars, P. A. 1979. The diet of worms: a study of polychaete feeding guilds. *Oceanography and Marine Biology: An Annual Review* **17**, 193-284.

Fett, T. 1982. Crack opening displacement of a penny-shaped crack in an infinite body loaded by internal pressure over a circular area. *International Journal of Fracture* **20(4)**, R135-R138.

Fountain, A. G., Jacobel, R. W., Schlichting, R. & Jansson, P. 2005. Fractures as the main pathways of water flow in temperate glaciers. *Nature* **433**, 618-21.

Frankel, L. & Mead, D. J. 1973. Mucilaginous matrix of some estuarine sands in Connecticut. *Journal of Sedimentary Petrology* **43**, 1090-5.

Full, R. J., Yamauchi, A. & Jindrich, D.L. 1995. Maximum single leg force production: cockroaches righting on photoelastic gelatin. *Journal of Experimental Biology* **198**, 2441-2452.

Geng, J., Howell, D., Longhi, E., Behringer, R. P., Reydellet, G., Vannel, L., Clement, E. & Luding, S. 2001. Footprints in sand: The response of a granular material to local perturbations. *Physical Review Letters* **87**, 035506: 4 pp.

Goldenberg, C. & Goldhirsch, I. 2005. Friction enhances elasticity in granular solids. *Nature* **435**, 188-91.

Gordon, J. E. 1976. *The New Science of Strong Materials: or Why You Don't Fall Through the Floor.* Princeton, NJ: Princeton University Press.

Grall, J. & Chauvaud, L. 2002. Marine eutrophication and benthos: the need for new approaches and concepts. *Global Change Biology* **8**, 813-30.

Gray, J. S. 1974. Animal-sediment relationships. *Oceanography and Marine Biology: An Annual Review* **12**, 223-261.

Hamilton, E. L. 1980. Geoacoustic modeling of the sea floor. *The Journal of the Acoustical Society of America* **68**, 1313-1340.

Harris, J. 1978. A photoelastic substrate technique for dynamic measurements of forces exerted by moving organisms. *Journal of Microscopy* **114**, 219-228.

Hartman, O. 1955. Endemism in the North Pacific Ocean, with emphasis on the distribution of marine annelids, and descriptions of new or little known species. In *Essays in the Natural Sciences in Honor of Captain Allan Hancock*. Los Angeles: University of Southern California Press, 39-60.

Hartman, O. 1958. Systematic account of some marine invertebrate animals from the deep basins off southern California. *Allan Hancock Pacific Expeditions* **22**, 69-215.

Hettiaratchi, D. R. P. & Ferguson, C. A. 1973. Stress-deformation behavior of soil in root growth mechanics. *Journal of Agricultural Engineering Research* **18**, 309-20.

Hollertz, K. & Duchene, J.-C. 2001. Burrowing behaviour and sediment reworking in the heart urchin *Brissopsis lyrifera* Forbes (Spatangoida). *Marine Biology* **139**, 951-7.

Hunter, R. D. & Elder, H. Y. 1989. Burrowing dynamics and energy cost of transport in the soft-bodied marine invertebrates *Polyphysia crassa* and *Priapulus caudatus*. *Journal of Zoology* **218**, 209-22.

Hunter, R. D., Moss, V. A. & Elder, H. Y. 1983. Image analysis of the burrowing mechanisms of *Polyphysia crassa* (Annelida: Polychaeta) and *Priapulus caudatus* (Priapulida). *Journal of Zoology* **199**, 305-23.

Jaeger, H. M. & Nagel, S. R. 1992. Physics of the granular state. *Science* **255**, 1523-31.

Johnson, B. D., Boudreau, B. P., Gardiner, B. S. & Maass, R. 2002. Mechanical response of sediments to bubble growth. *Marine Geology* **187**, 347-63.

Johnson, R. G. 1974. Particulate matter at the sediment-water interface in coastal environments. *Journal of Marine Research* **32**, 313-30.

Jones, M. L. 1968. On the morphology, feeding, and behavior of *Magelona* sp. *Biological Bulletin* **134**, 272-97.

Jumars, P. A. 1978. Spatial autocorrelation with RUM (Remote Underwater Manipulator): vertical and horizontal structure of a bathyal benthic community. *Deep-Sea Research* **25**, 589-604.

Jumars, P. A., Dorgan, K. M., Mayer, L. M., Boudreau, B. P., & Johnson, B. D. 2006. Material constraints on infaunal lifestyles: May the persistent and strong forces be with you. In *Trace Fossils: Concepts, Problems, Prospects*, W. Miller, III (ed.). Elsevier, 442-457.

Kanazawa, K. 1992. Adaptation of test shape for burrowing and locomotion in Spatangoid Echinoids. *Palaeontology* **35**, 733-50.

Keudel, M. & Schrader, S. 1999. Axial and radial pressure exerted by earthworms of different ecological groups. *Biology and Fertility of Soils* **29**, 262-9.

Koehl, M. A. R. 1982. Mechanical design of spicule-reinforced connective tissue: Stiffness. *Journal of Experimental Biology* **98**, 239-267.

Koenig, B., Holst, G., Glud, R. N. & Kuehl, M. 2001. Imaging of oxygen distributions at benthic interfaces: a brief review. In *Organism-Sediment Interactions*, J. Y. Aller et al. (eds), Columbia, South Carolina: University of South Carolina Press, 63-71.

Kudenov, J. D. 1977. The functional morphology of feeding in three species of maldanid polychaetes. *Zoological Journal of the Linnean Society* **60**, 95-109.

Lade, P.V. 2001. Engineering properties of soils and typical correlations. In *Geotechnical and geoenvironmental engineering handbook*. (ed. R. K. Rowe), pp. 43-68. Cambridge, MA: Springer.

Lastra, M., Dugan, J. E. & Hubbard, D. M. 2002. Burrowing and swash behavior of the Pacific mole crab *Hippa pacifica* (Anomura, Hippidae) in tropical sandy beaches. *Journal of Crustacean Biology* **22**, 53-8.

Levin, L. A. & Edesa, S. 1997. The ecology of cirratulid mudballs on the Oman margin, northwest Arabian Sea. *Marine Biology* **128**, 671-678.

Mach, K. J., Nelson, D. V. & Denny, M. W. 2007. Techniques for predicting the lifetimes of wave-swept macroalgae: a primer on fracture mechanics and crack growth. *Journal of Experimental Biology* **210**, 2213-2230.

Menand, T. & Tait, S. R. 2001. A phenomenological model for precursor volcanic eruptions. *Nature* **411**, 678-680.

Menand, T. & Tait, S. R. 2002. The propagation of a buoyant liquid-filled fissure from a source under constant pressure: An experimental approach. *Journal of Geophysical Research* **107** (B11), 2306, doi:10.1029/2001JB000589.

Meysman, F. J. R., Boudreau, B. P. & Middelburg, J. J. 2003. Relations between local, nonlocal, discrete and continuous models of bioturbation. *Journal of Marine Research* **61**, 391-410.

Meysman, F. J. R., Middelburg, J. J. & Heip, C. H. R. 2006. Bioturbation: a fresh look at Darwin's last idea. *Trends in Ecology and Evolution* **21**, 688-695.

Mulsow, S., Boudreau, B. P. & Smith, J. N. 1998. Bioturbation and porosity gradients. *Limnology and Oceanography* **43**, 1-9.

Nel, R., McLachlan, A. & Winter, D. P. E. 1999. The effect of sand particle size on the burrowing ability of the beach mysid *Gastrosaccus psammodytes* Tattersall. *Estuarine Coastal and Shelf Science* **48**, 599-604.

Nel, R., McLachlan, A. & Winter, D. P. E. 2001. The effect of grain size on the burrowing of two *Donax* species. *Journal of Experimental Marine Biology and Ecology* **265**, 219-38.

Nicolaisen, W., and Kanneworf, E. 1969. On the burrowing and feeding habits of the amphipods *Bathyporeia pilosa* Lindstrom and *Bathyporeia sarsi* Watkin. *Ophelia* **6**, 231-250.

Nowell, A. R. M., Jumars, P. A. & Eckman, J. E. 1981. Effects of biological activity on the entrainment of marine sediments. *Marine Geology* **42**, 155-72.

Nowell, A. R. M., Jumars, P. A., & Southard, J. B. 1989. Responses of intertidal macrofauna to ripple migration in a laboratory racetrack flume. In *Ecology of Marine Deposit Feeders*. G. R. Lopez et al. (eds), New York: Springer-Verlag, 247-268.

Purcell, E. M. 1977. Life at low Reynolds number. *American Journal of Physics* **45**, 3–11.

Quillin, K. J. 1998. Ontogenetic scaling of hydrostatic skeletons: Geometric, static stress and dynamic stress scaling of the earthworm *Lumbricus terrestris*. *Journal of Experimental Biology* **201**, 1871-83.

Quillin, K. J. 2000. Ontogenetic scaling of burrowing forces in the earthworm *Lumbricus terrestris*. *Journal of Experimental Biology* **203**, 2757-70.

Ramey, P. A., & Snelgrove, P. V. R. 2003. Spatial patterns in sedimentary macrofaunal communities on the south coast of Newfoundland in relation to surface oceanography and sediment characteristics. *Marine Ecology Progress Series* **262**, 215-227.

Reed, D. C., Huang, K., Boudreau, B. P., & Meysman, F. J. R. 2006. Steady-state tracer dynamics in a lattice-automaton model of bioturbation. *Geochimica Cosmochimica Acta* **70**, 5855-5867.

Reiner, M. 1964. The Deborah number. *Physics Today* **17**, 62.

Rhoads, D. C., McCall, P. L. & Yingst, J. Y. 1978. Disturbance and production on the estuarine seafloor. *American Scientist* **66**, 557-86.

Riisgård, H. U., Berntsen, I. & Tarp, B. 1996. The lugworm (*Arenicola marina*) pump: characteristics, modelling, and energy cost. *Marine Ecology Progress Series* **138**, 149-56.

Rivalta, E., Bottinger, M., & Dahm, T. 2005. Buoyancy-driven fracture ascent: Experiments in layered gelatine. *Journal of Volcanology and Geothermal Research* **144**, 273-285.

Roast, S. D., Widdows, J., Pope, N. & Jones, M. B. 2004. Sediment-biota interactions: mysid feeding activity enhances water turbidity and sediment erodability. *Marine Ecology Progress Series* **281**, 145-54.

Rouse, G. W. & Pleijel, F. 2001. *Polychaetes*. Oxford: Oxford University Press.

Rozbaczylo, N. & Mendez, M. A. 1996. *Artacama valparaisiensis*, a new species of Terebellidae (Annelida: Polychaeta) from subtidal soft bottoms of Valparaiso Bay, Chile. *Proceedings of the Biological Society of Washington* **109**, 138-142.

Santamarina, J. C., Klein, K. A. & Fam, M. A. 2001. *Soils and Waves*. Chichester, England: John Wiley & Sons, Ltd.

Schiffelbein, P. 1984. Effect of benthic mixing on the information content of deep-sea stratigraphical signals. *Nature* **311**, 651-653.

Schinner, G. O. 1993. Burrowing behavior, substratum, preference, and distribution of *Schizaster canaliferus* (Echinoidea: Spatangoida) in the Northern Adriatic Sea. *Marine Ecology* **14**, 129-45.

Schlangen, E. & Garboczi, E. J. 1996. New method for simulating fracture using an elastically uniform random geometry lattice. *International Journal of Engineering Science* **34**, 1131-44.

Schmidt, J. L., Deming, J. W., Jumars, P. A. & Keil, R. G. 1998. Constancy of bacterial abundance in surficial marine sediments. *Limnology and Oceanography* **43**, 976-82.

Self, R. F. L. & Jumars, P. A. 1988. Cross-phyletic patterns of particle selection by deposit feeders. *Journal of Marine Research* **46**, 119-43.

Seymour, M. K. 1969. Locomotion and coelomic pressure in *Lumbricus terrestris* L. *Journal of Experimental Biology* **51**, 47-58.

Seymour, M. K. 1971. Burrowing behaviour in the European lugworm *Arenicola marina* (Polychaeta: Arenicolidae). *Journal of Zoology, London* **164**, 93-132.

Sharples, K. 1981. Photoelastic stress analysis. *Chartered Mechanical Engineer* **28**, 42-50.

Sherwood, C. R., Drake, D. E., Wiberg, P. L. & Wheatcroft, R. A. 2002. Prediction of the fate of DDT in sediments on the Palos Verdes margin. *Continental Shelf Research* **22**, 1025-58.

Shull, D. H. & Yasuda, M. 2001. Size-selective downward particle transport by cirratulid polychaetes. *Journal of Marine Research* **59**, 453-73.

Sih, G. C. 1973. *Handbook of stress intensity factors: Stress intensity factor solutions and formulas for reference*. Bethlehem, PA, Lehigh University.

Solan, M. & Kennedy, R. 2002. Observation and quantification of in situ animal-sediment relations using time-lapse sediment profile imagery (t-SPI). *Marine Ecology Progress Series* **228**, 179-91.

Sperling, L. H. 2001. *Introduction to physical polymer science*. New York: John Wiley & Sons, Inc.

Stanley, S. M. 1970. *Relation of Shell Form to Life Habits of the Bivalvia (Mollusca)*. Boulder, CO: The Geological Society of America, Inc.

Stovold, R. J., Whalley, W. R. & Harris, P. J. 2003. Dehydration does not affect the radial pressures produced by the earthworm *Aporrectodea caliginosa*. *Biology and Fertility of Soils* **37**, 23-8.

Timmerman, K., Christensen, J. H. & Banta, G. T. 2002. Modeling of advective solute transport in sandy sediments inhabited by the lugworm *Arenicola marina*. *Journal of Marine Research* **60**, 151-69.

Torquato, S. 2001. Random Heterogeneous Materials: Microstructure and Macroscopic Properties. New York: Springer.

Trevor, J. H. 1977. The burrowing of *Nereis diversicolor* O. F. Muller, together with some observations on *Arenicola marina* (L.) (Annelida: Polychaeta). *Journal of Experimental Marine Biology and Ecology* **30**, 129-45.

Trevor, J. H. 1978. The dynamics and mechanical energy expenditure of the polychaetes *Nephtys cirrosa*, *Nereis diversicolor*, and *Arenicola marina* during burrowing. *Estuarine and Coastal Marine Science* **6**, 605-19.

Trueman, E. R. 1970. The mechanism of burrowing of the mole crab, *Emerita*. *Journal of Experimental Biology* **53**, 701-10.

Trueman, E. R. 1975. *The Locomotion of Soft-bodied Animals*. New York: American Elsevier Publishing Company, Inc.

Trueman, E. R. 1983. Locomotion in molluscs. In *The Mollusca*, A. S. M. Saleuddin & K. M. Wilbur (eds), New York: Academic Press, Inc., 155-98.

Trueman, E. R. & Brown, A. C. 1992. The burrowing habit of marine gastropods. In *Advances in Marine Biology*, J. H. S. Blaxter & A. J. Southward (eds.), San Diego, CA: Academic Press, 389-431.

Trueman, E. R. & Foster-Smith, R. L. 1976. The mechanism of burrowing of *Sipunculus nudus*. *Journal of Zoology, London* **179**, 373-386.

Trueman, E. R. & Jones, H. D. 1977. Crawling and burrowing. In *Mechanics and Energetics of Animal Locomotion*, R. M. Alexander & G. Goldspink (eds), London: Chapman & Hall, 204-21.

Tzetlin, A. B. 1994. Fine morphology of the feeding apparatus of *Cossura* sp. (Polychaeta, Cossuridae) from the White Sea. *Memoires du Museum National d'Histoire Naturelle, Paris* **162**, 137-43.

Tzetlin, A. B. & Filippova, A. V. 2005. Muscular system in polychaetes (Annelida). *Hydrobiologica* **535/536**, 113-126.

Tzetlin, A. B., Zhadan, A., Ivanov, I., Muller, M. C. M. & Purschke, G. 2002. On the absence of circular muscle elements in the body wall of *Dysponetus pygmaeus* (Chrysopetalidae, 'Polychaeta', Annelida). *Acta Zoologica (Stockholm)* **83**, 81-5.

Voparil, I. M., Burgess, R. M., Mayer, L. M., Tien, R., Cantwell, M. G. & Ryba, S. A. 2003. Digestive bioavailability to a deposit feeder (*Arenicola marina*) of polycyclic aromatic hydrocarbons associated with anthropogenic particles. *Environmental Toxicology and Chemistry* **23**, 2618-26.

Watling, L. 1988. Small-scale features of marine sediments and their importance to the study of deposit feeding. *Marine Ecology Progress Series* **47**, 135-44.

Wethey, D. S. & Woodin, S. A. 2005. Infaunal hydraulics generate porewater pressure signals. *Biological Bulletin* **209**, 139-145.

Wilkes, J. O. 1999. *Fluid Mechanics for Chemical Engineers*. Upper Saddle River, NJ: Prentice-Hall PTR.

Yannicelli, B., Palacios, R. & Gimenez, L. 2002. Swimming ability and burrowing time of two cirolanid isopods from different levels of exposed sandy beaches. *Journal of Experimental Marine Biology and Ecology* **273**, 73-88.

Yonge, C. M. & Thompson, T. E. 1976. *Living Marine Molluscs*. London: Collins.

Appendix A

SUPPLEMENTARY METHODS FOR BURROW EXTENSION BY CRACK PROPAGATION: PHOTOELASTIC STRESS ANALYSIS

Photoelastic stress analysis, common in materials engineering, has been used to measure forces of moving organisms (Harris 1978, Full et al. 1995). To restrict wall effects while still clearly visualizing animals and stress fields, a 21-L (5.5-gallon) aquarium was filled with gelatin mixed with seawater at double the normal concentration (28.35 g gelatin/L seawater). A photographic light table produced a uniform light field. We adapted previous methods (Full et al. 1995) from two to three dimensions by assuming that the light field was bilaterally symmetrical and using data only from worms travelling straight downward with the crack oriented perpendicular to the camera. Because we were more interested in magnitude than direction of forces, we used circularly, rather than linearly, polarized light. This procedure eliminates isoclinic fringes, which provide information about directions of stresses, to more clearly show isochromatic fringes, which provide information about magnitudes (Sharples 1981). Light from the light table went through a linear polarizer, then a quarter-wave retardation plate to become circularly polarized, through the gelatin, through another quarter-wave retardation plate, and finally a linear polarizing filter. Forces were calculated from the videotaped area of the stress field in individual frames over time.

Using a weighted test tube containing known volumes of water resting on the gelatin surface, we calibrated stress-field areas. Least-squares regression between force (mass of test tube plus water x gravity) per unit area of the test tube touching the surface (measured from frame grabs via Image J) and area of the stress field (thresholded using

Matlab to the same value as the stress field around worms) predicted stress. We assumed

that force exerted by the round bottom of the test tube against the flat surface of the

gelatin accurately mimicked force exerted by the curved pharynx against the relatively

flat wall of the crack. Stresses were converted to forces by multiplication with the area of

the everted pharynx (from a dorsal view, calculated with Image J). Because we could not

see the area of the pharynx exerting the force while the pharynx was being everted and

retracted, we scaled the maximum area by the ratio of dorso-ventral thickness at a given

time to thickness at full eversion (squared, to convert length to area). The ratio varied

from approximately 1/3 when the pharynx was retracted to unity at full eversion. Care

was taken to match the range of stresses caused by test-tube weight to those exerted by

the worm, although often when the pharynx was retracted, no pixels exceeded threshold

value. We conservatively assumed when no light was detected that the maximum stress

possible without detection was present. Calculated work in any case is small from these

threshold forces because of the small distances involved.

Appendix B

METHOD VALIDATION FOR BURROWING IN MARINE MUDS BY CRACK PROPAGATION: KINEMATICS AND FORCES

Experimental validation of calibration method

Because worms burrow in 3-D, we conducted tests to evaluate whether the linear relationship between stress and the area of the primary compression fringe observed in shallow, flat gelatin plates (Harris 1978, Full et al. 1995) holds for deep, 3-D aquaria and whether a surface calibration is appropriate to measure forces around a worm burrowing within the gelatin. We first calculated regressions between pixel areas and stresses and forces applied to the surface by objects of varied sizes and shapes to determine both whether the linear relationship between stress and area of pixels held for 3-D stress fields and whether the test tube had appropriate geometry to mimic the everted pharynx. These objects included balloons with varying volumes of water, Play-doh^{TM} objects of varying weights and shapes, and test tubes and flat-bottomed cylinders of varying sizes. Using a larger test tube resulted in larger pixel areas for a given stress (Figure B.1A), but plotting force instead of stress gave similar results across test tubes sizes (Figure B.1B). Curved pieces of Play-doh^{TM} and balloons showed similar stress fields to those of test tubes, but flat, rigid objects had smaller patches of stress along the edges with little stress in the middle of the object, very different than the stress fields around worms. Rigid, flat objects create constant displacements in gelatin, exerting high stress at the ends and low stress in the middle (a parabolic stress field), most noticeable by photoelastic stress analysis for light objects exerting small stresses.

Figure B.1. Pixel area as a function of force and stress for modeled and experimental data. A) Pixel area resulting from stresses applied to the surface of gelatin by test tubes and flat-bottomed cylinders of different diameters ($r^2 = 0.11$; n = 44). B) Pixel area as a function of force instead of stress for the data in A ($r^2 = 0.94$; n = 44). C) Results of finite element model of calibration showing thresholded pixel area as a function of stress (500, 750, and 1000 Pa) for three different modeled radii (0.005, 0.010, and 0.015 m) ($r^2 = 0.16$; n = 9). D) Pixel area as a function of force instead of stress for the data in C ($r^2 = 0.996$; n = 9).
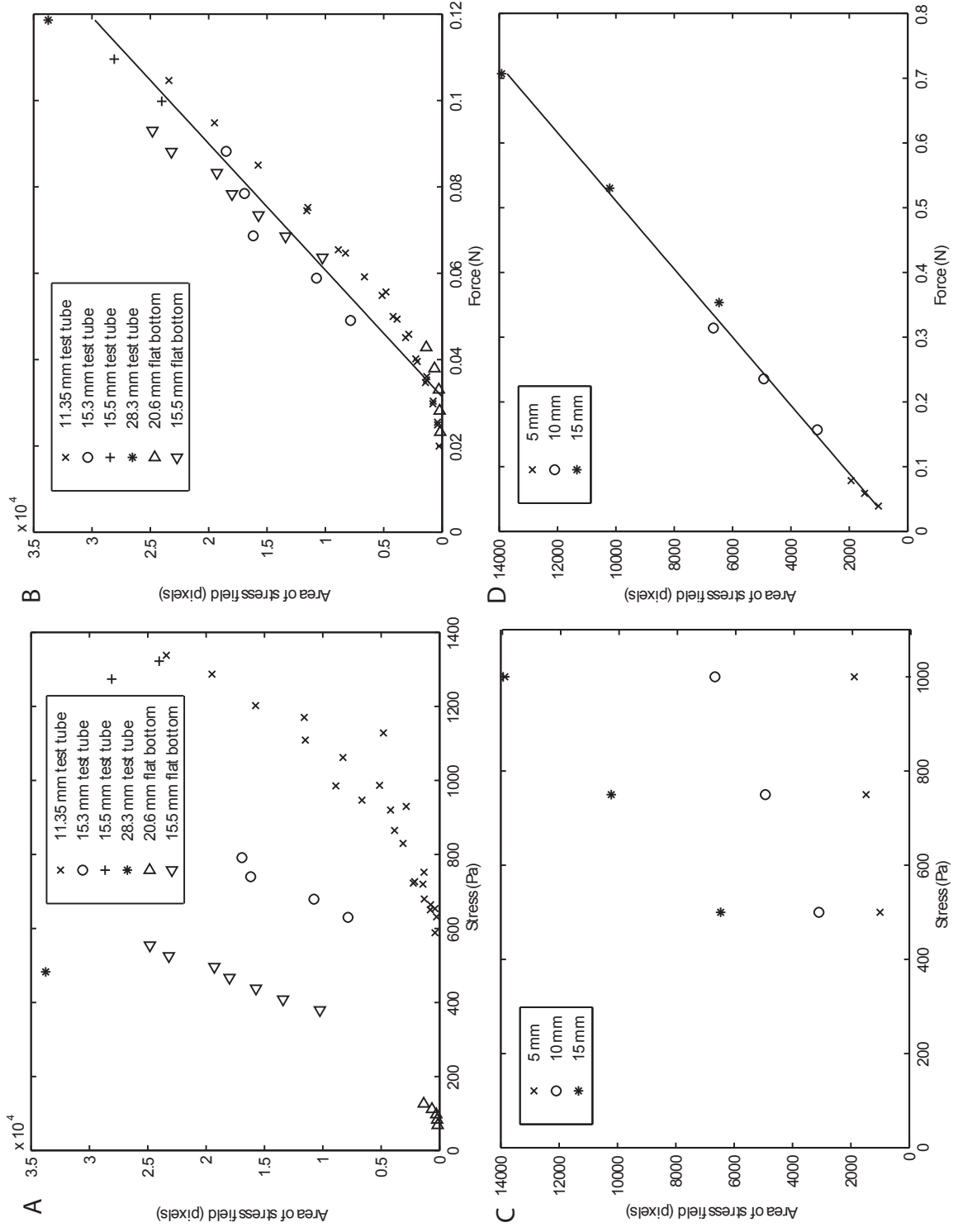
We then used finite element modeling to apply simulated stresses over different areas. A 2-D axisymmetric model of half of the gelatin tank (the x-z plane) with stress applied to the surface from the top corner of rotation (corresponding to the center of the aquarium) to a distance simulating the radius of a test tube was used to evaluate the effects of radius and magnitude of stress on areas of primary compression fringes (high stress). Again, the relationship between force and pixel area was much more linear than between stress and pixel area (Figure B.1C, D). Relationships for both calibration tests are linear rather than quadratic because the forces are larger (compare to x's in Figure 4.2).

Because worms move within gelatin, exerting forces on two walls, and our calibration involves only one surface, we also compared the test-tube calibration with data from a balloon inflated in the gelatin. The balloon was stretched over a curved wire to form a flat disk and was attached to a syringe and a 1 PSI gauge pressure transducer (Honeywell, Columbus, OH) connected through a data-acquisition device (National Instruments USB 6008) to a computer running LabView (Fig. B.2). The balloon was filled with enough water to give a pressure reading close to zero, inserted into the sediment (or gelatin), inflated to known volume, and pressure, measured. The balloon was deflated, removed from the gelatin, then re-inflated in air to the same volume to determine the pressure needed to inflate the balloon without resistance. Subtracting this pressure removed the stress needed to stretch the balloon, leaving only the stress applied to the gelatin. This approach assumes that balloon and gelatin stiffnesses are additive, which is approximately valid in this experiment since balloon and gelatin displacements must remain compatible. Forces exerted were calculated by multiplying pressure by the

Figure B.2. Balloon and pressure transducer set-up. The balloon is stretched to a 2-D disk using a wire and is glued to the end of a tube (grey line), which is connected to a Luer lock adapter (thicker grey line). The adapter is connected to a syringe filled with water and a pressure transducer. The balloon, syringe, and pressure transducer were held in the horizontal x-y plane, as shown in the top-view scheme, to minimize variations in pressure (P) with water height.

Top View
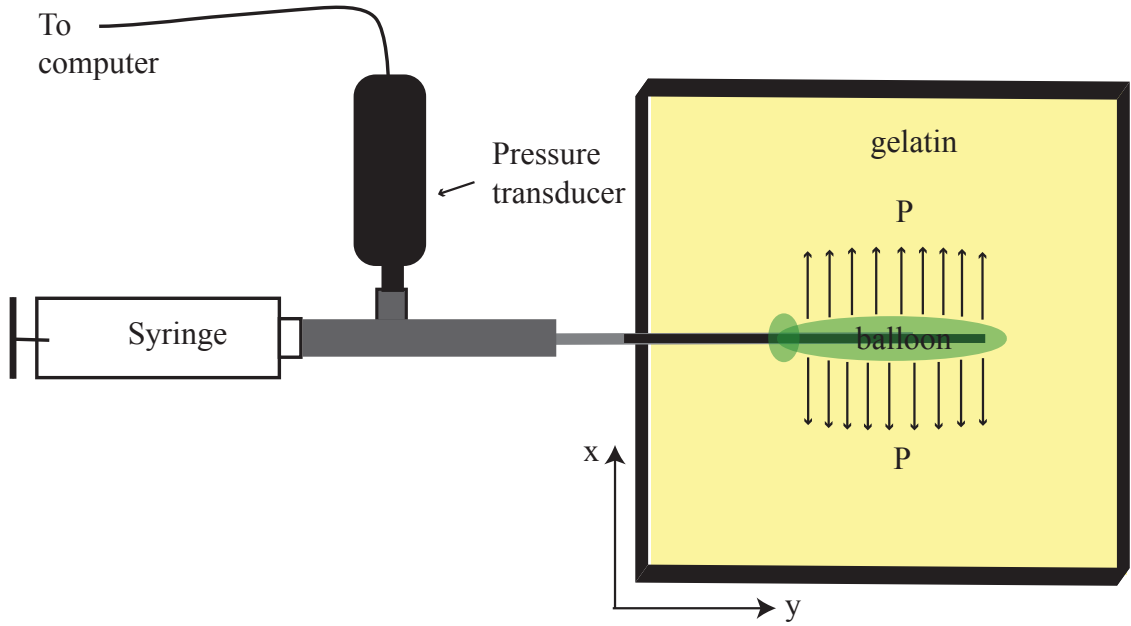
Side View
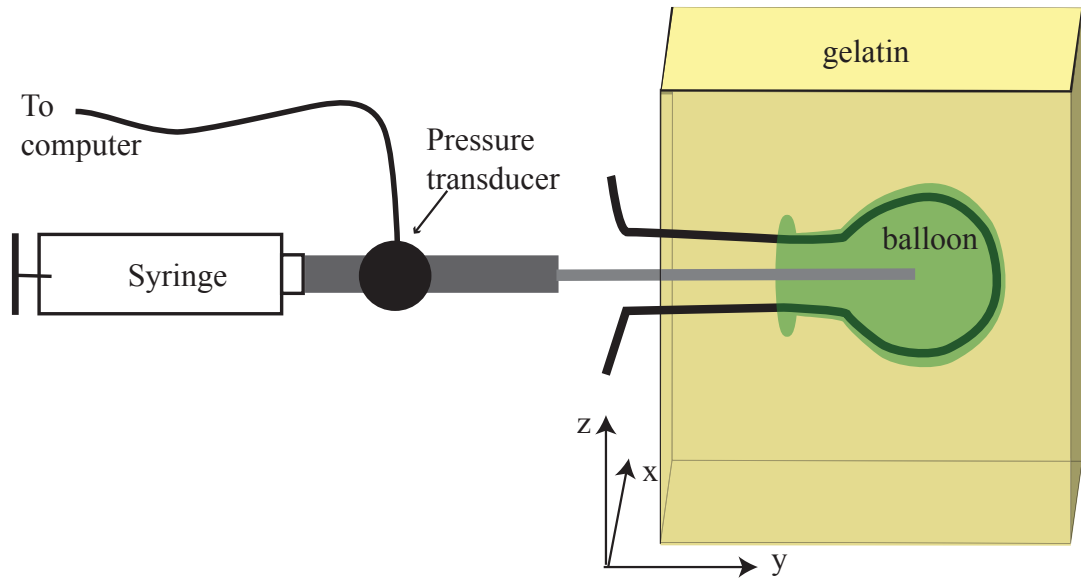
planar area of the balloon in contact with the gelatin. The planar area of the balloon

overestimated area over which stress was applied for small volumes of water that did not

fully inflate the balloon. We were unable to quantify the error in the planar area

measurements, but this error seems to explain the discrepancy between the regressions

using the test tube and balloon (Figure B.3A). Overestimating the area over which stress

is applied overestimates the calculated force (= stress x area) for small volumes of water;

shifting those points to the left would bring the balloon regression closer to the test-tube

regression, although the variation around the balloon regression is still very high.

Although the experimental data were less conclusive than we had hoped, they did not

reveal any obvious problems with the surface calibration method.

Finite element modeling to evaluate the difference in geometry between the crack

tip and the surface of the gelatin was more convincing. Stress was applied in a 2-D plane

strain model (again, a simplification of the 3-D state) to the top surface of modeled

gelatin and along the wall of the crack near the tip (Figure B.3B). Applying stress of 500

Pa along 0.0089 m starting at the crack tip resulted in a slightly smaller region above the

threshold stress than the same stress applied along the same length at the crack surface

(42 and 64 pixels, respectively). However, moving the stress 0.002 m back from the

crack tip (the distance between the fully everted pharynx and the crack tip; see results)

yielded more similar stress distribution to the surface (58 and 64 pixels, respectively).

Reduction in compressive stress fringe size at the crack tip likely resulted from

interference by the tensile stress at the crack tip (cf. Figure 4.3), visible as an asymmetry

in the tensile stress field in the middle frame of Figure B.3B compared to the right frame.

This interference would be overestimated in the model compared to the experiment

Figure B.3. Calibration curve comparing weight exerted by a test-tube on the surface to pressure exerted by a balloon inflated in a crack in the gelatin. A) The areas of the primary compression fringes on each side of the balloon were measured separately (* and +), and regressions are shown as dotted lines (r^2 = 0.65 and 0.62; n = 13). The regression through the test-tube data (x; solid line; r^2 = 0.998; n = 6) was extended through the ranges of the balloon data. B) Stress contours from franc2d models of stress on the surface (left), along the crack starting at the tip (center), and along the crack starting 0.002 m up from the tip (right). The models are 2-D representations of the y-z plane in the 3-D experiments. Stress (500 Pa) is exerted along 0.0089 m in each model and is indicated by vectors. In each image, red and white colors indicate compressive stress; blue is tensile stress. Images were thresholded to the light red/white boundary (scale bar = 0.005 m).

A

B

206
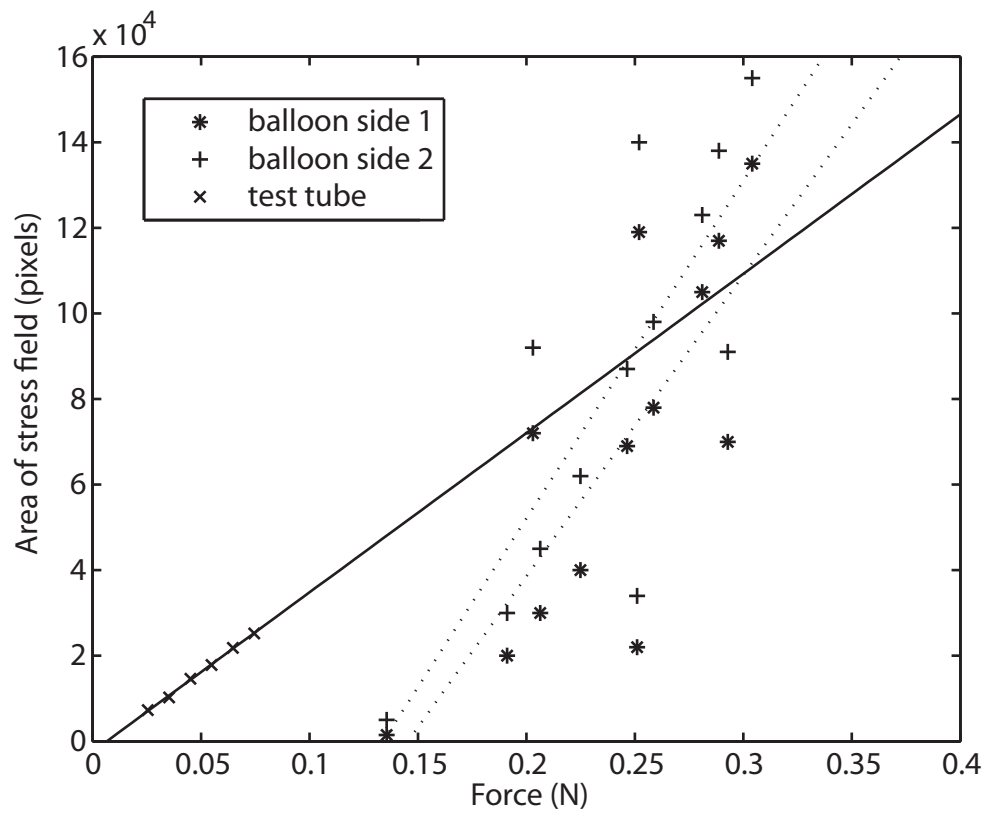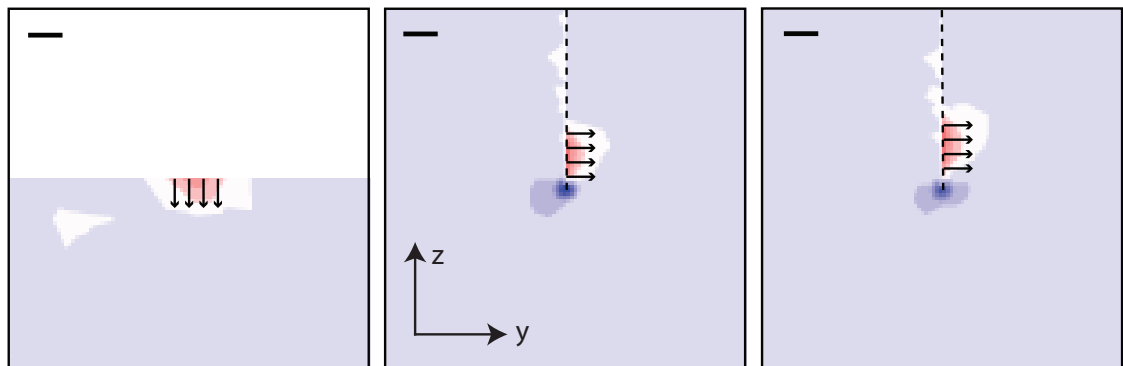
because observed stress fringes are narrower and extend farther from the surface than modeled stresses. This difference suggests that stresses in the experiment are less uniform than modeled stresses because the curved shape of the test tube (and worm pharynx) exerts more stress in the center than at the edges and/or the model ignores effects of displacements on shape of the stress field.

We performed the calibration with several different threshold values to calculate forces exerted. Calculated force increased with threshold value at low thresholds, reaching an asymptote at higher threshold values (data not shown). This increase is likely due to interference between compressive stress around the pharynx and tensile stress at the crack tip. Using a higher threshold value yields a smaller area of the primary compression fringe that is better resolved from the tensile stress field.

Slope of the quadratic calibration curve was higher for smaller numbers of pixels; using too high a threshold increases error in converting from pixels to force. However, using low thresholds underestimates force because of influence of the tensile stress field. To restrict error, we used the highest threshold (close to the asymptote) that resulted in areas of at least 300 pixels.

Experimental validation of modeling technique

To test for appropriate displacements under applied stresses, we modeled a control system with known stress and displacement. A balloon attached to a pressure transducer and inflated with a syringe (Figure B.2) was inserted through a vertical slot in the side of a 16.5- x 21-cm container of sediment that had been fully mixed and allowed to settle for two weeks. The same methods as for the calibration validation were used,

and the experiment was repeated in both sediment and gelatin with two balloon sizes. Volumes of the combined balloon, wire, and added water were measured.

Balloons were modeled in franc2d as an internal crack in an axisymmetric model of the container of sediment (or gelatin). Measured pressures were applied to the crack and volume of displaced sediment was compared to measured volume of the balloon and water. In both media, model results approximated actual volumes (Table B.1).

Table B.1. Results from model validation. Measured volumes of balloons in gelatin and muddy sediments are compared to volumes of displacements in finite element models using measured stresses and diameters of balloons.

	Material	Pressure (Pa)	Measured Volume (cm^3)	Modeled Volume (cm^3)
Balloon 1	Gelatin	675	0.75	0.74
		860	1.10	0.94
	Sediment	3000	0.55	0.57
		4156	0.75	0.78
Balloon 2	Gelatin	820	3.35	3.71
		859	3.45	3.88
	Sediment	1882	1.55	1.45
		2454	1.95	1.87

BIOGRAPHY OF THE AUTHOR

Kelly Dorgan was born in Newport News, Virginia on November 10, 1979. She was raised in Yorktown, Virginia and graduated from York High School in 1997. She attended the University of California, Santa Cruz and graduated in 2001 with a Bachelor's degree in Marine Biology. She entered the Oceanography graduate program at The University of Maine in the summer of 2002.

After receiving her degree, Kelly will be starting a post-doc at University of California, Berkeley in the Department of Integrative Biology. Kelly is a candidate for the Doctor of Philosophy degree in Oceanography from The University of Maine in December, 2007.